THE UNIVERSITY OF MANITOBA

A STUDY OF VIBROIMPACT SYSTEMS

BY

CHARUSHEEL NARAYAN BAPAT

A THESIS

SUBMITTED TO THE FACULTY OF GRADUATE STUDIES

IN PARTIAL FULFILLMENT OF THE REQUIREMENTS FOR THE DEGREE

DOCTOR OF PHILOSOPHY

DEPARTMENT OF MECHANICAL ENGINEERING

WINNIPEG, MANITOBA, CANADA

FEBRUARY 1982

A STUDY OF VIBROIMPACT SYSTEMS

BY

CHARUSHEEL NARAYAN BAPAT

A thesis submitted to the Faculty of Graduate Studies of
the University of Manitoba in partial fulfillment of the requirements
of the degree of

DOCTOR OF PHILOSOPHY

ABSTRACT

A general theory is developed for the general stable periodic motion of an Impact-Pair and impact damper when subjected to a prescribed, sinusoidally time varying external load or displacement. Any one impact is considered instantaneous and representable by the somewhat macroscopic coefficient of restitution. The theory is compared with previous but sparse theoretical results and more comprehensively with new experimental data. Agreement is found to be quite good. The presently employed procedure for designing an impact damper seems reasonable for constant speed mechanisms operating at or just above their fundamental natural frequency. Similarities between various vibroimpact mechanisms is demonstrated for specific conditions. This procedure offers a useful means of generalising the applicability of several vibroimpact idealisations often used in practice.

ACKNOWLEDGEMENTS

The author wishes to express his grateful appreciation for the invaluable guidance and help given by his academic advisor, Dr. N. Popplewell.

The author wishes to acknowledge gratefully Dr. K. R. McLachlan, Dr. S.F. Masri, Dr. A.B. Thornton-Trump and Dr. A. Shah for their advice and suggestions. Many thanks to Mr. Y. Muzyka, Mr. J.E. Sewell and Mrs. Paulette Giardino for typing this manuscript.

Finally, the author wishes to thank the Government of India for the financial support in the form of a scholarship for study abroad.

TABLE OF CONTENTS

LIST OF FIGURES

Figure | Page

LIST OF TABLES

NOMENCLATURE

A	maximum amplitude of absolute displacement of primary system alone due to prescribed sinusoidal displacement or force
C	viscous damping constant of primary system
d	clearance between primary and secondary system when both stationary
F_o	maximum amplitude of external sinusoidal force
I	ratio of duration between three consecutive impacts for stable two impacts/cycle
K	linear spring stiffness of primary system in case of an impact-damper
k	odd number of cycles of prescribed sinusoidal displacement or force
M	mass of primary system
m	mass of secondary system
N	integer number of impacts between m and M during a periodic unit of time T_o
$[P]$	a matrix product $[P_N]\,[P_{N-1}] \ldots [P_1]$ or $[P_{N+}]\,[P_{(N-1)+}] \ldots [P_{1+}]$ in case of Impact-Pair and impact damper respectively
$[P_i]$	a square matrix that relates perturbation vector at time $t_{(i+1)}$ to corresponding perturbations at time t_i in case of an Impact-pair
$[P_{i+}]$	a square matrix that relates perturbation vector immediately after the (i+1)th impact to corresponding perturbations immediately after the ith impact in case of an impact damper
R_i	a coefficient of restitution at the ith impact
R_1, R_2	constant coefficients of restitution due to collisions on side 1 and 2 respectively
R	constant coefficient of restitution when $R_1 = R_2 = R$
r	frequency ratio, Ω/ω
R_o	periodicity of motion
t	time elapsed after the first impact

t_i	time elapsed between the first impact and the ith impact with t_i zero
V_{ia}	absolute velocity of secondary mass immediately after the ith impact
V_{ib}	absolute velocity of secondary mass just before the ith impact
X	absolute displacement of primary mass at any instant
X_i	absolute displacement of primary mass at the ith impact
X_{ia} or X_{1+}	absolute displacement of primary mass just after the ith impact
X_{ib} or X_{i-}	absolute displacement of primary mass just before the ith impact
X_{max}	maximum displacement of primary system with impacts
ΔX_{i+}	small perturbation in value of X_i immediately after the ith impact
$\dot{X}_{ia}$ or $\dot{X}_{i+}$	absolute velocity of primary mass just after the ith impact
$\dot{X}_{ib}$ or $\dot{X}_{i-}$	absolute velocity of primary mass just before the ith impact
$\Delta\dot{X}_{i+}$	small perturbation in value of $\dot{X}_{i+}$
Y	relative displacement of secondary mass with respect to primary mass at any instant
Y_i	relative displacement of secondary mass at the ith impact
$\dot{Y}$	relative velocity of secondary mass with respect to primary mass
Z	absolute displacement of secondary mass at any instant
Z_i	absolute displacement of secondary mass at the ith impact
ΔZ_i	small perturbation in value of Z_i
$\dot{Z}$	absolute velocity of secondary mass
$\Delta\dot{Z}_i$	small perturbation in absolute velocity of secondary, $\dot{Z}_i$, at time t_i

$\Delta\dot{Z}_{i+}$ small perturbation in absolute velocity of secondary mass just after the ith impact

α_i product, Ωt_i

α_o product, ΩT_o

ξ fraction of critical viscous damping

μ mass ratio, m/M

ω undamped natural circular frequency of primary system alone

Ω circular frequency of excitation

τ phase angle (initially unknown) of presumed first impact with respect to prescribed displacement or force

σ the ratio, 2A/d

$\frac{d}{dt}$ or $\cdot$ derivative with respect to time, t superscript

SYMBOLS USED GENERALLY IN FIGURES FOR VARIOUS STABILITY ZONES:

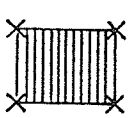

two equispaced impacts/three cycles of the external force or prescribed displacement+

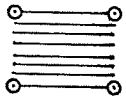

two equispaced impacts/cycle

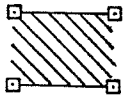

two unequispaced impacts/cycle

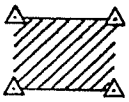

three impacts/cycle

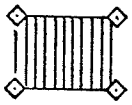

four impacts/cycle

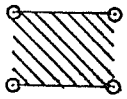

five impacts/cycle

Symbols employed solely when the coefficients of restitution are unequal i.e. $R_1 \neq R_2$

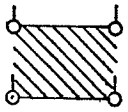

one impact on steel and many impacts on tape/cycle

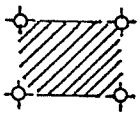

two impacts on steel and many impacts on tape/cycle

+It will be understood that the subsequent abbreviation of a cycle infers implicitly a cycle either of the external force or the prescribed displacement.

CHAPTER 1

INTRODUCTION

An impact arises normally from a collision of masses which produces finite (discontinuous) changes in their velocities over an extremely small duration. Impacts occur in moving machines and mechanisms largely as a result of clearances between components. Then high transient stress and noise levels may be produced which may result in accelerated wear, malfunctioning or even failure [9-29]. On the other hand, impact interactions may be employed advantageously to suppress or amplify the displacement of a usually resonant vibrating system. Vibroimpact devices have been used, for example, to attenuate the oscillations of radar antennae, machine tools, beams and printing machines [49-68] and to exaggerate vibrations associated with pile driving and the crushing or conveying of materials [46-48, 69-75].

The impact process is complex at the microscopic level and depends at least upon the approach velocities, contact geometries and duration, normally local plasticity effects and external loads [34-43]. One of the simplest and widely used macroscopic idealisations stems from the concept of the coefficient of restitution and the assumption of an instantaneous contact [1-4, 46-48]. The coefficient gives the ratio of the relative velocity just after and before a collision of two bodies as a constant. More sophisticated representations

of contact surfaces to include linear [10] or nonlinear compliance [19, 20] have been employed too. However, the solution of the ensuing equations of motion usually requires analog or digital computation which can be very time consuming [20, 26].

The traditional coefficient of restitution and instantaneous interaction approach will be adopted here to evaluate the general behaviour of two periodically colliding bodies. One of these bodies oscillates with either a prescribed sinusoidal displacement or in response to a given sinusoidal external force. Its displacement amplitude is sufficiently large to overcome the clearance between the two bodies and ensure regular contact with the second, otherwise free body. Equations of motion will be formulated conventionally by using the conservation of linear momentum and by applying periodicity instead of initial conditions [30-33, 52-55]. Transient motions therefore will be disregarded. More universal solutions than generated hitherto [1-4, 28-33, 49-59] will be determined by assuming more general numbers and sequences of impacts in some repetition period. The repetition period will be related, as customarily, to the corresponding, not necessarily integer, number of cycles performed during this time by either the prescribed displacement or external force. Solutions will be categorized for convenience by the number of impacts repeated every specified number of cycles of the prescribed displacement or force. Reference to the prescribed displacement or force will be omitted when self-evident although, in any case, the two situations will be shown interchangeable

under certain conditions.

A vibroimpact system undergoing periodic motion is classified conventionally as asymptotically stable or unstable. The system is asymptotically stable if it returns eventually to the original periodic motion after a small perturbation [1, 53]. Consequently, all characteristics like the amplitude and form of a stable periodic motion should not ultimately be altered by any small disturbance. Several difficulties relating to the practical implementation of this theoretical definition can be envisaged easily. An arbitrarily long if not virtually infinite time is permitted in principle to regain the original periodic motion. This is obviously impractical experimentally especially when, in any eventuality, almost impossible to control draughts and extraneous building vibrations happen spasmodically. Additionally, a real disturbance's fulfillment of the theoretical definition of "small" cannot be guaranteed presently from a priori knowledge of the vibro-impact system. A less apparent trouble relates to the suggestion of previous researchers [1, 59] that any one theoretical solution may not be necessarily unique. The disregarded transient component presumably may become important under these circumstances. If so, extraneous experimental disturbances when viewed as transitional "initial" conditions to the subsequent transient motions, take greater significance. These vexatious questions will be discussed later and expedient compromises will be sought in lieu of difficult to achieve, complete answers.

A completely different theoretical approach [3], used possibly with a non-smooth transformation [79, 80], employs time averaging. Mean values are assumed much greater than the variations allowed in the vibroimpact system's parameters over the averaging time. The ensuing formulation has the advantage of not being based upon an assumed and uncertainly applicable number and sequence of impacts. On the other hand an assurance of stability,which is important practically when predictable machinery performance is needed [1, 4, 70-74], is not given. This deficiency coupled with applications otherwise more restricted by the requirement of small variations detered further investigations with the averaging technique.

Two basic types of vibroimpact systems and their physical derivatives will be considered in detail. The first type called "Impact-Pairs" are those systems which are composed ideally of rigid bodies alone. The second category consists of vibroimpact systems which not only have masses but some resilience and maybe damping too. Systems in this latter group are often termed "impact dampers". These two types of vibroimpact systems have tended historically to be viewed in isolation. This will be shown unnecessary under certain specified circumstances.

CHAPTER 2

VIBROIMPACT OF AN IMPACT-PAIR

2.1 Introduction

Clearances occur commonly in kinematic pairs of mechanisms such as linkages, gear trains, pinned connections, joints and automatic control systems [9-33]. They may arise from manufacturing tolerances, wear, lubrication spaces, backlash or may be incorporated intentionally to accommodate thermal expansion. The operation of mechanisms with clearances may produce high but transient impact stresses which may lead to hammer hardening, scoring, pitting or wear of intermittently contacting surfaces and high noise levels [10, 11, 14, 17, 21-24, 44]. The life-reducing and noisy phenomenon of knock and piston slap in an internal combustion engine, for example, arises from clearances in bearings [13, 25]. Although many uncertainties exist, intuition suggests that wear and noise increase generally with the rate, number and severity of impacts. Therefore it is quite important from a practical viewpoint to relate these characteristics to the external loads and structural properties like the masses, geometry, clearance and coefficient of restitution.

Idealised models of typical mechanisms with clearances are illustrated in Figure 2.1. The models represent an oscillating four bar linkage, a gear assembly and a pin connection with a clearance.

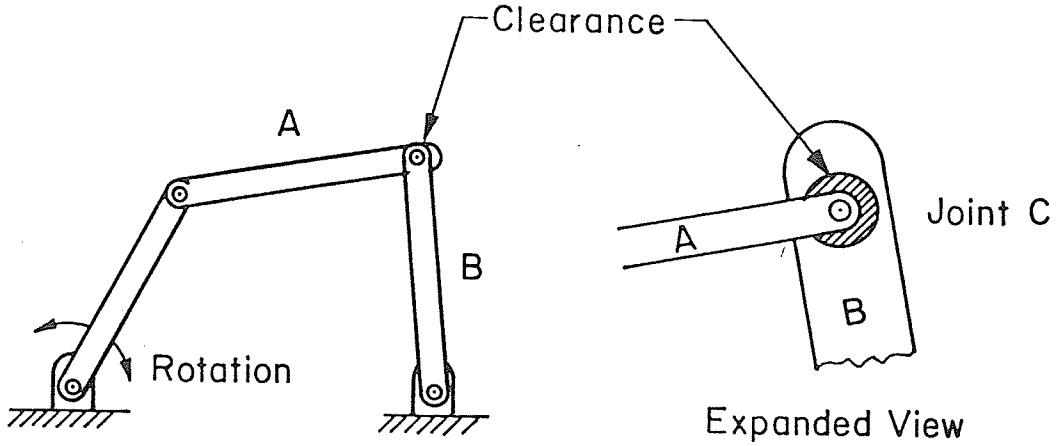

(a) Four bar mechanism with clearance.

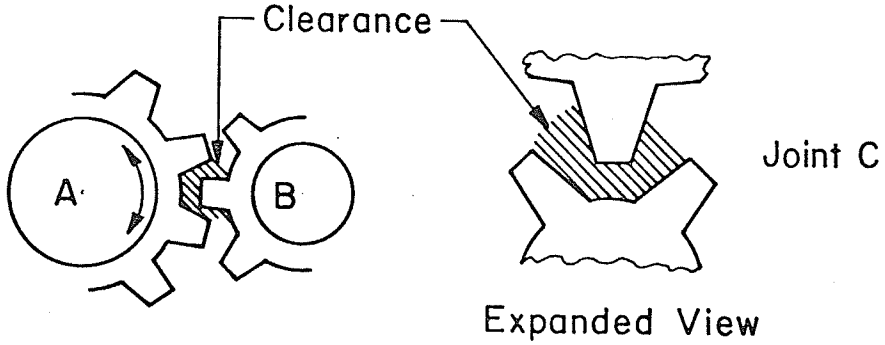

(b) Gear assembly with backlash.

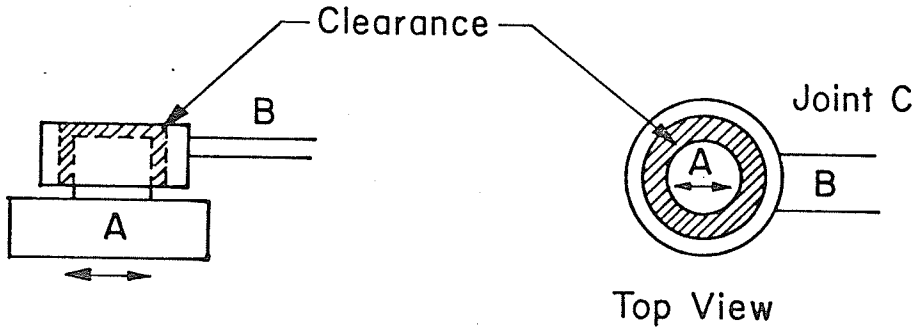

(c) Pin connection with clearance.

Figure 2.1. Mechanisms with clearances.

Motions of rigid members A and B are identical when the clearance is zero but can differ substantially otherwise. This latter situation can create practical problems like dynamic drift, high frequency oscillations or mismeasurement if member B with clearance at Joint C is connected to the measuring indicator of some instrument [1, 2, 3, 26-29]. A detailed study of the dynamics of joint C is required to understand and reduce these detrimental effects. In many cases such as slider-crank mechanisms, pin connections in linkages and fuel density meters, the displacement of member A varies sinusoidally in time whilst the motion of B is largely uniaxially. Linkages are normally considered rigid at low speeds of rotation. In such cases the significant features of joints C in the vibroimpact mechanisms are retained by the idealised model shown in Figure 2.2. In this figure mass m and slotted mass M, with a prescribed sinusoidal displacement, represent members B and A respectively. The model shown in Figure 2.2 is called traditionally an 'Impact Pair'.

While studying general mechanisms with clearances, both Kobrinskii [1, 2, 31, 32] and Stepanenko [33] observed that during k, k = 1, 3, 5.... periods of the prescribed displacement, successive impacts occur on alternate sides of the clearance. The prescribed displacement has been shown to be analogous in these cases to a prescribed external force on the Impact-Pair [2]. Kobrinskii et al [31] obtained an analytical solution by using the concept of the coefficient of restitution, conservation of linear momentum and applying periodicity instead of initial conditions. It was found

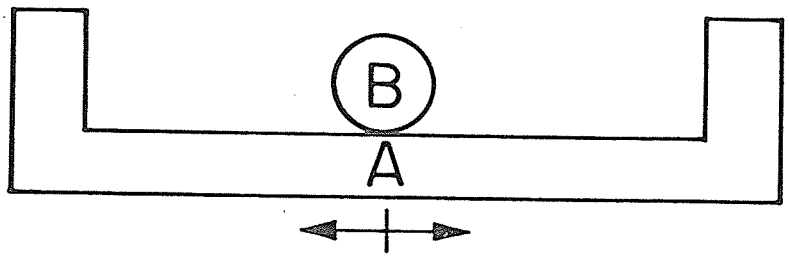

Figure 2.2. Simplest model of a mechanism with clearance.

that vibroimpact systems may have nonunique or multivalued solutions [1]. Kobrinskii et al [32] checked the asymptotic stability for small perturbations by using a concept analogous to the propagation of errors in difference equations. The problem of stability will be considered in detail later.

Dubowsky et al [10, 11] and Veluswami et al [19, 20] extended Kobrinskii's model by including linear and nonlinear surface compliances to explain multi-impact regions observed experimentally. The major advantage of this alternative approach to using the concept of a restitution coefficient is that the contact time, stresses, accelerations and surface deformations during an impact can be determined more directly. The direct analogue or digital solution of the resulting differential equations however can often be very time consuming [20, 26]. These direct techniques also have the extra disadvantage, shared with experimental observations, that a large number of cycles of a given periodic motion may have to be evaluated visually before a still often uncertain decision can be reached regarding stability. On the other hand, all theoretical approaches are restricted by the fact that the existence and uniqueness of a periodic solution has never been proved [1, 4, 53].

The contact between two colliding objects like a steel ball or bar on a steel plate or rigid base, typically lasts from 50 to 300 μ secs [10, 11, 19, 20, 35]. Such durations are negligible compared

with the usual characteristic times of dynamic engineering systems operating at speeds lower than 3000 rpm, say. Under such circumstances, the somewhat macroscopic concept of a restitution coefficient seems reasonable. Coefficients of restitution of impacting objects made from hard materials like metal are known to be fairly insensitive to their relative approach velocity [34-38]. Therefore the often employed first approximation of a constant coefficient of restitution for two given contact surfaces seems plausible. Consequently the more traditional approach will be taken here of simply describing a collision by some equivalent constant coefficient even though the impact process may be much more complicated [34, 40-43].

The only available analytical solution involves an Impact-Pair undergoing two symmetric impacts/odd number of cycles of the external force or prescribed displacement where all impacts have the same constant restitution coefficient [2, 31]. An extension to two unsymmetric impacts and unequal coefficients will be developed here. These theories however still do not cover more general periodic motions observed in practice to have more than two impacts in a periodic unit [1, 10, 11, 19, 20]. Consequently a computer orientated technique based upon the analytical approach of Kobrinskii [1] and Masri [59] will be presented to better accommodate such situations. The effect of commonly occurring fluctuations in the coefficients of restitution at different contact surfaces [1] will be investigated too. Results will be checked as far as possible with available data and additional

information to be determined from a specially constructed experimental simulation.

2.2 Theoretical Periodic Motions of an Impact-Pair

The general periodic motion of an Impact-Pair will be formulated when the absolute displacement of the primary mass, M, is prescribed. The amplitude A of this prescribed displacement is sufficient to ensure N impacts happening between M and the secondary mass, m, during the periodic unit of time T_o.

The idealised model of an Impact-Pair with clearance d between M and m is shown again for convenience in Figure 2.3. Although the proposed development is valid for varying coefficients of restitution R_i where $0 < R_i \leq 1$, i = 1, 2--N, each R_i will be restricted to a constant and known value R_1 or R_2. The R_1 and R_2 are associated with every collision at the sides labelled 1 and 2, respectively, in Figure 2.3. The start of time can be shifted arbitrarily to the instant of any one impact after the appropriate periodic motion has been established. This impact is numbered 1 in Figure 2.4(b) and can be seen from Figure 2.4(a) to have a phase τ relative to the prescribed displacement. The integer N impacts described by the Y_i in Figure 2.4(c) occur before the sequence is repeated exactly after time T_o. The N, T_o and the distribution in time of the impacts (i.e. t_1, t_2, --- and t_N in Figure 2.4(b) are assumed known.

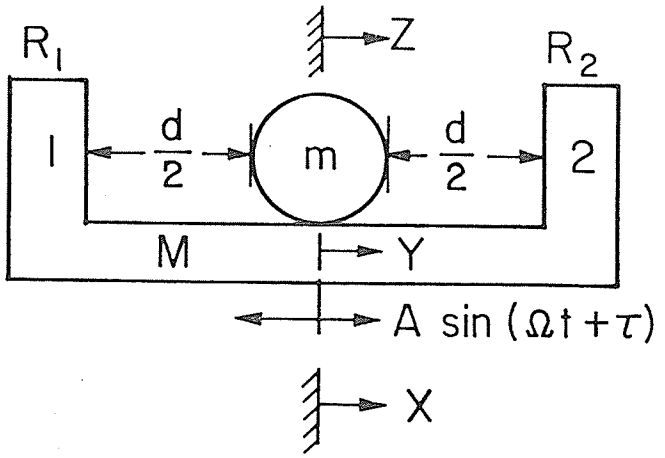

Figure 2.3. Dynamic model of an Impact-Pair.

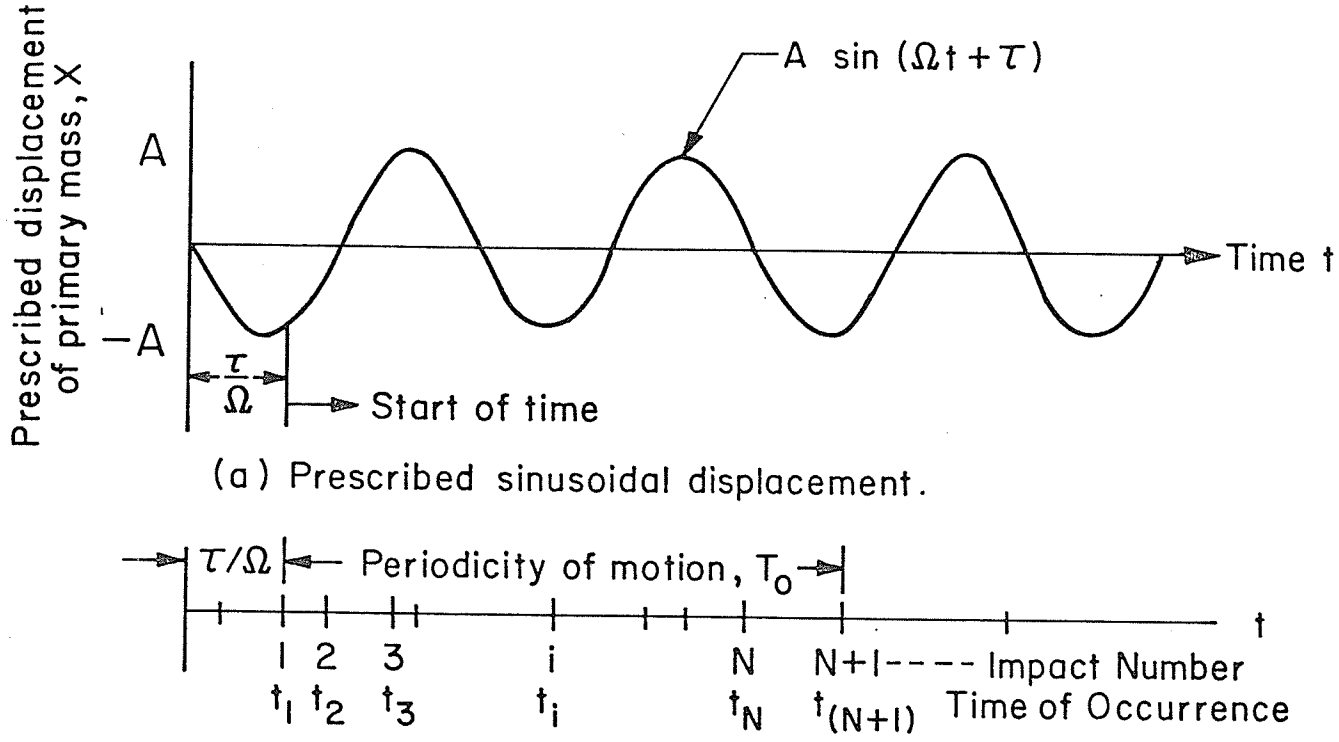

Figure 2.4. General motion of N impacts happening during period T_o.

The absolute displacement of M at time t is

$$X = A \sin (\Omega t + \tau) \tag{2.1}$$

and the time variation of X is implied.

If impacts between M and m occur at time t_i, i = 1, 2--N with t_1 zero, then the absolute displacement of M at these instants is given by

$$X|_{t=t_i} \equiv X_i = A \sin (\alpha_i + \tau), \; i = 1, 2,--N \tag{2.2}$$

where

$$\alpha_i = \Omega t_i, \; i = 1, 2,---N \quad . \tag{2.3}$$

Impacts occur only when the relative distance Y between m and M is $+\frac{d}{2}$ for a collision on the right side of M in Figure 2.3 and $-\frac{d}{2}$ for a collision on the left. Hence

$$Y_i = Z_i - X_i = \pm \frac{d}{2} \; , \; i = 1, 2,---N \tag{2.4}$$

at impacts because Figure 2.3 indicates that Z is the absolute displacement of m. All the relative displacements at impacts Y_i, i = 1, 2,--N, are presumed known. The velocity of m remains constant between impacts because no external forces then act upon it. Consequently the velocity, V_{ia}, of m between the i and (i + 1) impacts is identical to its velocity after the i th impact. Therefore V_{ia} is simply the ratio of the absolute

distance travelled by m between the i and (i + 1) impacts and the time elapsed between these impacts. Mathematically,

$$V_{ia} = \frac{Z_{(i+1)} - Z_i}{t_{(i+1)} - t_i} \quad , \; i = 1, 2, \text{--}N \quad . \tag{2.5}$$

Substituting equation (2.3) and (2.4) into equation (2.5) gives

$$V_{ia} = \frac{\Omega[X_{(i+1)} + Y_{(i+1)} - X_i - Y_i]}{\alpha_{(i+1)} - \alpha_i} \quad , \; i = 1, 2, \text{--}N \quad . \tag{2.6}$$

Similarly the velocity, V_{ib}, of m between the (i - 1) and i th impacts equals

$$V_{ib} = \frac{\Omega[X_i + Y_i - X_{(i-1)} - Y_{(i-1)}]}{\alpha_i - \alpha_{(i-1)}} \quad , \; i = 1, 2, \text{--}N \quad . \tag{2.7}$$

The basic definition of the coefficients of restitution are [1]

$$R_i = - \frac{\dot{X}_{ia} - V_{ia}}{\dot{X}_{ib} - V_{ib}} \quad , \; i = 1, 2, \text{--}N \tag{2.8}$$

where $\dot{X}_{ib}$ and $\dot{X}_{ia}$ are the velocities of the primary mass immediately before and after the typical i th impact, respectively. However the primary mass' displacement and its time derivatives are prescribed to be continuous regardless of the collisions. Therefore

$$\dot{X}_{ib} = \dot{X}_{ia} = \frac{d}{dt}\left[A \sin (\Omega t + \tau)\right]\Big|_{t=t_i}$$

or

$$\dot{X}_{ib} = \dot{X}_{ia} = A\,\Omega\cos(\alpha_i + \tau),\ i = 1, 2, \text{--}N \quad . \tag{2.9}$$

Equation (2.9) can be combined with equation (2.8) to produce

$$R_i = -\frac{A\,\Omega\cos(\alpha_i + \tau) - V_{ia}}{A\,\Omega\cos(\alpha_i + \tau) - V_{ib}},\ i = 1, 2, \text{--}N \tag{2.10}$$

or, alternatively,

$$V_{ia} = -R_i V_{ib} + (1 + R_i)\,A\,\Omega\cos(\alpha_i + \tau),\ i = 1, 2, \text{--}N \quad . \tag{2.11}$$

By employing equation (2.6) and (2.7), equation (2.11) can be rewritten as

$$\frac{\Omega[X_{(i+1)} + Y_{(i+1)} - X_i - Y_i]}{\alpha_{(i+1)} - \alpha_i} = (1 + R_i)\,A\,\Omega\cos(\alpha_i + \tau)$$

$$- R_i \frac{\Omega\,[X_i + Y_i - X_{(i-1)} - Y_{(i-1)}]}{\alpha_i - \alpha_{(i-1)}},\ i = 1, 2, \text{--}N \quad . \tag{2.12}$$

Now the sequence of N impacts is repeated every ΩT_o or, from equation (2.3), α_o so that

$$\alpha_{i+N} = \alpha_i + \alpha_o \;,\; X_{(i+N)} = X_i,\; R_{(i+N)} = R_i$$

$$Y_{i+N} = Y_i,\; X_{(i+N-1)} = X_{(i-1)},\; \alpha_{(i+N-1)} = \alpha_{(i-1)} + \alpha_o. \quad (2.13)$$

Consequently by using $\alpha_{(i+N-1)}$, $\alpha_{(i+N)}$ and $X_{(i+N-1)}$ instead of $\alpha_{(i-1)}$, α_i and $X_{(i-1)}$, respectively, and expanding $A\sin(\alpha_i+\tau)$ and $A\cos(\alpha_i+\tau)$, equation (2.3) and (2.11) can be manipulated into

$$X_i - \sin\alpha_i \cdot A\cos\tau - \cos\alpha_i \cdot A\sin\tau = 0,\; i = 1, 2, --N \quad (2.14)$$

and

$$\frac{X_{(i+1)}}{\alpha_{(i+1)} - \alpha_i} + \frac{R_i}{X_i\left[\frac{1}{\alpha_{(i+N)} - \alpha_{(i+N-1)}} - \frac{1}{\alpha_{(i+1)} - \alpha_i}\right]}$$

$$- X_{(i+N-1)}\left[\frac{R_i}{\alpha_{(i+N)} - \alpha_{(i+N-1)}}\right] - (1+R_i)\cos\alpha_i \cdot A\cos\tau = -\left[\frac{Y_{(i+1)} - Y_{(i)}}{\alpha_{(i+1)} - \alpha_i}\right]$$

$$+ (1+R_i)\sin\alpha_i \cdot A\sin\tau \qquad -R_i\left[\frac{Y_{(i+N)} - Y_{(i+N-1)}}{\alpha_{(i+N)} - \alpha_{(i+N-1)}}\right],$$

$$i = 1, 2, --N \;. \quad (2.15)$$

These last two, most general relationships form 2N linear simultaneous equations when all the i are substituted. There are (N + 2) unknowns if the periodicity and timing between impacts is assumed and all passive components like m, M and d are given. The unknowns are the N values of X_i, the amplitude of the prescribed displacement, A, and the phase

angle, τ. An exact, closed form solution is possible only when the number of equations and unknowns coincide (i.e. $2N = N + 2$ or $N = 2$). Otherwise a numerical technique like the least square fit method [7] has to be employed.

Further advancement of an analytical nature requires at least an assumption of the motion's periodicity, T_o. The standard assumption will be made that two impacts happen every k, k = 1, 3, 5,---, cycles of the prescribed displacement of the primary mass, M. Successive impacts occur on alternate sides of the slot within this mass. For convenience suppose that the first impact is on the left-hand surface of M labelled 1 in Figure 2.3. Then the subsequent impact is on the right-hand surface, 2. The corresponding constant coefficients of restitution are R_1 and R_2, respectively, where R_1 and R_2 may or may not be equal.

The periodicity condition leads immediately to

$$\alpha_o = \Omega T_o = 2\pi k \quad . \tag{2.16}$$

Equation (2.3) takes the particular form

$$\alpha_1 = 0 \text{ and } \alpha_2 = \alpha_2 \text{ and } 0 < \alpha_2 < 2\pi k \quad . \tag{2.17}$$

On the other hand, equation (2.4) still gives

$$Y_1 = -\frac{d}{2} \text{ and } Y_2 = \frac{d}{2} \quad . \tag{2.18}$$

Then equation (2.14) and (2.15) can be shown, by using the last three equations, to take the special form

$$\left.\begin{aligned} X_1 - A\sin\tau &= 0 \\ X_2 - \sin\alpha_2 \cdot A\cos\tau - \cos\alpha_2 \cdot A\sin\tau &= 0 \end{aligned}\right\} \tag{2.19}$$

and

$$\left.\begin{aligned} L_1 \cdot X_1 - L_1 \cdot X_2 - (1 + R_1)\, A\cos\tau &= dL_1 \\ L_2 \cdot X_1 - L_2 \cdot X_2 - (1 + R_2)\cos\alpha_2 \cdot A\cos\tau & \\ + (1 + R_2)\sin\alpha_2 \cdot A\sin\tau &= dL_2 \end{aligned}\right\} \quad . \tag{2.20}$$

The two coefficients L_1 and L_2 depend upon α_2 and can be expressed as

$$L_1 = \left[\frac{R_1}{2\pi k - \alpha_2} - \frac{1}{\alpha_2}\right] \text{ and } L_2 = \left[\frac{1}{2\pi k - \alpha_2} - \frac{R_2}{\alpha_2}\right] . \tag{2.21}$$

Variables X_1 and X_2 can be eliminated from the two equations numbered (2.20) by using equations (2.19). This procedure produces the two equations

$$[1 - \cos\alpha_2]\, L_1 \cdot A\sin\tau - [L_1 \sin\alpha_2 + (1 + R_1)] \cdot A\cos\tau = dL_1 \tag{2.22a}$$

and

$$\left.\begin{aligned} &[L_2(1 - \cos\alpha_2) + (1 + R_2)\sin\tau_2]\cdot A\sin\tau \\ &+ [-L_2\sin\alpha_2 - (1 + R_2)\cos\alpha_2]\cdot A\cos\tau \end{aligned} = dL_2 \right\} \quad (2.22b)$$

When the impact timing sequence parameter α_2 is known in addition to T_o, L_1 and L_2 can be determined from equation (2.21) given k so that the only remaining unknowns are A and τ.

The solutions of equation (2.22a) and (2.22b) fall into two categories depending whether these equations are independent or essentially identical. This last situation arises when α_2 equals one-half the periodicity parameter α_o given by equation (2.16) and R_1 is the same as R_2. The physical interpretation of the requirement for α_2 is that the durations between any three consecutive impacts are equal. Then the impacts will be termed "equispaced". (Conversely analogous unequal durations will be called "unequispaced". If no adjective is used in conjunction with impacts/cycle then unequispaced is implied.) Therefore under the special conditions

$$\alpha_2 = \pi k \quad \text{and} \quad R_1 = R_2 = R \quad (2.23)$$

both equation (2.22a) and (2.22b) take the simpler form

$$\sin\tau + \frac{\pi k}{2}\left(\frac{1 + R}{1 - R}\right)\cos\tau = \frac{d}{2A} \quad . \quad (2.24)$$

Then it is more convenient to assume A and compute τ by manipulating the last equation into

$$\sin\tau = \frac{\frac{d}{2A} \pm \frac{\pi k}{2}\left(\frac{1+R}{1-R}\right)\left[\left(\frac{1+R}{1-R}\right)^2 \frac{\pi^2 k^2}{4} + 1 - \left(\frac{d}{2A}\right)^2\right]^{\frac{1}{2}}}{\left(\frac{1+R}{1-R}\right)^2 \frac{\pi^2 k^2}{4} + 1} \quad . \tag{2.25}$$

Equation (2.24) and (2.25) coincide with the equations given in reference 2 specifically for two equispaced impacts/k cycles. It is shown in Appendix A1 that a necessary condition for two equispaced impacts/k cycles (k = 1, 3, 5,---) to occur is for R_1 to equal R_2.

The second more generally applicable category exists if

$$\alpha_2 \neq \pi k \quad . \tag{2.26}$$

Then equation (2.22a) and (2.22b) are two independent equations in the two unknowns A and τ. It can be shown straightforwardly that

$$\left.\begin{aligned} A &= [L_3^2 + L_4^2]^{\frac{1}{2}} \\ \text{with} \qquad & \\ \sin\tau &= \frac{L_3}{A} \quad \text{and} \quad \cos\tau = \frac{L_4}{A} \quad . \end{aligned}\right\} \tag{2.27}$$

Coefficients L_3 and L_4 can be expressed as

$$L_3 = \frac{+[L_1 \sin\alpha_2 + (1 + R_1)]\, dL_2 + dL_1\, [-L_2 \sin\alpha_2 - (1 + R_2)\cos\alpha_2]}{S}$$

and

$$L_4 = \frac{[1 - \cos\alpha_2]\, dL_1 L_2 - [L_2\,(1 - \cos\alpha_2) + (1 + R_2)\sin\alpha_2]\, dL_1}{S} \qquad (2.28)$$

where

$$S = [1 - \cos\alpha_2]\,[-L_2 \sin\alpha_2 - (1 + R_2)\cos\alpha_2]\, L_1 + [L_1 \sin\alpha_2 + (1 + R_1)]\,[L_2\,(1 - \cos\alpha_2) + (1 + R_2)\sin\alpha_2] \quad . \qquad (2.29)$$

These coefficients can be enumerated given α_2 distinct from πk ($k = 1, 3, 5, \text{---}$) and A and then τ can be determined from equation (2.27).

Analytical solutions have been given in principle for general periodic motions having two impacts/k cycles of the prescribed displacement of the primary mass. The k can be any odd integer although it is restricted normally in practice to the two lowest. Impacts may be equispaced or unequispaced in time. A necessary condition for equispaced impacts has been demonstrated for the first time to be equal coefficients of restitution, R_1 and R_2. Then the general analytical solution degenerates into an existing, more specific one, equation (2.25). The closed form solution (2.27) developed for two unequispaced impacts/k cycles however is novel.

Only computationally orientated methods are feasible when the number of impacts is greater than two in any periodic unit. This situation arises because the number of equations exceeds the number of unknowns in relationship (2.14) and (2.15) even after the periodicity and timing of impacts is assumed. Then a numerical solution was computed based upon the least square subroutine LLSQF of the IMSL Library [45]. Values of the unknowns were finalised when the square of the difference, ε^2, between the left- and right-hand sides of relation (2.14) and (2.15) was truly minimised and ε was less than 3% of these values. Truncation errors were reduced by using double precision arithmetic throughout. Numerical calculations were performed on an AMDAHL V7 digital computer.

2.2.1 Stability of Periodic Motion

A vibroimpact system is asymptotically stable if it returns eventually to the original periodic motion after a small perturbation [1, 53]. Substantial information of a quantitative nature is sadly lacking regarding the return time and the definition of small. In this work the first variable will be fixed somewhat arbitrarily and the likely magnitude of the second will be investigated experimentally. Previous theoretical and experimental work [1,59] indicates that multivalued solutions occur for given parameters which may or may not all be stable. If both stable and unstable periodic motions appear simultaneously feasible, then a vibroimpact

system seems inclined to vibrate in the stable mode [1, 55, 65]. The need for continued stability is especially important in forging, material conveying and ploughing where predictable machinery performance is required regardless of parameter changes [1, 4, 70-74].

The asymptotic stability of any periodic motion can be determined by generalizing the results obtained independently by Kobrinskii [1, 2] and Masri [53]. Their approach is analogous to evaluating the propagation of small errors in difference equations. It basically relates the effect of perturbing the absolute displacement Z and velocity $\dot{Z}$ of the secondary mass at the time t_1 of the chosen first contact to corresponding changes, ΔZ_i and $\Delta \dot{Z}_i$, at later contact instants t_i, i = 2, 3,---. These relationships were developed in reference 1 and 59 by using the equations of motion, conservation of linear momentum and the definition of the coefficient of restitution. The initial perturbation was considered "small" if corresponding products are negligible compared to all terms typically involving ΔZ_i and $\Delta \dot{Z}_i$. Then it was shown that

$$\begin{Bmatrix} \Delta Z_{N+1} \\ \Delta \dot{Z}_{N+1} \end{Bmatrix} = [P] \begin{Bmatrix} \Delta Z_1 \\ \Delta \dot{Z}_1 \end{Bmatrix} \tag{2.30a}$$

where

$$[P] = [P_N]\,[P_{N-1}] \text{ --- } [P_1] \tag{2.30b}$$

and the representative 2 x 2 component matrix $[P_i]$ relates the changes at impact time t_{i+1} to those at t_i. Elements P_i (p, q), p and q equal one or two, of $[P_i]$ are

$$\left.\begin{aligned} P_i(1,1) &= -R_{(i+1)} \\ P_i(1,2) &= -R_{(i+1)}\,[\alpha_{(i+1)} - \alpha_i]/\Omega \\ P_i(2,1) &= [1 + R_{(i+1)}] \cdot H \cdot \Omega^2/G \\ \text{and} \\ P_i(2,2) &= -R_{(i+1)} + [1 + R_{(i+1)}] \cdot H \cdot \Omega \cdot [\alpha_{(i+1)} - \alpha_i]/G \end{aligned}\right\} \qquad (2.31a)$$

where

$$\left.\begin{aligned} H &= A \sin [\alpha_{(i+1)} + \tau] \\ \text{and} \\ G &= \frac{\Omega[X_{(i+1)} + Y_{(i+1)} - X_i - Y_i]}{[\alpha_{(i+1)} - \alpha_i]} - A\Omega\cos [\alpha_{(i+1)} + \tau] \end{aligned}\right\} \qquad (2.31b)$$

when the nomenclature of the previous section is used. Terms like R_i in equation (2.31a) were constant previously but the coefficient of restitution can be variable now. The periodic motion is asymptotically stable if and only if all the modulii of the eigenvalues of matrix [P] given by equation (2.30b) are strictly less than unity

[53, 59]. Double precision arithmetic was used in conjunction with the readily available subroutine EIGRF of the IMSL library to compute the eigenvalues of [P] by employing Hessenberg's method [45, 8]. Computer programmes are listed in reference 82.

The theory outlined in this and the previous section will be used to review various stable periodic motions of particular examples of Impact-Pairs considered less comprehensively elsewhere. Results will be given in the form of various stability zones each shown as a hatched area bounded by two curves with a common symbol. Any one curve will be called a stability boundary and the modulii of the maximum eigenvalues are unity there. All points within two associated boundaries are stable and have an identical form of periodic motion. This form will be denoted by the number of impacts happening in a usually different number of cycles of the prescribed displacement.

2.2.2 Theoretical Results

Non-uniform coefficients of restitution can be expected in practice because small differences occur even in carefully conducted laboratory experiments [1]. The likely practical consequences of such differences will be assessed by using equal ($R_1 = R_2 = R$) and unequal ($R_1 \neq R_2$) coefficients of restitution in the previously detailed theory.

2.2.2.1 Identical Coefficients of Restitution

The governing equations of motion are equations (2.14) and (2.15) when the coefficients of restitution both equal R. Terms like $(Y_{(i+1)} - Y_i)$ in the latter equation can be seen from equation (2.4) to be a multiple of d. A simple division by d would non-dimensionalise both equations leaving the motion to be described in terms of A/d (or, more conventionally $\sigma/2$) and R for a given α_i and τ or pattern of impacts. The equations and, hence, their solutions are independent of both masses m and M.

Theoretical, asymptotically stable zones are presented in Figure 2.5 for two equispaced and two unequispaced impacts per one and three cycles. The stable three, four and five impacts/cycle zones are given too. Zones of two unequispaced and three impacts/cycle can be seen to overlap for all R whilst most zones overlap another one at values of R below about 0.2. This indicates that any one theoretical solution may not be unique. Then the appropriate solution under such circumstances probably depends upon the particulars of the initial conditions. A similar observation has been made previously in theoretical studies of loaded Impact-Pairs [1], vibrohammers and vibrotampers [4, 46]. Clarification of the phenomenon will be sought experimentally.

The widely studied two equispaced impacts/cycle stability zone occurs predominantly below a unity σ. Its height grows slightly with increasing R. Other zones however do not necessarily have the same

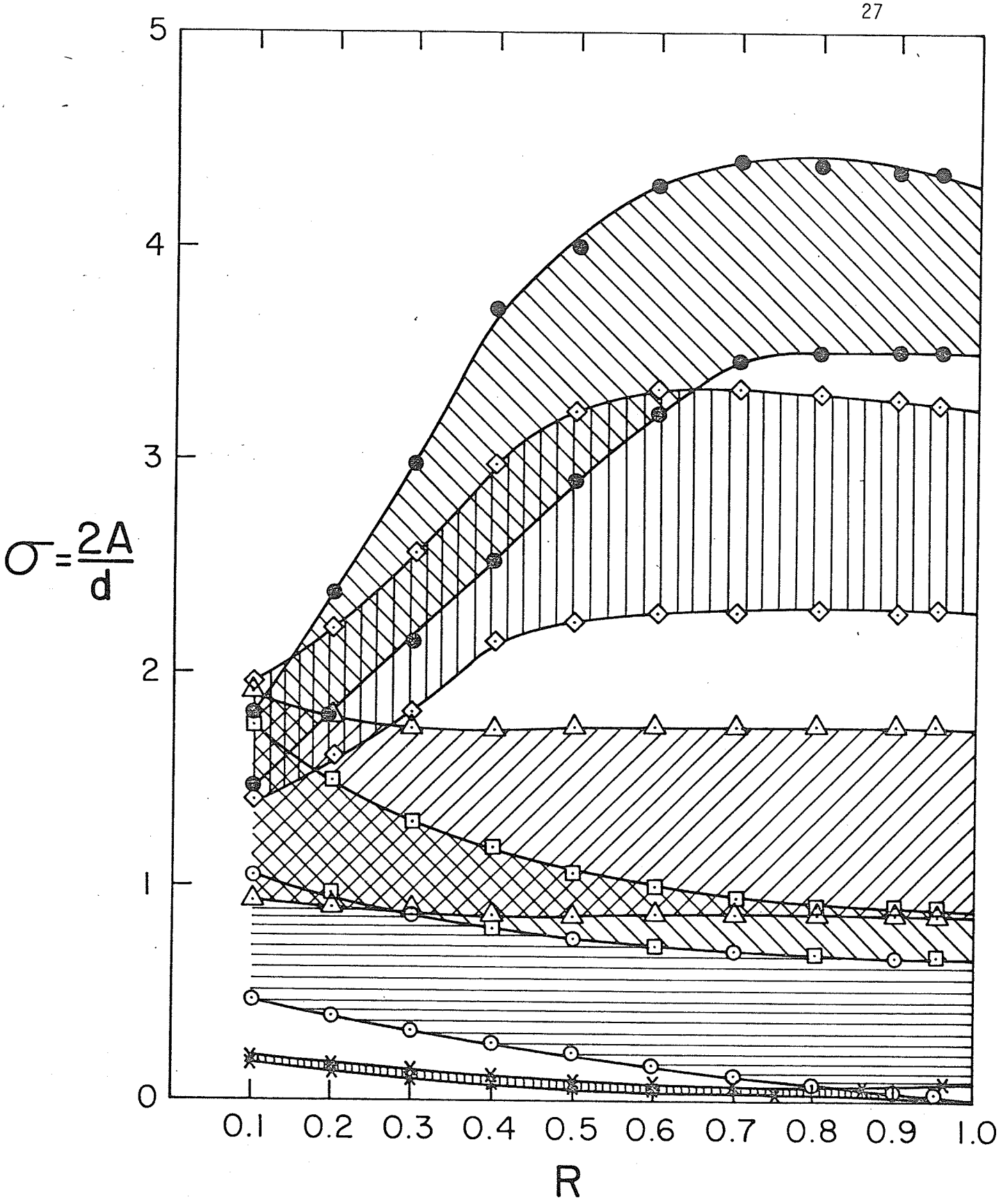

Figure 2.5. Theoretical stability zones of an Impact-Pair with identical coefficients of restitution, R.

tendency. The height of the two unequispaced impact/cycle zone, for example, decreases with larger R. Therefore it cannot be assumed automatically that a characteristic of the two equispaced impacts/cycle zone adequately reflects the corresponding property of another stability zone. In addition, the heights of the three and higher numbered impacts/cycle zones are larger than both the two impacts/cycle zones in the commonly occurring range of $0.4 < R < 1.0$. Consequently there appears to be a greater chance of higher number impact sequences for σ or ratios of A to d greater than one.

The variation of the maximum absolute eigenvalue of matrix P in equation (2.30b) is shown for completeness within the two unequispaced impacts/cycle stability zone in Figure 2.6. Various σ and representative values of R are employed. The maximum is unity on the two stability boundaries and diminishes invariably with greater penetration of the zone's interior. The minimum attained for the maximum absolute eigenvalue is presented in Figure 2.7 for more comprehensive values of R. It appears to vary as R^2. However the range of σ over which the minimum holds seems, from Figure 2.6, to decrease with R.

Figure 2.8 shows the ratio, I, of the durations between three consecutive impacts for stable, two unequispaced and also two equispaced impacts/cycle motion. Three intermediate values of R are employed which leads to σ being between 0 and 1.5. The vertical line $I = 1$ naturally corresponds to equal durations or equispaced impacts

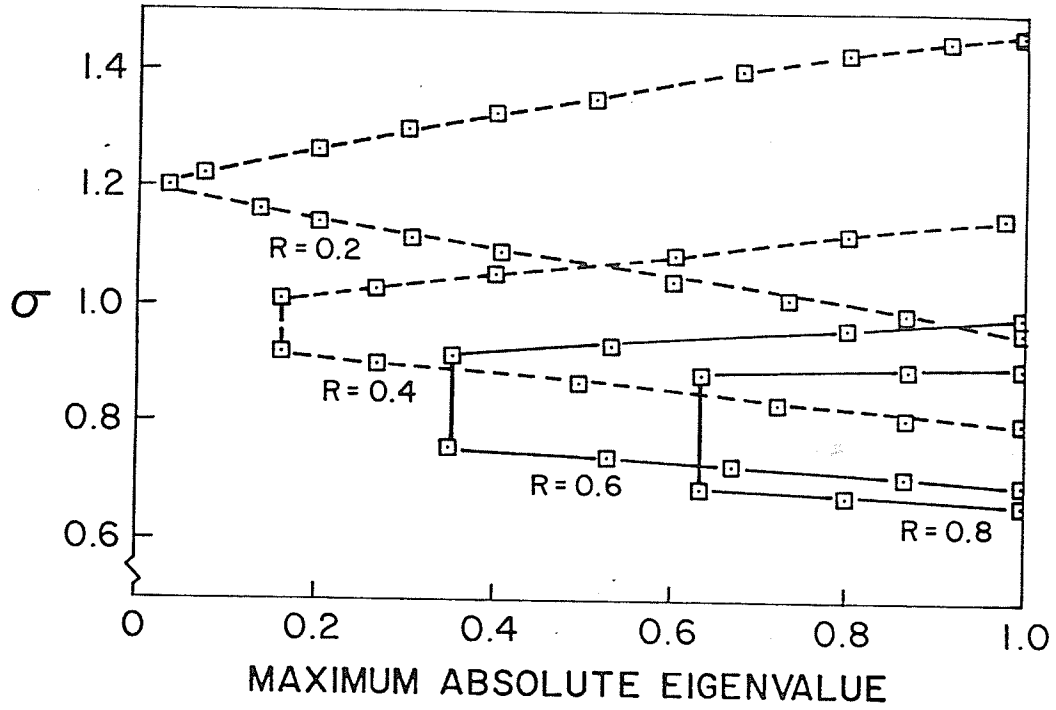

Figure 2.6. Maximum absolute eigenvalue for two unequispaced impacts/cycle. Coefficients of restitution are identical and given by the assigned R.

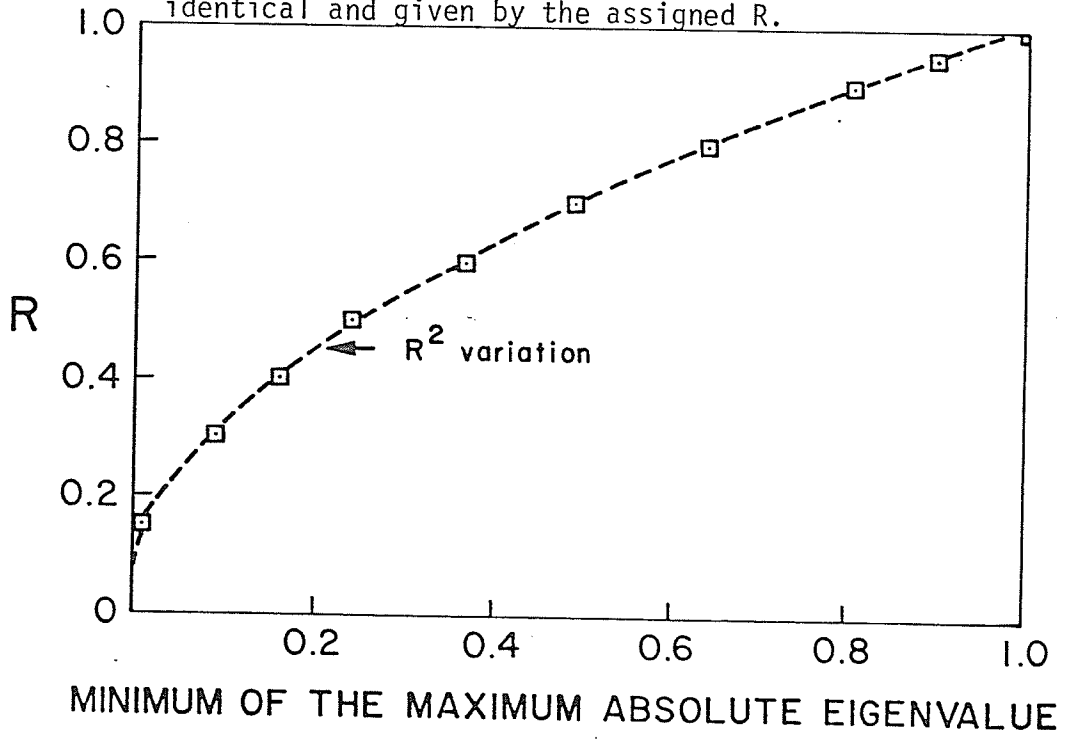

Figure 2.7. Variation with R of the minimum of the maximum absolute eigenvalue.

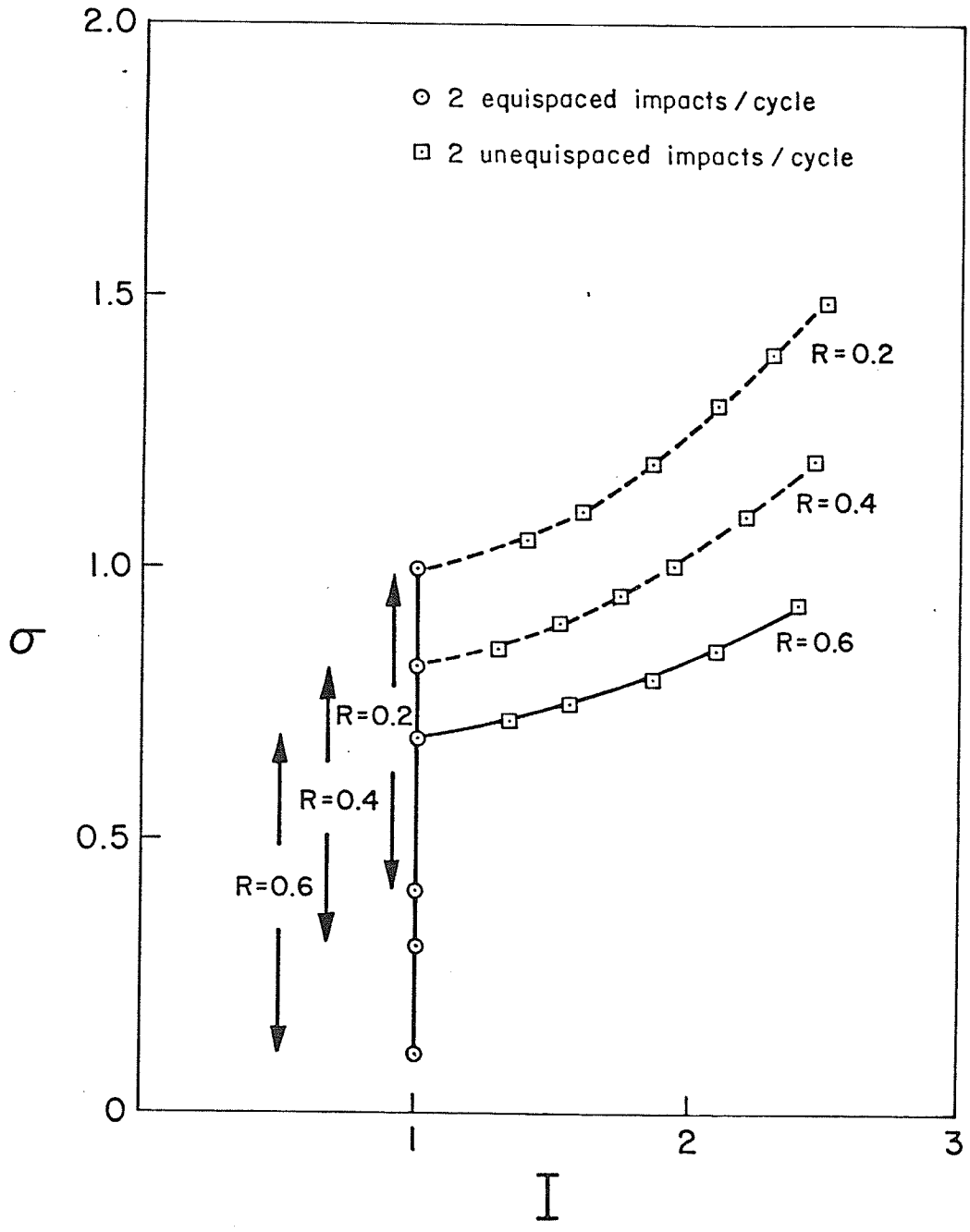

Figure 2.8. Ratio of durations between three consecutive impacts, I, for stable two impacts/cycle. Coefficients of restitution are identical and given by R.

regardless of R. However the value of I increases with σ for the unequispaced impacts ($I \neq 1$) in a similar fashion for all three remaining curves.

Repeated collisions of an Impact-Pair will produce wear and, hence, a changing clearance. Figure 2.8 may be used to find the instantaneous clearance without dismantling the pair if:

1) the amplitude A of the prescribed displacement of the primary mass is controllable and measurable; and
2) the initially equal coefficients of restitution are not altered by the repeated collisions.

The first requirement may be reasonable when the cyclical impact motion can be sustained noticeably for slow run-ups or run-downs of motor driven systems. The second assumption is still questionable and will be commented upon later.

Amplitude A has to be controlled such that I remains constant throughout and, for convenience, the easily observed, two unequispaced impacts/cycle motion is always obtained. Then the previous assumptions ensure that σ is invariable, i.e.

$$\sigma_{new} = \sigma_{old} \tag{2.32}$$

where the subscripts are self-explanatory. The σ has been defined as 2A/d so that

$$d_{new} = \frac{A_{new}}{A_{old}} \cdot d_{old} \qquad (2.33)$$

from equation (2.32) after cross-multiplication. Both subscripted values of A can be measured so that the new clearance, d_{new}, can be calculated by using equation (2.33). The initial clearance, d_{old}, is supplied normally by the machinery manufacturer.

2.2.2.2 Different Coefficients of Restitution

Corresponding figures to Figure 2.5 and 2.8 obtained for normally different rather than equal coefficients of restitution R_1 and R_2 are shown as Figure 2.9 and 2.10, respectively. The R_1 is a constant 0.75 in the latter figures because this value is fairly representative of metals like steel. Theoretical stability zones are limited in Figure 2.9 to two unequispaced and three impacts/cycle for greater clarity. Two zones, one labelled ABCDE and the other FGHDE, with region CDEF in common are shown for the case of three impacts/cycle. The three impacts of stability zone ABCDE are composed of two on side 1 and one impact on side 2 of the primary mass. These same numbers are associated with the reverse sides for zone FGHDE. All the stability boundaries were determined for R_2 incremented by 0.05 in the range from 0.05 to 1.00. A few only of the ensuing results are shown explicitly in Figure 2.9. Also only a selected representative sample of these R_2 values was utilised in the computation of Figure 2.10. The vertical line I = 1 in this last figure indicates again that impacts are equispaced. Figure 2.10

therefore substantiates that equispaced impacts require at least R_1 and R_2 equal. Similarly the stability zone for two equispaced impacts/cycle can be shown only as the lowest dashed line at R_2 equal 0.75 (R_1 a constant 0.75) in Figure 2.9. The other dashed lines at R_2 equal 0.75 indicate the range of the remaining two pertinent stability zones taken from Figure 2.5.

Figure 2.9 indicates that a given stability zone is neither uniform in height nor horizontal with R_1 constant and R_2 increasing. The space between the two extreme zones appears largest at the left of this figure where the difference between R_1 and R_2 is greatest. It naturally tends to decrease as R_2 approaches the value of R_1 and subsequently grows again when R_2 increases beyond R_1. Except for the common upper three impacts/cycle stability boundary, the slopes of all boundaries are fairly smooth and reasonably horizontal in the area near R_2 equal R_1. Despite the more rapidly changing upper boundary, the height of both three impacts/cycle zones does not vary dramatically in this area for fluctuations of around 5% in R_2. Similar R_2 fluctuations also do not seem to significantly affect ratio I in Figure 2.10. A variation of around 5% is typical of careful practice at fixed operating conditions [1, 35, 36, 55]. Such variations would appear not to particularly change the character of two of the lower impact numbered stability zones. Variations progressively greater than 5% however should be expected to become increasingly more important.

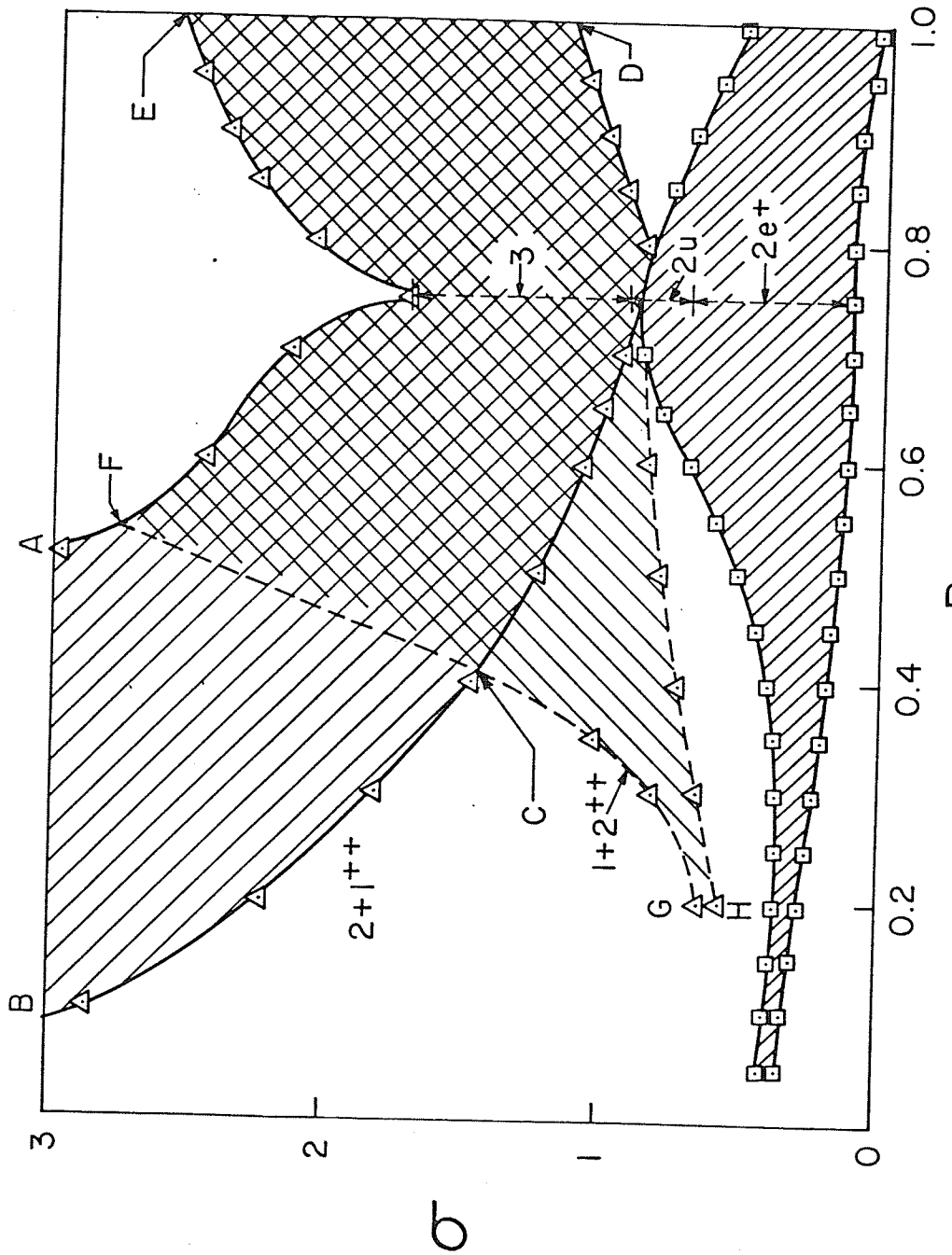

Figure 2.9. Theoretical stability zones for two and three impacts/cycle. The R_1 is a constant 0.75 and R_2 varies as shown.

+Range of two equispaced, two unequispaced and three impacts/cycle designated respectively 2e, 2u and 3 taken from Figure 2.5 when $R_1 = R_2 = 0.75$.

++$n_1 + n_2$ indicates n_1 and n_2 impacts, respectively, on side 1 and 2 of primary.

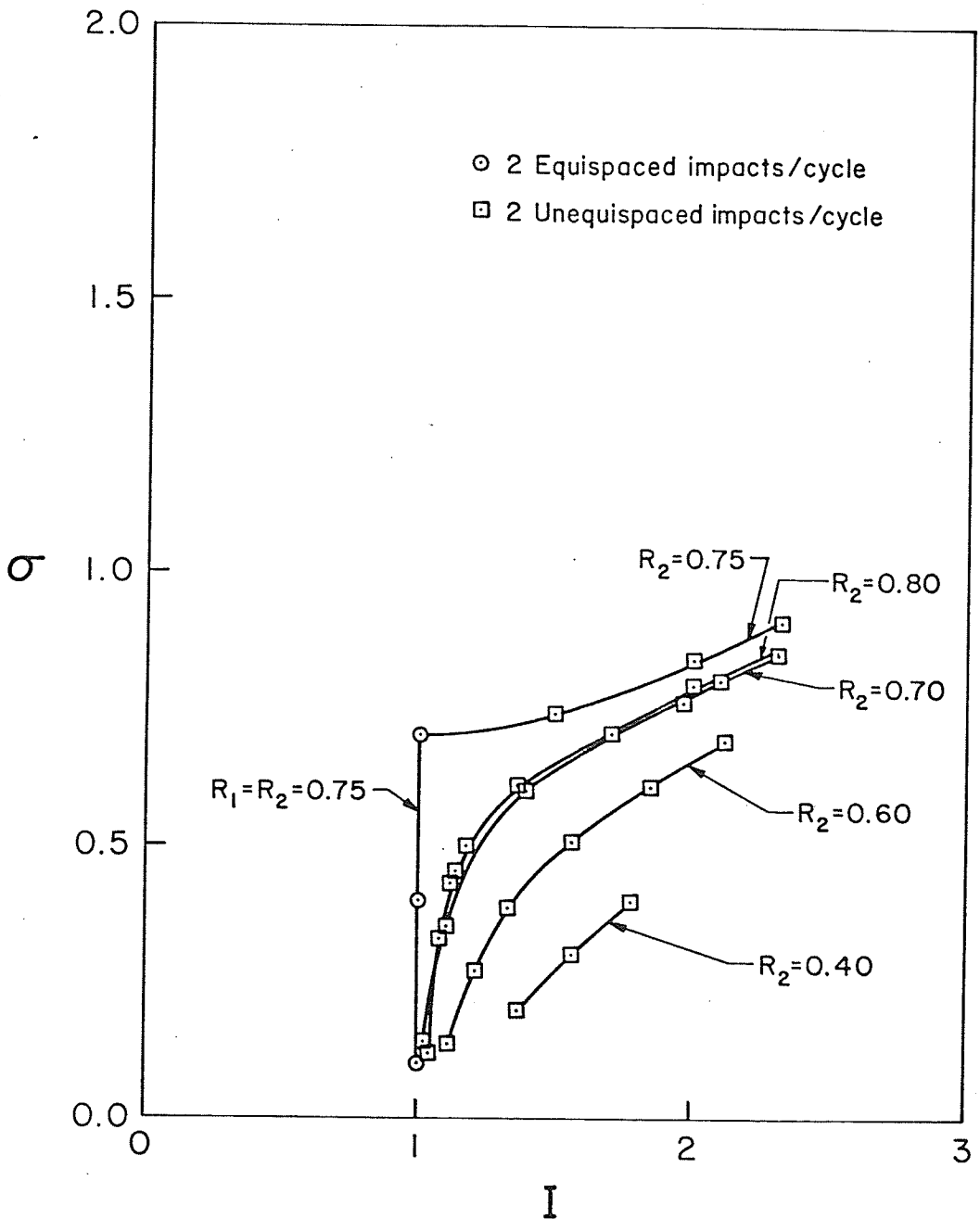

Figure 2.10. Ratio I of durations between three consecutive impacts for two impacts/cycle. The R_1 is a constant 0.75 and differs normally from the various R_2.

Theoretical predictions will be checked next by comparing them with experimental data. Details of the apparatus, built as far as practical to satisfy the theoretical assumptions, will be presented in the following section.

2.3 Details of the Experimental Apparatus and Instrumentation

The experimental apparatus is displayed in Figure 2.11 with important details of the masses shown in Figure 2.12. The primary mass was made of hardened die tool steel to minimise possible indentations from repeated impacts. A rectangular slot was machined inside the steel taking care that surfaces with which the secondary masses collide were flat, parallel and 0.7000 $\pm$ 0.0005 inch apart. This primary mass was fixed essentially rigidly to the electromagnetic shaker by using a light, non-magnetic aluminium adapter. Non-magnetic stainless steel and brass secondary masses were employed primarily to observe the effect of various coefficients of restitution. However, an additional secondary mass was made from a magnetic sensitive, mild steel to assess the effect of the shaker's magnetic field on the motion of the masses.

All secondary masses were machined as integral dumbells with a spherical like contact surface. Consequently a secondary mass is always contacted at some point even if it rotates about vertical AA' in Figure 2.12(b) or, to a less extent, about a perpendicular axis. This mass was suspended virtually frictionless and 34.25 $\pm$ 0.05 ins.

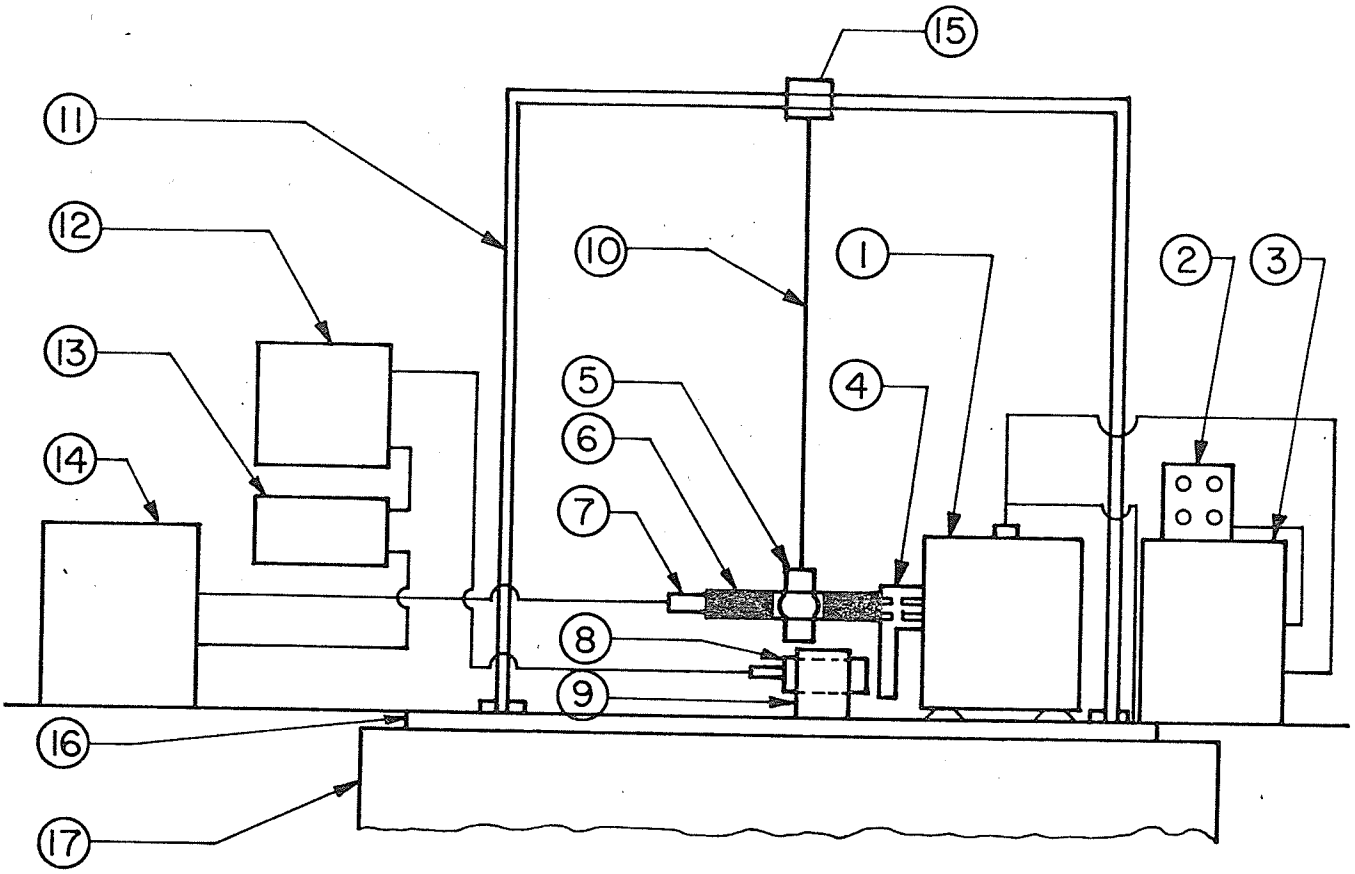

Figure 2.11. Details of the experimental apparatus and instrumentation.

Key:

(1) Electromagnetic shaker, Ling Model 400 Series 192

(2) Hewlett-Packard Function Generator 3110B

(3) Amplifier Ling Model PA200

(4) Aluminum adapter

(5) Secondary mass made from either steel or brass

(6) Slotted primary mass of die tool steel

(7) Bruel & Kjaer accelero-meter Type 4333

(8) Wayne Kerr capacitance transducer

(9) Support for capacitance probe

(10) Two-light cotton threads

(11) Solid frame

(12) Wayne-Kerr Feedback amplifier TE MK II

(13) Hewlett-Packard multimeter 5306A

(14) Tektronix double beam storage oscilloscope 7313

(15) Adjusting mechanism

(16) Cold rolled plate

(17) Heavy concrete block

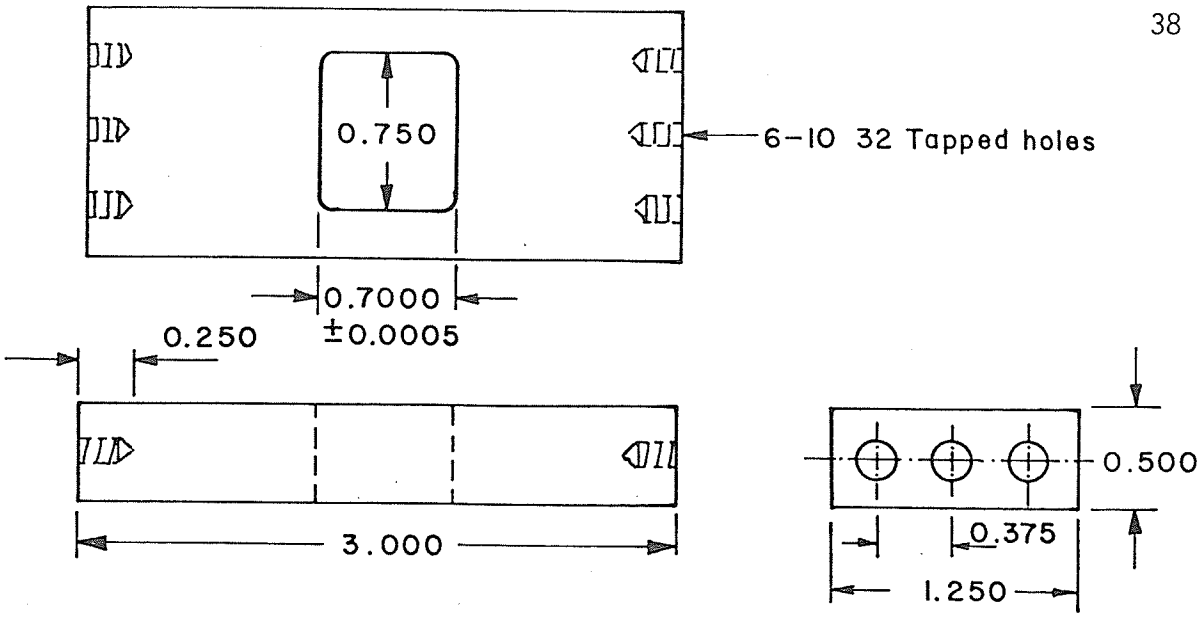

(a) Primary mass of die tool steel RC 62.

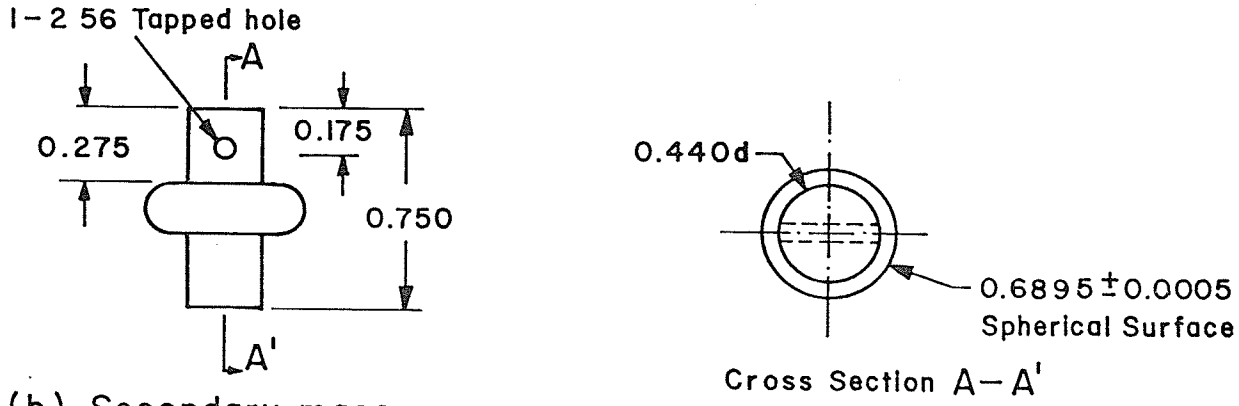

(b) Secondary mass

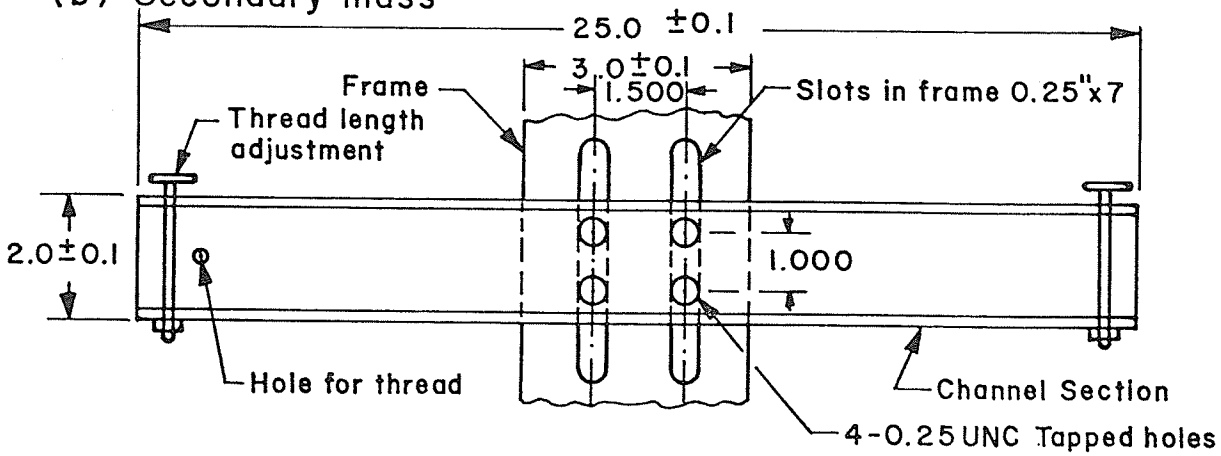

(c) Adjusting mechanism

All dimensions are in inches and those tolerances not specified are ±0.001 inches.

Figure 2.12. Details of the primary and secondary masses and adjusting mechanism.

from a solid frame, item 11 in Figure 2.11, by two light cotton strings. These strings were arranged so that the angle between them ($38.5° \pm 0.5°$) was maximised to prevent rotation, θ, about the vertical. It was found from preliminary experiments that the greatest θ then occurring (at the largest prescribed displacements) was reduced from about 90° to 15°. By also employing the dumbell rather than a spherical secondary mass, rotations about other axes were substantially less. Therefore the experimental secondary mass simulated the free, horizontal unidirectional movement assumed theoretically. Possible superfluous effects of varying contact geometries and, hence, coefficients of restitution were minimised.

The adjusting mechanism highlighted in Figure 2.11 enabled the initial stationary position of the secondary mass to be modified in order to evaluate the influence, if any, of the initial conditions on the final periodic motion. This mechanism, like the capacitance transducer, item 8 in Figure 2.11, was supported by a solid connection from a level, horizontal plate, 16, seated on the very heavy concrete block, 17. The electromagnetic shaker, 1, was situated also on the horizontal plate. Consequently, any extraneous building vibrations should likely affect all major mechanical components equally so that the prescribed absolute displacement of the primary mass can be measured with the capacitance transducer, 8. The additional precaution of performing all experiments during quiet nights was taken to further reduce extraneous events. Impacts were monitored most easily by displaying the signal from the accelerometer, numbered 7 in Figure 2.11, on the

storage oscilloscope, item 14. All the equipment was calibrated according to manufacturer's instructions. The accuracy of any one instrument was generally within $\pm$ 0.5%.

The prescribed frequency and amplitude of the sinusoidal displacement of the primary mass was generated by controlling carefully the motion of the rigidly coupled shaker using a function generator and amplifier. Sinusoids were varied in frequency from 10 to 50 Hz in steps of 5 Hz. This frequency range was well below the individual first mode natural frequencies of the secondary mass alone and the primary mass system, respectively about 10 kHz and 15 kHz. It was also above the fundamental pendulum frequency, 0.53 $\pm$ 0.02 Hz., of the strung secondary mass. Therefore the secondary pendulum behaved essentially as a mass [20] which, like the primary, reasonably satisfied the theoretical assumption of rigidity.

Prescribed displacement amplitude of the primary mass was restricted practically to less than about 0.05 in. by the limited range of the capacitance transducer. On the other hand the secondary mass began noticeably to rotate increasingly about the horizontal and rise (termed "lifting") with larger displacements of the primary mass. This was likely the result of not truly horizontal impact forces due to the secondary's pendulum motion and directional distortions from the shaker. The effect became excessive when the prescribed displacement rose above 0.02 in. and 30 Hz, so that measurements were then terminated. Another, solely practical phenomenon was the change in the amplitude

of the prescribed displacement caused by the collisions of the primary and secondary masses. These changes increased with a diminishing prescribed amplitude but were never greater in magnitude than a 5% of the overall displacement amplitude.

There are no clear quidelines regarding an appropriate amplitude for "small" perturbations in the determination of asymptotic stability. This question was explored experimentally by using a pulse to disturb an existing periodic motion. The pulse was produced with an Interstate Sweep Generator Model F77 so that its amplitude, 0 to 5 volts, and duration, 1 to 100 μ sec., could be controlled. The system was considered asymptotically stable if it returned to the prior periodic motion within two minutes of the pulse's application. The somewhat arbitrary two minutes corresponded to at least 1200 cycles of the prescribed displacement. Although desirable in principle, more cycles would have been progressively time consuming and increased the possibility of uncontrolled vibrations from external sources becoming influential. Experience gained in this exercise was useful in assessing reasonable perturbation characteristics for subsequent stability checks of all experimental periodic motions.

2.4 Comparison of Experimental and Theoretical Results

Experimental data will be reported in a form fairly compatible with the theoretical stability zones of Figure 2.5 and 2.9. The non-dimensional parameter σ (2A/d) will form the ordinate again but the

usually conjectured constant experimental coefficient of restitution will be replaced as abscissa by the frequency of the prescribed displacement. In principle stable periodic motions should be independent of frequency. However they have been observed to vary somewhat in practice due to changes in the coefficient of restitution arising from differences in the relative approach velocities of the colliding masses [34]. Similar variations, although never investigated before, may stem from surface changes due to repeated collisions. Such effects were assessed separately by utilising high speed photography and the apparatus described in the previous section. Details of these experiments are given in Appendix A4. They suggest that collisons repeated intermittently over six months may cause the coefficients of restitution of the materials investigated to change around 5 to 10%. A number of separate coefficients were employed additionally by independently using non-magnetic stainless steel and brass for secondary masses and discriminately applying tape to stainless steel primary mass.

2.4.1 Equal Coefficients of Restitution

Stability zones are presented in Figure 2.13 and 2.14 for the various coefficients of restitution employed experimentally. Experimental data are plotted as curves whereas corresponding theoretical predictions, independent of frequency, are illustrated as vertical lines. These predictions were obtained from Figure 2.5 by using the observed number and spacing of impacts/cycle and the

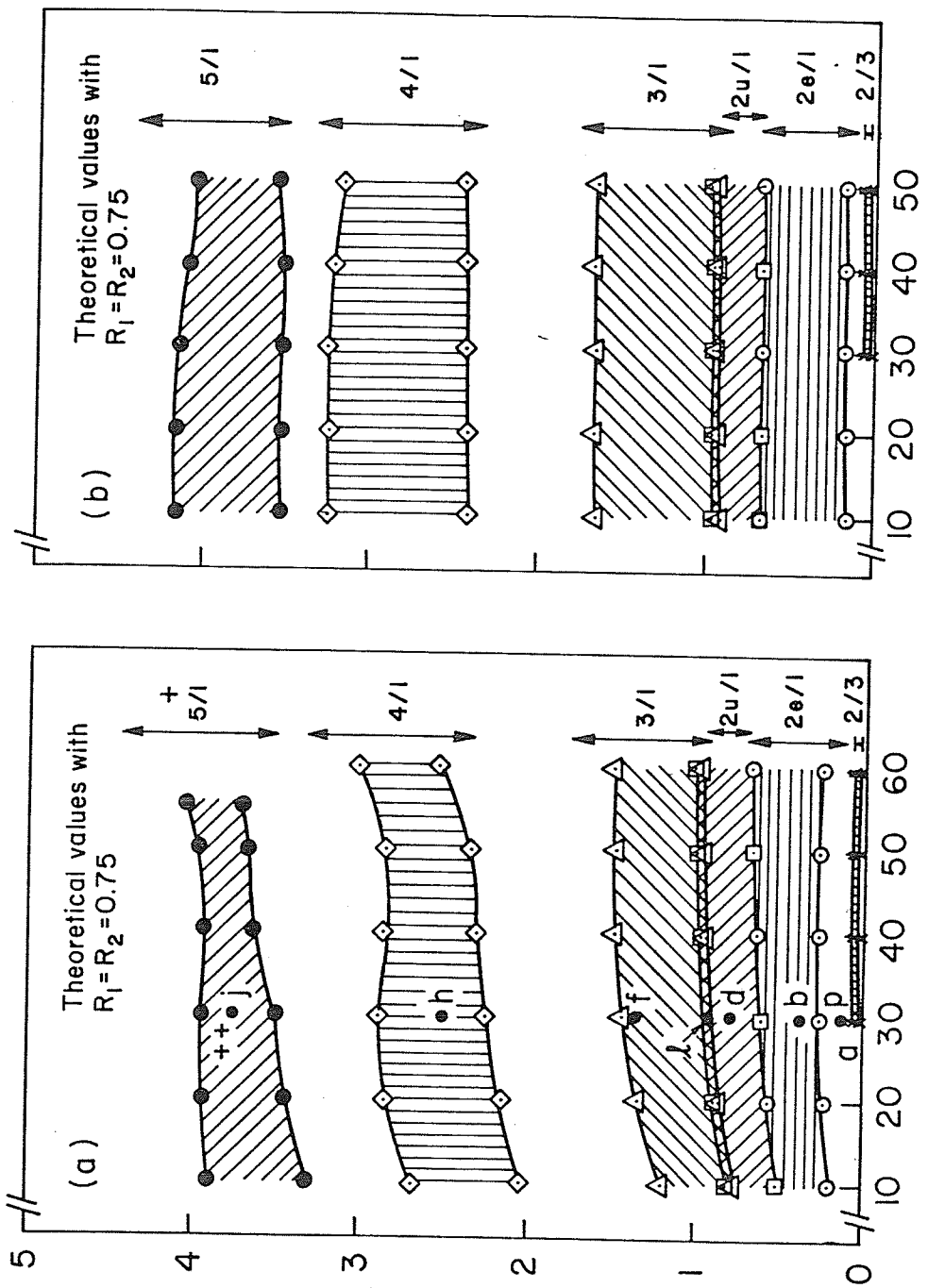

Figure 2.13. Experimental stability zones with non-magnetic stainless steel secondary mass. Gap size is 0.0105 + 0.0005 in. Data (a) gives results immediately after systems manufacture and (b) after intermittent use of six months.

+Number of impacts/cycle of prescribed displacement. Unequispaced impacts are implied or given by u when not obvious and e denotes equispaced impacts.

++Time histories are shown with corresponding lettered photographs in Figure 2.15 through 2.18.

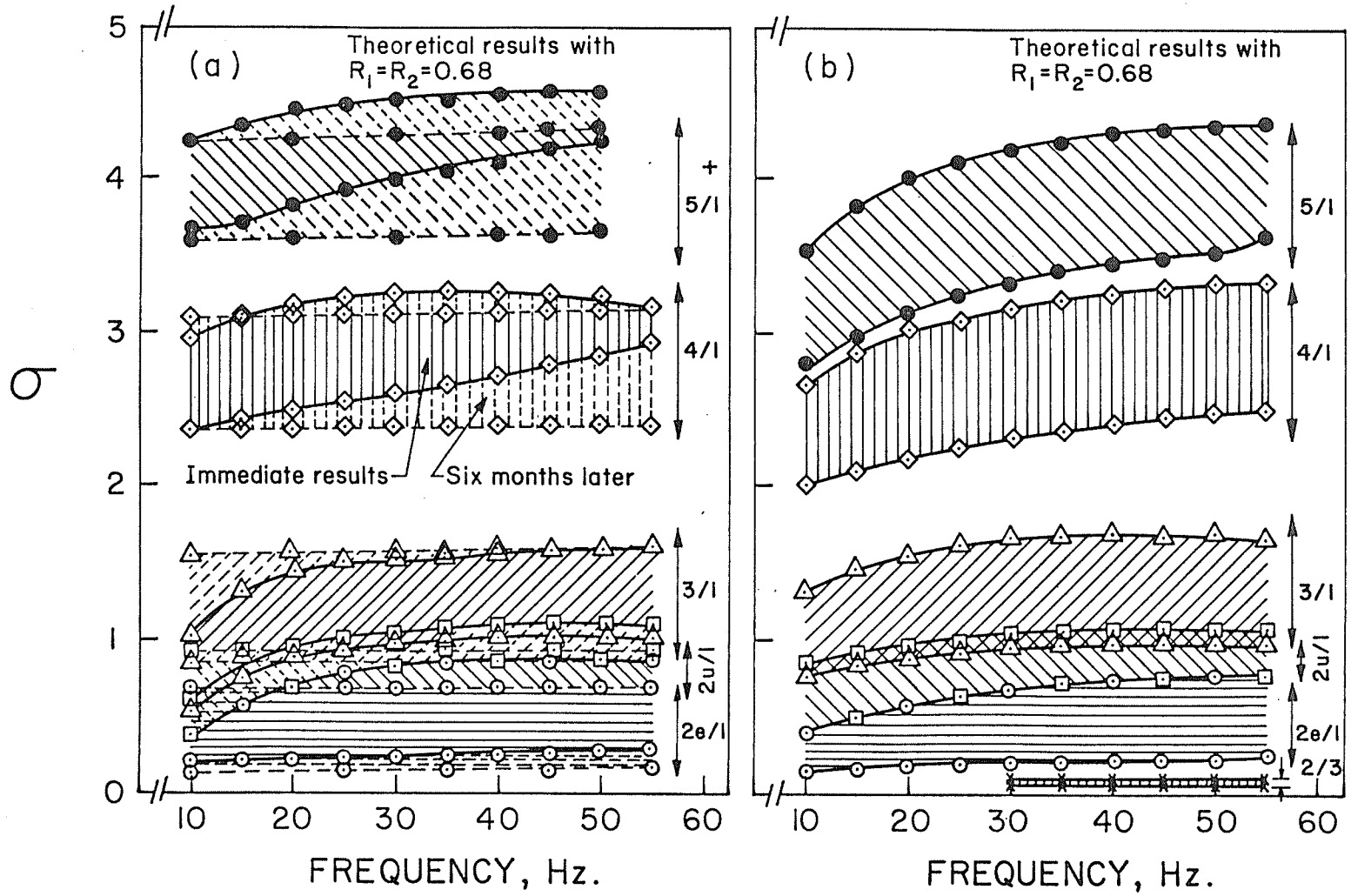

Figure 2.14. Experimental stability zones with (a) brass secondary mass, and (b) stainless steel secondary mass and both sides of primary mass taped. (a) 0.0100 ± 0.0005 in. and (b) 0.0057 ± 0.0005 in.

+Notation is identical to that in Figure 2.13.

experimentally determined coefficients of restitution in Table A4.1. Errors introduced by simply assuming that coefficients of restitution are constant in theory and equal at collisions on opposite sides of the primary mass will be discussed later. The cumulative effect of intermittently regular contacts between experimental masses over six months may be determined by the differences in Figure 2.13(a) and 2.13(b) and in Figure 2.14 between the full and corresponding dashed curves. Typical motions under the conditions (a) through (p) in Figure 2.13(a) are shown by the correspondingly lettered photographs in Figure 2.15 through 2.18. The upper and lower signature of those photographs having dual traces respectively present the time history of the absolute displacement and acceleration. Acceleration of the primary mass was modified by a low band-pass filtering from 6 to 250 Hz to improve clarity of phase planes. Phase plans help to determine the spacing and number of impacts per cycle of the primary mass' prescribed displacement. The two vertical spikes in Figure 2.15(c) and 2.15(e), for example, indicate clearly two impacts/cycle. Equal arc separations between spikes in Figure 2.15(c) demonstrates that these two impacts, unlike those in Figure 2.15(e), are equispaced. This information can be observed less directly from the spacing and number of sudden acceleration changes in a time history relative to one period of the corresponding displacement of the primary mass. The number of impacts per period, or cycle, and their spacing in the case of two impacts/cycle alone is stated for convenience under virtually all time histories.

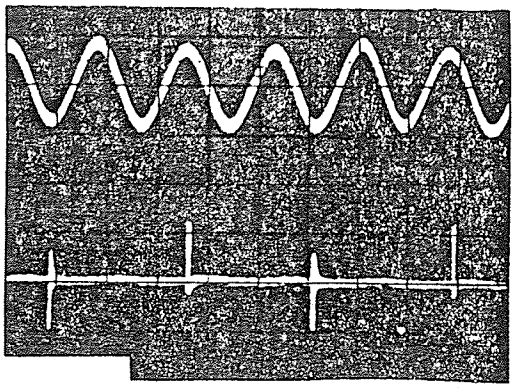

(a) Two impacts/three cycles

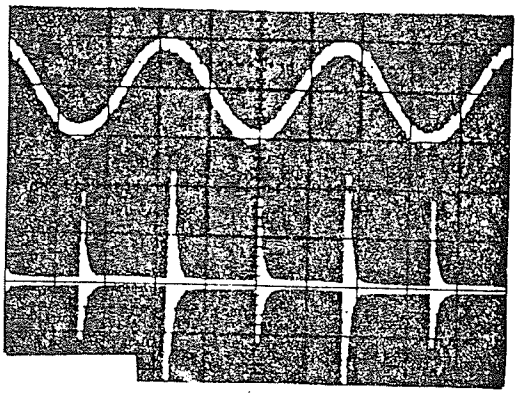

(b) Two equispaced impacts/cycle

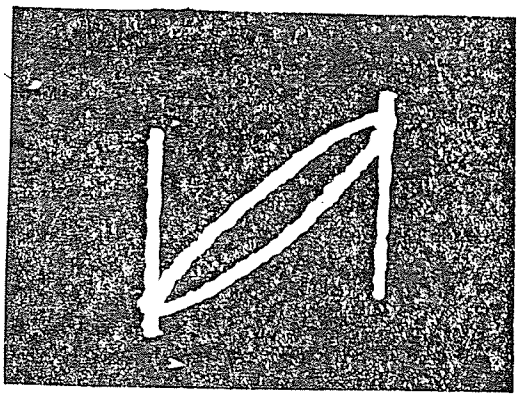

(c) Phase plane representation of (b)

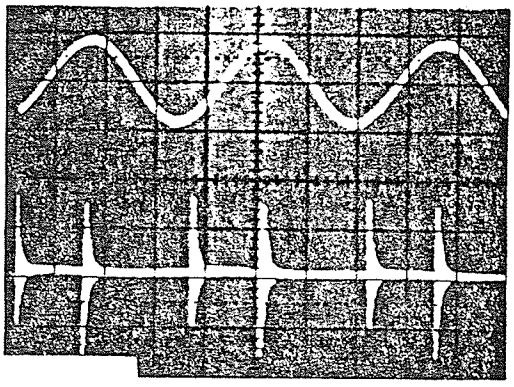

(d) Two unequispaced impacts/cycle

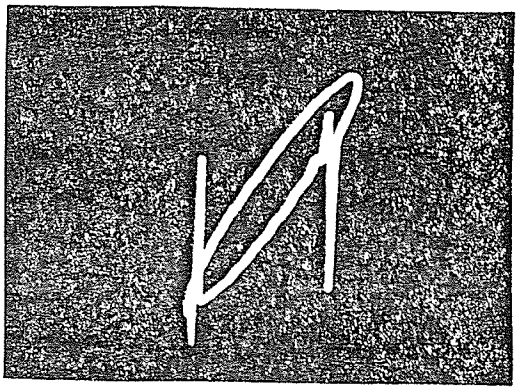

(e) Phase plane representation of (d)

→TIME (10 msec./division unless shown otherwise)

→DISPLACEMENT

Figure 2.15. Typical experimental time history and phase plane of two impacts/three cycles and two impacts/cycle periodic motions of the primary mass. Traces from top to bottom on the left-hand side alternately represent the absolute displacement and acceleration.

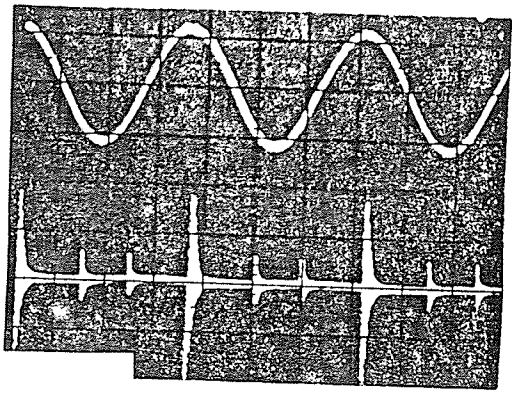

(f) Three impacts/cycle

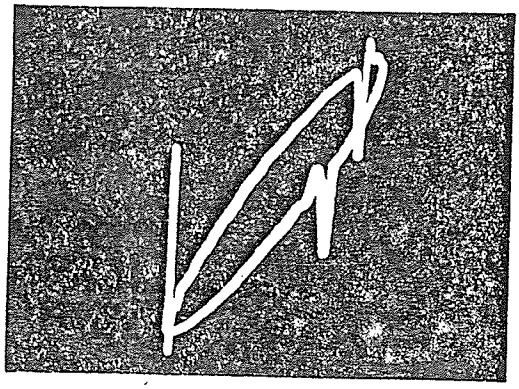

(g) Phase plane representation of (f)

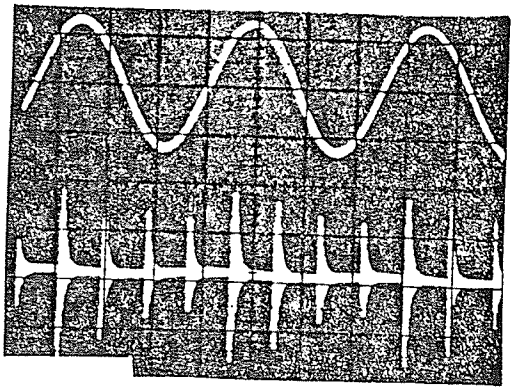

(h) Four impacts/cycle

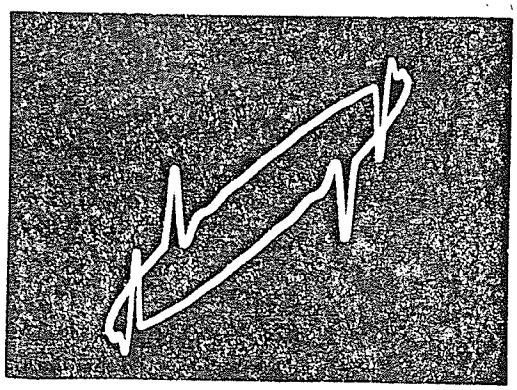

(i) Phase plane representation of (h)

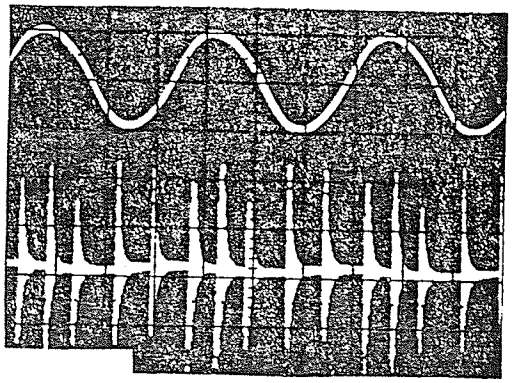

(j) Five impacts/cycle

→TIME (10 msec./division unless shown otherwise)

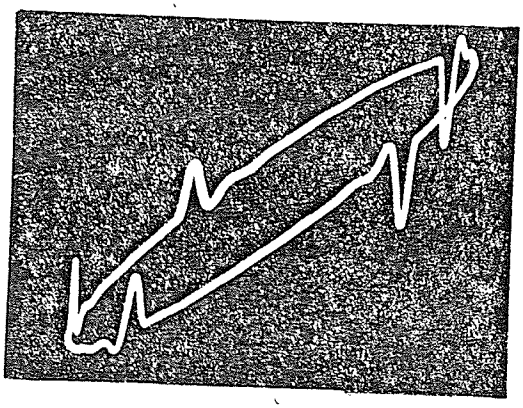

(k) Phase plane representation of (f)

→DISPLACEMENT

Figure 2.16. Experimental three, four and five impacts/cycle periodic motions of primary mass. Outlay is similar and conventions are identical to those in previous figure.

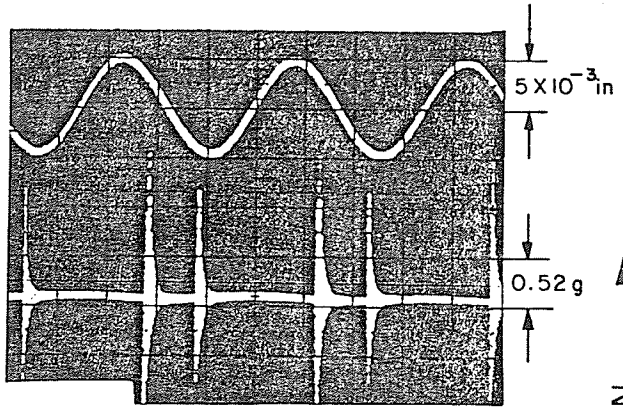

(l) Two unequispaced impacts/cycle

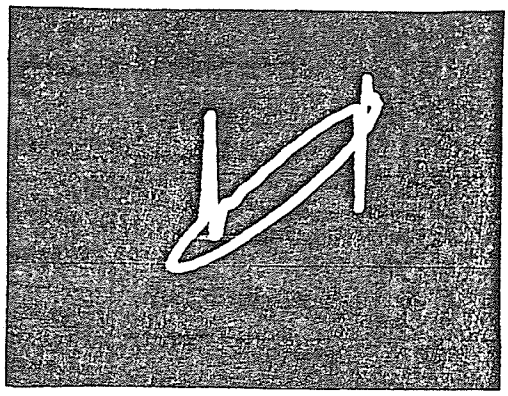

(m) Phase plane representation of (ℓ)

ACCELERATION

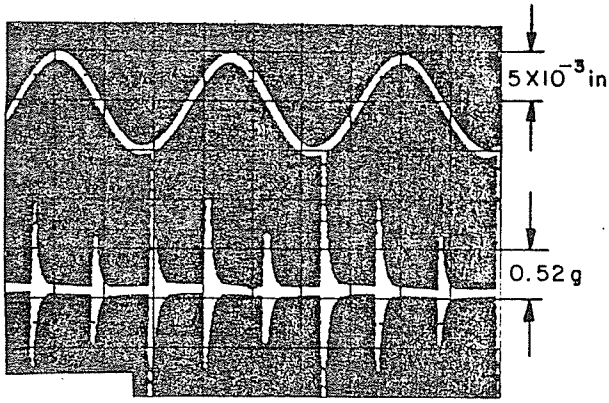

(n) Three impacts/cycle

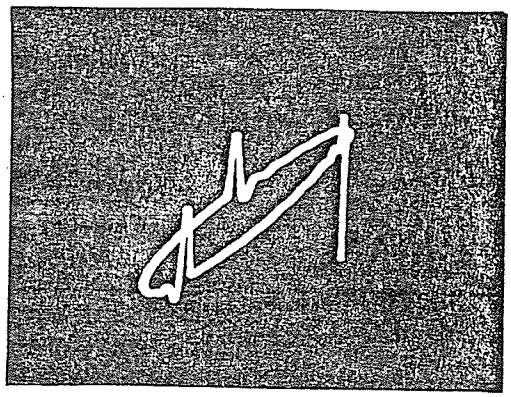

(o) Phase plane representation of (n)

→TIME (10 msec./division unless shown otherwise)

→DISPLACEMENT

Figure 2.17. Illustrating the probable non-uniqueness of theoretical stable periodic solutions. Convention is identical to that in Figure 2.15.

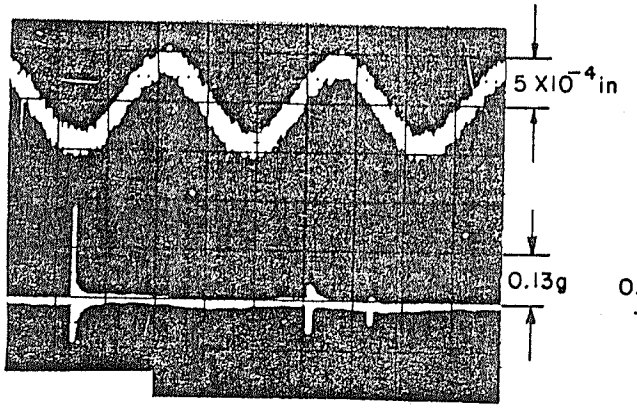

(p) Initial unstable aperiodic motion

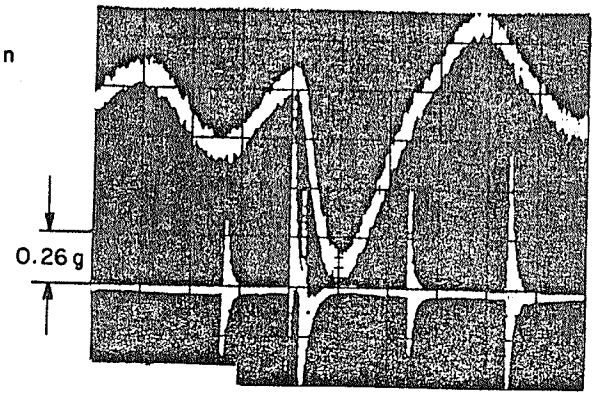

(q) Subsequent perturbation of (p)

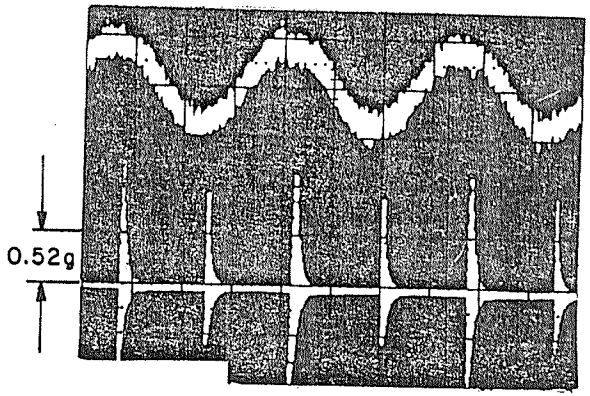

(r) Later unstable 2 equispaced impacts/cycle motion

TIME (10 m sec/ division)

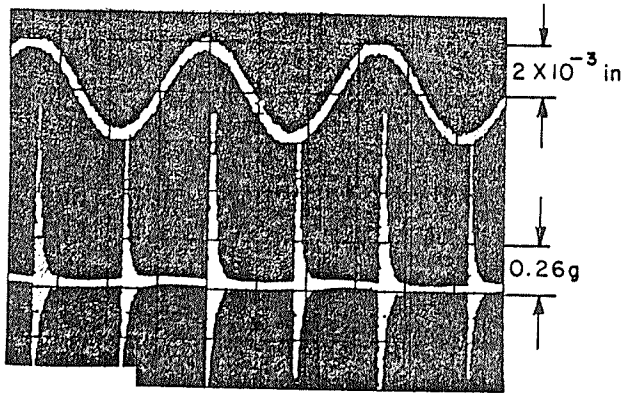

(s) Initially stable, two equi-spaced impacts/cycle motion

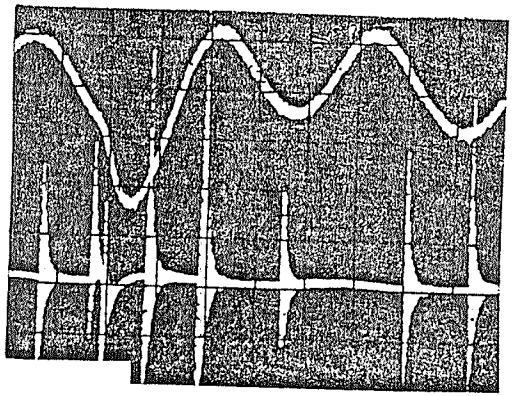

(t) Subsequent perturbation of (s)

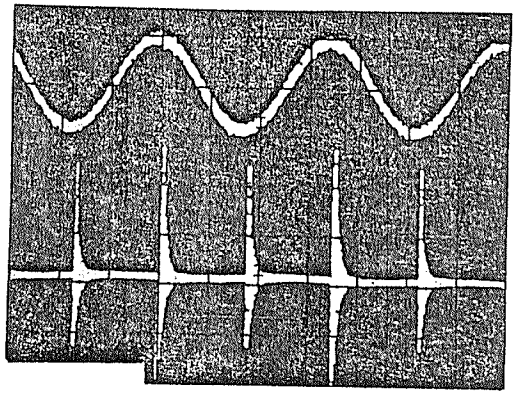

(u) Later stable, two equispaced impacts

Figure 2.18. Experimental perturbations of aperiodic and stable, two equispaced impacts/cycle motion of primary mass. Convention is identical to that for the time histories of Figure 2.15.

Experimental and theoretical results generally agree quite well as may be seen in Figures 2.13 and 2.14. The various stability zones appear in exactly the same order and tend to overlap similarly. A comparable degree of agreement was found in the corresponding time histories. Figure 2.13 and 2.14 clearly indicate the basic tendency of experiment and theory to correlate best, after six months of intermittent usage. The largest differences occur at the lowest frequencies of the immediate experimental values. Then experimental curves generally decrease with frequency especially below about 25 Hs. Corresponding results after six months of usage are horizontal or independent of the prescribed frequency of displacement. The last, unlike the former trend agrees with theoretical predictions.

Veluswami et al. [19] found in contrast to the experimental results presented here and by Kobrinskii [1] that stability boundaries tended to decrease rather than increase at the lowest frequencies. Similar electromagnetic shakers seem to have been employed to obtain these contradictory trends. However Veluswami et al. appear to have taken no precautions to attenuate the magnetic field of the shaker or to use, as here, non-magnetic materials for the secondary masses. Consequently a secondary mass made of a magnetic sensitive mild steel was employed to investigate possible extraneous effects of the

magnetic field. The primary mass was again coupled directly to the shaker by using the original magnetic insensitive brass studs and, additionally, by magnetic prone, mild steel studs. Previous experimental procedures were followed to produce the data displayed in Figure 2.19. It can be seen clearly that the likely consequence of stray magnetism decreases with more effective precautions. A noticeable effect appears restricted however to the single two equispaced impacts/cycle stability boundary at frequencies below 40 Hz. Therefore extraneous magnetism is not the major cause of the invariable low frequency discrepancy between all the immediate experimental data and the theoretical results of Figure 2.13 and 2.14. The downward trend with decreasing stray magnetism does suggest conversely that the low frequency, immediate experimental values in these figures are plausible.

Theoretical accelerations were considered to change instantly at any one impact. Experimental accelerations on the other hand can be seen from Figure 2.15 through 2.18 to have a finite but small "ring down" duration after a collision. Stress waves travel during this time between the surfaces of each mass with progressively attenuated amplitudes. Ring down was completed before the subsequent impact and complementary research [88] suggests that the theoretical assumption is then justified.

Coefficients of restitution R_1 and R_2 were assumed identical and constant in theoretical computations. Accurate and extensive high speed

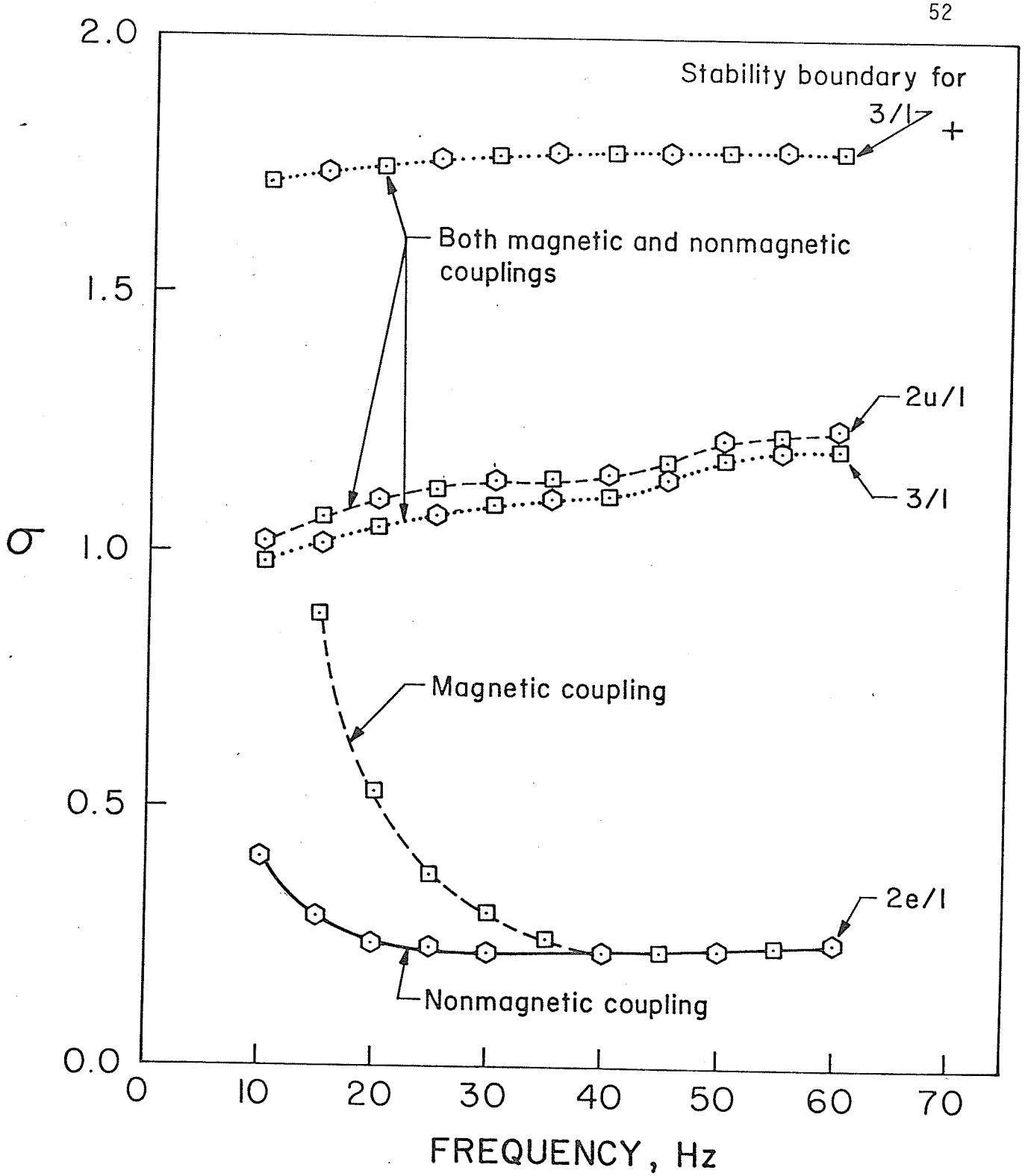

Figure 2.19. Influence of electromagnetic shaker's magnetic field. Secondary mass is magnetic mild steel and gap clearance is 0.0307 + 0.0005 in. Results obtained by using (a) non-magnetic brass studs (⬡--⬡) and (b) magnetic steel studs (□--□) connections between shaker and primary mass.

+Number of impacts/cycle of displacement. Unequispaced impacts are implied or given by u when not obvious and e denotes equispaced impacts.

photography indicated that R_1 and R_2 were invariably within 3% for the mature stainless steel secondary mass. A similar correlation was obtained for the brass secondary mass but only at one operating condition. Comparable differences should be expected however over the entire range of experimental conditions because the same vigilance was taken in the manufacture of both secondary masses. The 3% is within normal careful practice and has been shown in principle to hardly affect the lowest stability zones. Therefore R_1 and R_2 are sufficiently close to be considered identical to a common value R. Consequently, these differences were neglected in measurements of the coefficient of restitution. On the other hand Figure A4.2 of Appendix A4 suggests that the short-term coefficient of restitution R of the mature stainless steel secondary mass varied by about 8% over the entire range of experimental conditions. The constant employed computationally was enumerated in the manner described in Appendix A4. Its value was generally lower and higher than the measured coefficients below and above 25 Hz, respectively. Figure 2.5 indicates that an increasing theoretical value of R in the pertinent region around 0.75 might lower the stability boundaries somewhat below 25 Hz, but only consistently for those zones involving two impacts. Therefore the inevitable and pronounced downward shift of all the immediate experimental stability zones below 25 Hz remains largely unexplained. Approximations more sophisticated than a constant R would seem to offer only marginal improvements.

Effects of prolonged use were evaluated neither comprehensively nor in a strictly compatible fashion. Restitution coefficients were

only assessed initially by using the conventional method of determining the rebound height of the secondary pendulum from the free end of the tightly held primary mass. They were measured this way and, for stainless steel alone, more accurately six months later with the help of high speed photography. Discrepancies in the three sets of coefficients for the stainless steel secondary mass appeared no worse than errors associated with the pendulum technique. Consequently the effect of repeated collisions could not be determined from these limited direct measurements. Costs were too prohibitive to repeat the photography for the softer brass and taped steel masses. A visual inspection revealed that the contact surface of the brass was smoothed by the elimination of very small "high spots" somewhat more than the plain stainless steel after similar use. A comparable process has been noted for gears [23, 24]. Although the stability boundaries for stainless steel and brass are similar originally, a comparison of Figure 2.13(b) and the dashed curve of Figure 2.14(a) suggests that slopes are slightly more horizontal at higher impact numbers and frequencies for the mature brass. The somewhat more repeatable collision conditions for the older brass seem to counteract its greater rotation and lifting. Counterbalancing is slightly less presumably for all original and for the final materials harder than brass. Variations in the impact conditions of original masses are exaggerated at low frequencies by the sudden increase of R and by the growing effect of collisions on the primary mass' displacement amplitude at small σ.

2.4.2 Unequal Coefficients of Restitution

A difference of over 20% in the coefficients of restitution at opposite sides of the primary mass was obtained by taping only one side and using the stainless steel secondary mass. As far as could be discerned from pendulum tests, the tape gave a consistent coefficient of restitution even after impacts repeated continuously over thirty minutes. Experimental and theoretical procedures were identical to previous tests and the presentation of data in Figure 2.20 and 2.21 follows the same format.

Figure 2.20 indicates that the most frequently studied two equispaced impacts/cycle stable motion observed for equal coefficients of restitution could predictably, not be found for such widely dissimilar coefficients. The agreement between experimental and theoretical two unequispaced and three impacts/cycle is as good or better than noted for equal coefficients of restitution. Much more complex stable motions were seen experimentally, however, at σ over one. They involve one or two impacts on the steel and many impacts subsequently on the tape. Such motions are displayed in Figure 2.21(d) and 2.21(e). The much larger transient accelerations in these figures were generated by collisions on the steel. These motions were not observed for equal coefficients of restitution. They appeared to be similar to the phenomenon of sliding where a large number of impacts with decreasing strength happen in a small but finite duration [47, 48]. Major theoretical modifications needed to adequately describe this particular behaviour could not be justified.

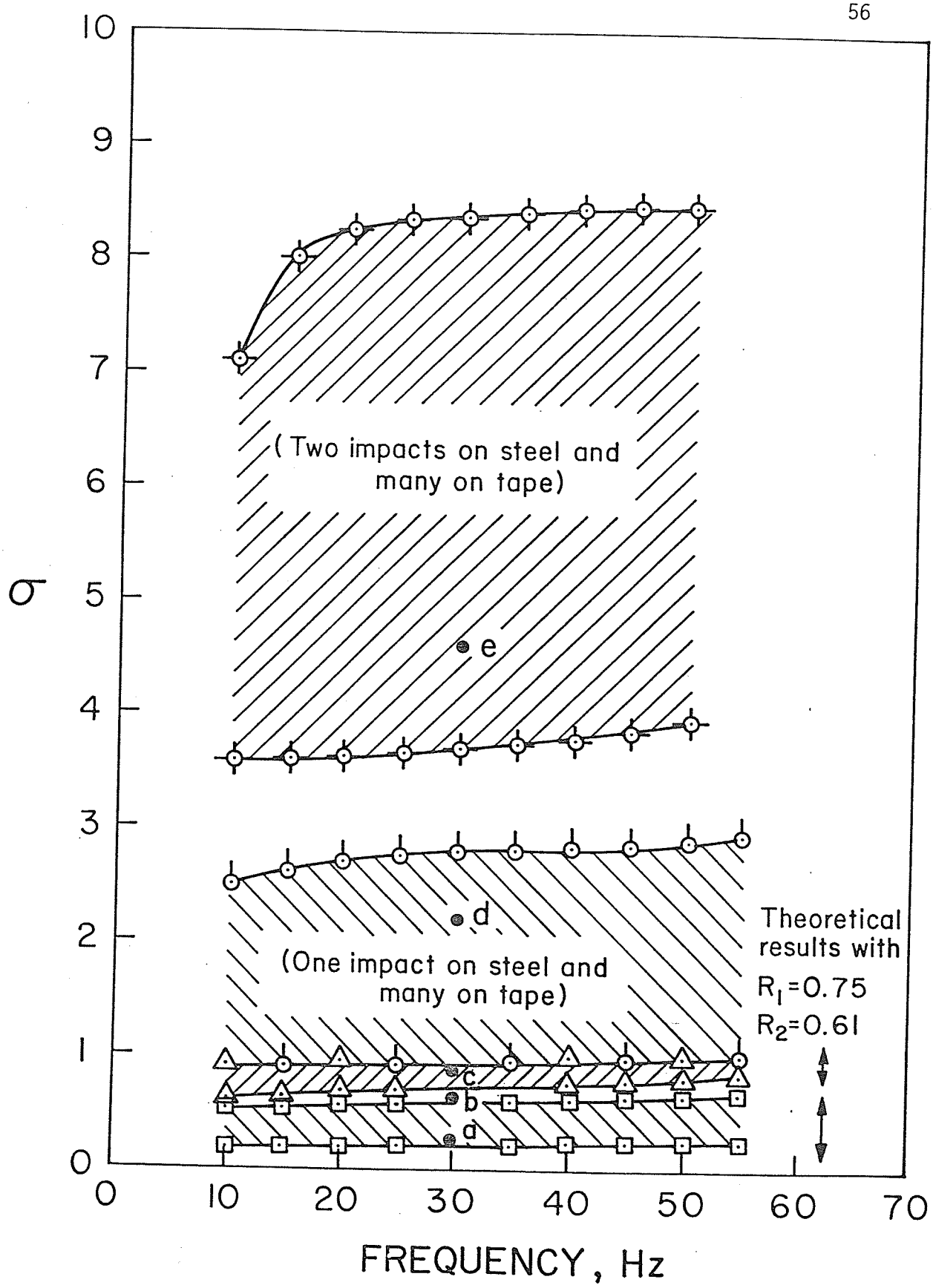

Figure 2.20. Stability zones of experimental periodic motions for stainless steel secondary mass and only one side of primary mass taped. Gap clearance is 0.0081 ± 0.0005 in.

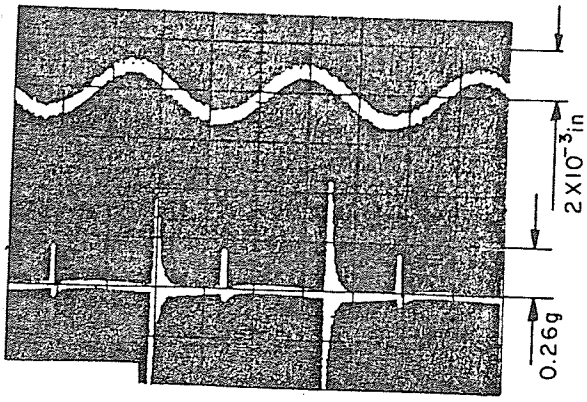

(a) Two unequispaced impacts/cycle

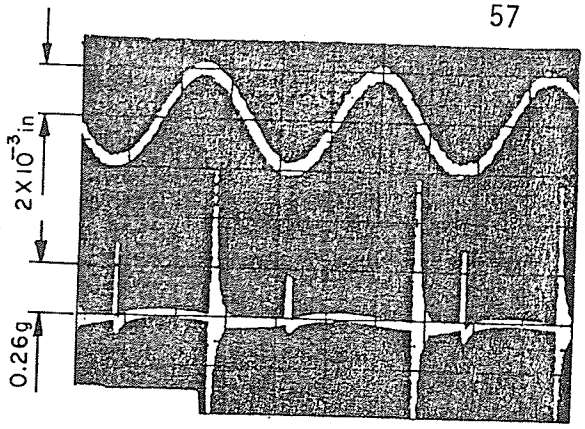

(b) Complex periodic motion of two unequispaced impacts/cycle

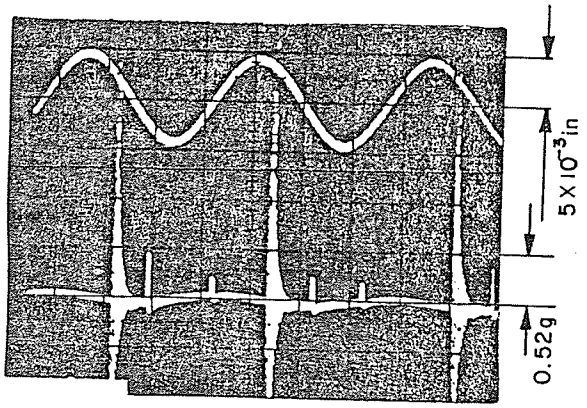

(c) Three impacts/cycle

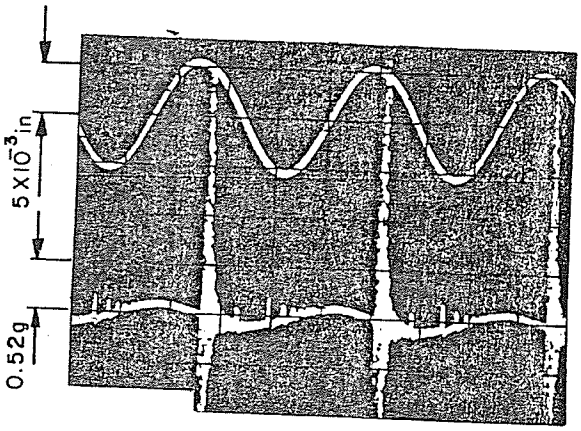

(d) One impact on steel and many on tape

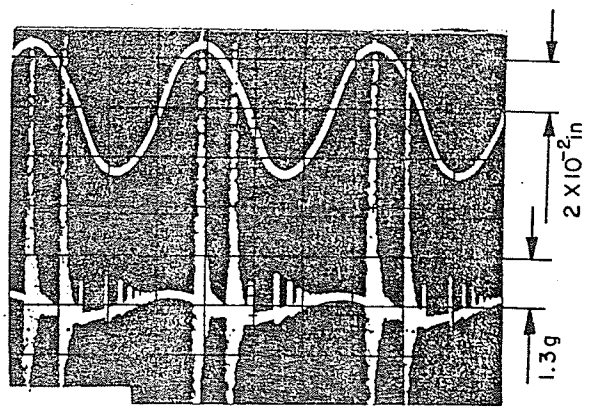

(e) Two impacts on steel and many on tape

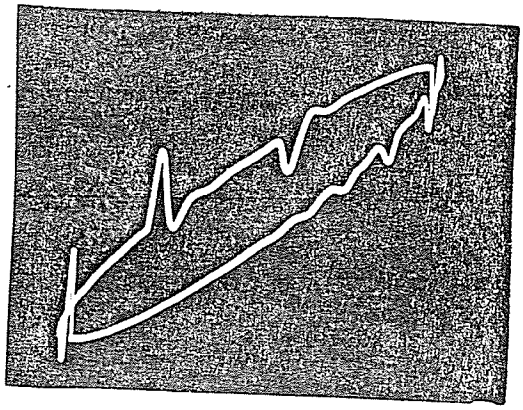

(f) Phase plane of e

ACCELERATION

→TIME (10 msec./division unless shown otherwise)

→DISPLACEMENT

Figure 2.21. Experimental time histories and phase planes of primary mass when coefficients of restitution are unequal. Traces from top to bottom on left-hand side alternately represent absolute displacement and acceleration.

2.5 Conclusions

Previous theory has been generalised and a more comprehensive set of stability charts have been computed for an Impact-Pair. The general theory subsumes previous theories without conflict. In addition correlates well with experiments covering a wide range of conditions. The worst, yet still minor disagreements occurred generally at the lowest prescribed frequencies and highest numbered stability zones for recently manufactured secondary masses. Differences occur due to not absolutely non-uniform contact surfaces, lifting of the secondary mass, fluctuations in the coefficients of restitution and in a supposedly constant prescribed displacement were contributory and sometimes compensatory. Coefficients of restitution need not be equal at opposite sides of the primary mass but interactions like sliding with appreciable contact times cannot be accommodated presently.

A simple technique has been proposed in principle which employs the general theory to conveniently determine the clearance of an Impact-Pair. Regular measurements may be necessary however to ensure that the coefficients of restitution do not change significantly in the interim.

The presence of a particular periodic motion was found experimentally to presence depend upon the initial conditions of the secondary mass only when:

1) the value of σ was so small (typically less than about one) that collisions never happened; and
2) different periodic motions had stable points in common. (A typical example is displayed in Figure 2.17). Figure 2.18(s),

2.18(t) and 2.18(u) illustrate that even a perturbation so large as to virtually double the original displacement amplitude of the primary mass did not seem to influence a periodic motion permanently if its stability zone was distinct. Conversely, Figure 2.18(p), 2.18(q) and 2.18(r) demonstrate that a perturbation may transform an initially aperiodic motion into an unstable periodic one.

CHAPTER 3

GENERAL MOTION OF AN IMPACT-DAMPER

3.1 Introduction

An impact damper is used to reduce the resonant displacement of a vibrating mechanical system. It is envisaged usually as a light but rigid mass moving unidirectionally without friction. The mass impacts against either a container attached solidly to the vibrating system or the ends of a slot within the system. A properly designed impact damper can be quite effective despite the transitional high accelerations generated at impacts [49-68]. It also is less sensitive to small changes in either the vibrating system's parameters or external load than a conventional dynamic neutralizer [6, 53].

Periodic, two equispaced impacts per cycle of sinusoidal excitation have been considered almost exclusively previously [1, 2, 49-56, 61]. Impacts have been assumed to be instantaneous and idealised by using identical coefficients of restitution. An exact, closed form solution was obtained independently by Warburton [52] and Korbrinskii [1] using periodicity in the manner of boundary conditions. Masri [53] subsequently applied the concept of error propagation in difference equations to determine the asymptotic stability.

Limited experimental and theoretical studies by Sadek [57] and Dittrich [58] suggests that unequispaced impacts are more likely than equi-

spaced periodic impacts near the fundamental resonance of the original mechanical system. Sadek also inferred form careful experimentation that "equally spaced impacts hardly ever occur" even away from this resonance [57]. The differen-es in views [54, 57] could arise from the not always consistent influence of gravity in the various experiments. They are more likely the result however of ignoring small variations in the coefficients of restitution at consecutive impacts.

Both Sadek [57] and Masri [59] attempted to generalise the theory for two equispaced impacts per excitation cycle. Sadek did not account properly for the velocity discontinuity at an impact [57] whilst Masri's iterative proposal may converge slowly and be computationally time consuming. A more efficient algorithm will be developed here. The usual concept of assuming the duration known between any two equispaced impacts will be replaced by presuming a priori knowledge of all durations between any periodic N impacts per periodicity period T_o. The ensuing 2N linear simultaneous equations in (N + 2) unknowns will be solved exactly when N equals two and otherwise approximately by using a method of least square fit [7]. Computed values will be compared with the theoretical results of previous investigators and more extensively with experimental data. The effect of unequal coefficients of restitution on the general motion of an impact damper will be investigated as well.

3.2 Theoretical Development of the General Periodic Motion of an Impact Damper

An idealised vibroimpact device is shown in Figure 2.1. The primary system consists of a linear spring with stiffness K, a

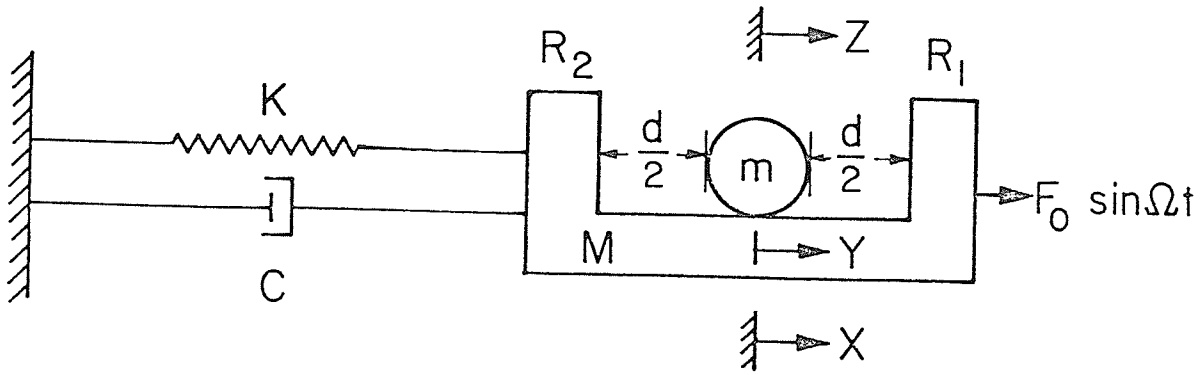

Figure 3.1. Model of a single degree-of-freedom system with an impact damper.

viscous dashpot having damping constant C and mass M excited by the external harmonic load, $F_0 \sin\Omega t$. The secondary system is composed of a rigid mass m which can move uniaxially without generating frictional forces in a slot inside the usually much heavier mass M. Motion of m is provoked only by contacts between it and M which are intermittent due to a clearance, d, between the two masses. Any one impact i is assumed, for metal-like masses, to be instantaneous and to be described adequately by a coefficient of restitution, R_i. This coefficient is assumed for simplicity to be invariant with time and any parameter changes of the vibroimpact

device or external load. However the initial coefficients associated with collisions on the right- and left-hand sides of the slot in Figure 3.1, R_1 and R_2 respectively, need not necessarily be identical. Then the conjectured periodic motion is identical to that shown in Figure 2.4 with the exception that the external load rather than the primary mass' displacement is prescribed. The sequence of and the durations between, consecutive collisions of generally N impacts in the periodic duration T_o are presumed. Conversely the amplitude of the external load F_o, its phase with respect to an arbitrarily selected first impact and the absolute displacement of M at each of the N impacts are considered unknown, initially.

The equation of motion of mass M between impacts is

$$M\ddot{X} + C\dot{X} + KX = F_o \sin\Omega t \tag{3.1}$$

where X(t) represents the absolute displacement of the primary mass M. A dot superscript indicates differentiation with respect to time, t. The solution of equation (3.1) can be obtained conventionally by superimposing free and forced motions [5]. A typical solution between the i and the (i + 1) impacts is

$$X(t) = \exp\left[-\frac{\xi}{r}(\Omega t - \alpha_i)\right]\cdot\left[a_i \sin\frac{\eta}{r}(\Omega t - \alpha_i) + b_i \cos\frac{\eta}{r}(\Omega t - \alpha_i)\right] + A \sin(\Omega t - \Psi)$$

$$t_{i+} \leq t \leq t_{(i+1)-} \quad . \tag{3.2}$$

Subscripts i, i+ and i- respectively represent quantities at, just after and just before the typical i th impact. For example, t_{i+} is the instant immediately after the occurrence of the i th impact. Variables ξ, η, ω, A, r and Ψ are given conventionally by

$$\left.\begin{aligned} &\xi = C/2\ (KM)^{\frac{1}{2}}\ ,\quad \omega = (K/M)^{\frac{1}{2}}\ ,\quad r = \frac{\Omega}{\omega} \\ &\eta = (1 - \xi^2)^{\frac{1}{2}}\ ,\quad \Psi = \tan^{-1} 2\xi r/(1 - r^2) \end{aligned}\right\} \tag{3.3}$$

and

$$A = \frac{F_o}{K}\left[(1 - r^2)^2 + (2\xi r)^2\right]^{-\frac{1}{2}}\ .$$

The remaining variables used in equation (3.2) are defined as

$$\alpha_i = \Omega t_i,\ X_i \equiv X(t_i),\ \dot{X}_{ia} \equiv \dot{X}(t_{i+}) \tag{3.4}$$

and

$$\theta_i = \alpha_i - \Psi,\quad b_i = X_i - A\sin\theta_i \tag{3.5a}$$

$$\mu = \frac{m}{M}\ ,\quad a_i = \frac{1}{\eta}\left[\frac{1}{\omega}\dot{X}_{ia} - Ar\cos\theta_i + \xi b_i\right]\ . \tag{3.5b}$$

If t_1 is chosen arbitrarily as the temporal origin after the initiation of periodic motion, then equation (3.2) can be expressed as

$$\begin{aligned} X(t) = \exp\left[-\frac{\xi}{r}(\Omega t - \alpha_i)\right]\left[a_i \sin\frac{\eta}{r}(\Omega t - \alpha_i)\right. \\ \left. + b_i \cos\frac{\eta}{r}(\Omega t - \alpha_i)\right] + A\sin(\Omega t + \tau) \\ t_{i+} \leq t \leq t_{(i+1)-}\ ,\ i = 1, 2\text{---}N\ , \end{aligned} \tag{3.6a}$$

where invariably

$$\alpha_1 = 0,\ \tau = \Omega t_1 - \Psi\ ,\ \theta_i = \tau + \alpha_i \tag{3.6b}$$

and the t in equation (3.6a) implies $(t - t_1)$. Equations (3.4) through (3.6) hold between any of the N impacts occurring in the basic period, T_o. This implies that they can be generalised straightforwardly by letting i equal one through N. Impacts occur only when the relative displacement Y between m and M is $+\frac{d}{2}$ for a collision on the right side of M in Figure 3.1 and $-\frac{d}{2}$ for a collision on the left. Hence at impacts,

$$Y_i = Z_i - X_i = \pm\frac{d}{2}\ ,\quad i = 1, 2,\text{----}N \tag{3.7}$$

where Z_i is the absolute displacement of the secondary mass at contact time t_i. All of the N Y_i are determinable after accounting for collision locations.

The absolute displacement of the primary mass is continuous at any one impact so that [1, 59]

$$X_{i-} \equiv X_{ib} = X(t_i) = X_{ia} = X_{i+}\ ,\ i = 1, 2\text{----}N \tag{3.8}$$

for all N impacts. Velocities on the other hand are discontinuous at the impacts. The absolute velocity of M just before the representative i th impact can be determined by substituting the

instant of this impact, t_i, into the time derivative of equation (3.6a). Expressed more generally,

$$\dot{X}_{i-} = \dot{X}_{ib} = \dot{X}(t_i) \quad , \quad i = 1, 2\text{----}N \quad . \tag{3.9}$$

Its velocity immediately after the i th impact, $\dot{X}_{ia}$ is related to $\dot{X}_{ib}$ by the conservation of momentum and the definition of the coefficient of restitution. Applying these principles to the vibroimpact device shown in Figure 3.1 leads to

$$M\,\dot{X}_{ib} + m\,V_{ib} = M\,\dot{X}_{ia} + m\,V_{ia}, \; i = 1, 2\text{---}N \quad . \tag{3.10}$$

and

$$R_i = -\frac{\dot{X}_{ia} - V_{ia}}{\dot{X}_{ib} - V_{ib}} \quad , \quad i = 1, 2\text{----}N \quad . \tag{3.11}$$

The V_{ib} and V_{ia} are the absolute velocities of the secondary mass, m, just before and after the i th impact, respectively. Equation (3.10) and (3.11) can be solved to give

$$\dot{X}_{ib} = k_{7i} \cdot V_{ib} + k_{8i} \cdot V_{ia}, \; i = 1, 2\text{----}N \quad . \tag{3.12a}$$

and

$$\dot{X}_{ia} = k_{9i} \cdot V_{ib} + k_{10i} \cdot V_{ia}, \; i = 1, 2\text{----}N \quad . \tag{3.12b}$$

Expressions for the coefficients k_{7i} through k_{10i} are given in Appendix A2 and the nomenclature is clarified in Figure 3.2.

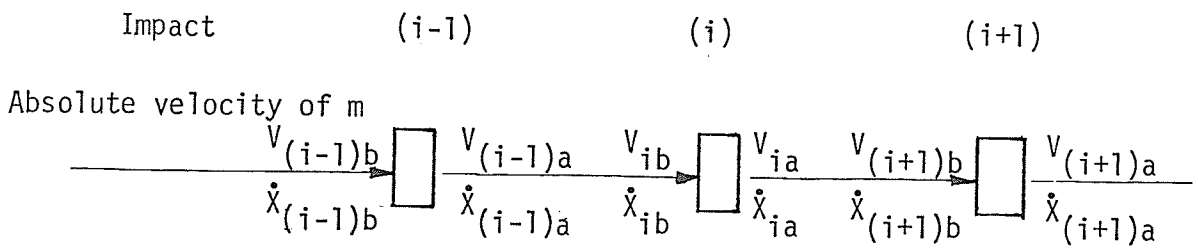

Absolute displacement of M

$X_{(i-1)}$ X_i $X_{(i+1)}$

Absolute displacement of m

$Z_{(i-1)}$ Z_i $Z_{(i+1)}$

Relative displacement between masses

$Y_{(i-1)}$ Y_i $Y_{(i+1)}$

Coefficient of restitution

$R_{(i-1)}$ R_i $R_{(i+1)}$

Contact instant

$t_{(i-1)}$ t_i $t_{(i+1)}$

Figure 3.2. Nomenclature of variables describing the (i-1) through (i+1) impacts.

Calculation of the V_{ib} and V_{ia} in equation (3.12a) and (3.12b) is simplified by the assumption that no external forces act upon m between impacts. The velocity of m therefore remains constant between impacts. Consequently its velocity V_{ia} between ith and (i+1)th

impacts, for example, is simply the ratio of the absolute distance travelled by m and the time elapsed between these two impacts. Mathematically,

$$V_{ia} = \frac{Z_{(i+1)} - Z_i}{t_{(i+1)} - t_i}, \quad i = 1, 2\text{----}N \quad . \tag{3.13}$$

Substituting equation (3.4) and (3.7) into equation (3.13) produces

$$V_{ia} = \frac{\Omega[X_{(i+1)} + Y_{(i+1)} - X_i - Y_i]}{\alpha_{(i+1)} - \alpha_i}, \quad i = 1,2\text{----}N \quad . \tag{3.14}$$

Similarly the velocity of the secondary mass just before the i th impact, V_{ib}, equals its velocity between the (i-1) and i impacts. Therefore

$$V_{ib} = \frac{\Omega[X_i + Y_i - X_{(i-1)} - Y_{(i-1)}]}{\alpha_i - \alpha_{(i-1)}}, \quad i = 1, 2\text{----}N \quad . \tag{3.15}$$

These expressions for V_{ia} and V_{ib} can be substituted directly into equation (3.12) to give

$$\dot{X}_{1b} = \frac{k_{7i}\,[X_i + Y_i - X_{(i-1)} - Y_{(i-1)}]\Omega}{\alpha_i - \alpha_{(i-1)}} + \frac{k_{8i}\,[X_{(i+1)} + Y_{(i+1)} - X_i - Y_i]\Omega}{\alpha_{(i+1)} - \alpha_i}, \quad i = 1,2\text{----}N \tag{3.16}$$

and

$$\dot{X}_{ia} = + \frac{k_{9i}\,[X_i + Y_i - X_{(i-1)} - Y_{(i-1)}]\Omega}{\alpha_i - \alpha_{(i-1)}} \frac{k_{10i}\,[X_{(i+1)} + Y_{(i+1)} - X_i - Y_i]\Omega}{\alpha_{i+1} - \alpha_i}, \quad i = 1, 2\text{----}N \; . \tag{3.17}$$

The relationship for $\dot{X}_{ia}$ can be used in conjunction with equation (3.5a) and (3.5b) to express coefficient a_i in the equation (3.6a) for the absolute displacement of M as

$$a_i = \frac{1}{\eta} \left\{ \frac{1}{\omega} \left[\frac{k_{9i}\,\{X_i + Y_i - X_{(i-1)} - Y_{(i-1)}\}\Omega}{\alpha_i - \alpha_{(i-1)}} + \frac{k_{10i}\,\{X_{(i+1)} + Y_{(i+1)} - X_i - Y_i\}\Omega}{\alpha_{(i+1)} - \alpha_i} \right] - Ar\cos\theta_i + \xi b_i \right\}, \quad i = 1,2\text{---}N \; . \tag{3.18}$$

Given all passive components of the vibroimpact damper, parameters η,ω and r in this last expression can be determined from equation (3.3). All the Y_i, k_{9i} and k_{10i} can be evaluated explicitly for known coefficients of restitution from equation (3.7) and equation (A2.11a) and (A2.11b) of Appendix A2. The α_i can be detailed in a manner identical to that explained in Section 2.2 by using the assumed contact instants and periodicity in equation (3.4). On the other hand the X_i, i = 1,2, ----N, are still unknown. Coefficient b_i here and in equation (3.6a) is written already in equation (3.5a) as a function of the N of the X_i and the two other unknowns A and θ_i or, by combining the α_i in equation

(3.4) with equation (3.6b), A and τ. Therefore (N + 2) unknowns exist. They are determined by the imposition of condition (3.8) and satisfaction of identity (3.9). The particular X_{ia} in equation (3.8) is found directly in terms of the (N + 2) unknowns from equation (3.6a) applied at the contact instant t_i. The X_{ib} is determined similarly but from the counterpart of equation (3.6a) valid between the (i-1) and i rather than i and (i+1) impacts. Also the $\dot{X}_{ib}$ of relation (3.9) coincides identically with both the time derivative of equation (3.6a) at time t_i and the right-hand side of equation (3.16). Applying these two requirements for all N impacts produces 2N linear simultaneous equations in the (N + 2) unknowns. Details of the algebraic manipulations and all the resulting α_i dependent coefficients, $W1_i$ through $W6_i$ and $V1_i$ through $V7_i$, i = 1, 2---N, are supplied in Appendix 2. The 2N equations are shown to take the form

$$\left.\begin{aligned} & W2_i\, X_i + (1 - W1_i)\, X_{(i+1)} + W3_i\, X_{(i+N-1)} \\ & + W4_i\, A\cos\tau + W5_i\, A\sin\tau \end{aligned}\right\} = W6_i,\ i = 1, 2\text{----}N \qquad (3.19a)$$

$$\left.\begin{aligned} & V2_i\, X_i + V1_i\, X_{(i+1)} + V3_i\, X_{(i+2)} \\ & + V4_i\, X_{(i+N-1)} + V5_i\, A\cos\tau + V6_i\, A\sin\tau \end{aligned}\right\} = V7_i,\ i = 2\text{----}N \qquad (3.19b)$$

Exact solutions are not possible when N exceeds two (i.e. when the number of equations is larger than the number of unknowns). Then the (N + 2) unknowns of X_i where i = 1, 2,----N, the amplitude and phase factor, A and τ, were computed by using the least square fit method described in Section 2.2 [7]. If N equals two, equation (3.19a) and (3.19b) each give two equations which are independent normally. The resulting, solutions however involve very cumbersome expressions. Consequently these equations were left in the form of equation (3.19a) and (3.19b) which were solved numerically by using the IMSL library subroutine LEQT1F [45]. This subroutine solves a set of independent linear simultaneous equations by performing a Gaussian Elimination with partial pivoting [45]. Double precision arithmetic was employed throughout all numerical computations. However the two equations in both sets become essentially identical in the special case

$$\alpha_2 = \pi k \qquad \text{and } R_1 = R_2 = R \tag{3.20}$$

with k an odd integer and N still equal two. This situation is reminiscent of that observed from equation (2.23) for the Impact-Pair having two equispaced impacts/odd integer of cycles. A cycle corresponds here to a period of the prescribed external force rather than the displacement of the primary mass. Then the absolute displacement of M at the first collision, X_1, can be eliminated as before to produce a single equation in A and τ. The final equation is

identical to the one produced by Masri [53] algebraic certain change was made. Details are given in Appendix A3. It is more convenient again to calculate τ by first assuming some value for A. Unlike the Impact-Pair however only one value of k (i.e. k = 1) has been apparently considered in any detail for the vibroimpact damper.

A technique to assess the stability of any periodic motion of a vibroimpact damper will be evolved next. The technique is basically an extension of the method outlined in Section 2.2.1 for the Impact-Pair.

3.2.1 Stability

The methodology of determining the stability of general periodic motions of a vibroimpact damper is described essentially in Section 2.2.1. Therefore only major differences of detail will be reported here.

The external force is prescribed on M in the case of a vibroimpact damper as opposed to the displacement for an Impact-Pair. Consequently the absolute displacement and velocity of M, X and $\dot{X}$ respectively, are no longer constant. Therefore these additional two variables have to be perturbed initially along with the previously changeable Z and $\dot{Z}$ which describe the motion of m. Masri [59] on the other hand preferred to substitute the non-dimensional frequency parameter α_i given by equation (3.4) for the Z at collisions which

depends therefore upon the α_i. Subsequently he also systematically replaced changes at the contact times by corresponding changes just afterwards. However the end result is no different [2, 59]. The cause and effect relationship between the initial perturbation and subsequent changes still takes the form

$$\begin{Bmatrix} \Delta X_{(N+1)+} \\ \Delta \dot{X}_{(n+1)+} \\ \Delta \dot{Z}_{(N+1)+} \\ \Delta \alpha_{(N+1)+} \end{Bmatrix} = [P] \begin{Bmatrix} \Delta X_{1+} \\ \Delta \dot{X}_{1+} \\ \Delta \dot{Z}_{1+} \\ \Delta \alpha_{1+} \end{Bmatrix} \tag{3.20a}$$

which is analogous to equation (2.30a). Matrix [P] is given by

$$[P] = [P_{N+}]\,[P_{(N-1)+}]\text{----}[P_{1+}] \tag{3.20b}$$

where the typical $[P_{i+}]$ is now a 4 x 4 rather than the 2 x 2 matrix of before to accommodate the two additional variables X_{i+} and $\dot{X}_{i+}$.

Masri [59] derived explicit expressions for all representative components P_{i+} (p, q) of $[P_{i+}]$. He assumed again that corresponding products are negligible compared to all terms typically involving ΔX_{i+}, $\Delta \dot{X}_{i+}$, $\Delta \dot{Z}_{i+}$ and $\Delta \alpha_{i+}$ and that coefficients of restitution are invariably constant. The expressions were checked and modified to

incorporate possible changes in the coefficients of restitution. They are given more conveniently in Appendix A2. A periodic motion of the damper is asymptotically stable if and only if all the modulii of the eigenvalues of [P] in equation (3.20b) are again strictly less than unity. Computational details were described in Section 2.2.1 and will not be repeated here.

3.3 Checking the General Theory

Motions involving two equispaced impacts per cycle of sinusoidal force have been primarily studied previously [1, 2, 49-56, 61]. Much less theoretical data has been published for two unequispaced impacts/cycle [57, 59] and the result of only one, probably analog computed illustration of three impacts/cycle is available [59]. However these few examples which relate to specific vibroimpact dampers should form an adequate basis for checking the general theory of N impacts/cycle. Computations were performed for the general theory by using double precision arithmetic on an AMDAHL V7 digital computer. Single precision arithmetic which presumably is less accurate have been employed elsewhere [53].

A resulting comparison of the stability zone of two equispaced impacts/cycle predicted for a particular damper is illustrated in Figure 3.3. The convention will be adopted of giving damper characteristics (ξ, m/M, R_1 and R_2, etc.) in the upper right-hand corner of a figure. Differences

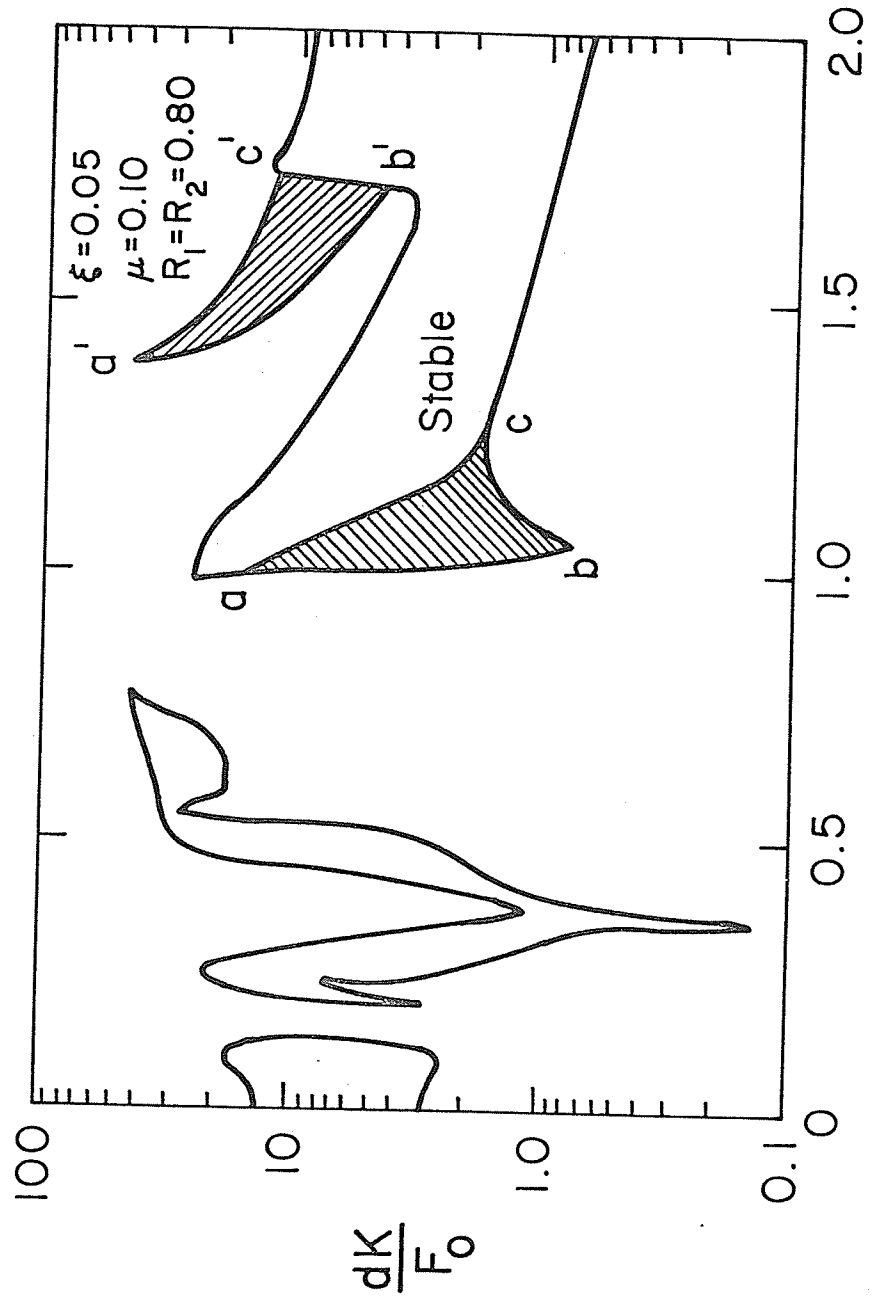

Figure 3.3. Comparison of uncorrected previous stability zone [53] and the special results of two equispaced impacts/cycle from general theory. Differences are indicated by the hatched regions abc and a'b'c'.

Parameters of primary and secondary system $\xi = 0.005$, $r = 0.94$, $\mu = 0.042$, $R_1 = R_2 = 0.75$, $\frac{d}{F_o/K} = 37$						
	2 equispaced[+]		2 equispaced		2 unequispaced	
	Present results	Previous results	Present results	Previous results	Present results	Previous results
α_2/π	1	1	1	1	1.37	1.37
$\Omega t_1/\pi$	0.68	0.68	-0.53	-0.53	0.52	0.52
τ/π	0.66	0.65	-0.56	-0.55	0.50	0.49
X_1	16.17	16.21	-5.10	-5.07	13.65	13.76
X_2	-16.17	-16.21	5.10	5.07	-9.31	-9.37
Z_1	34.67	34.71	13.41	13.42	32.15	32.26
Z_2	-34.67	-34.71	-13.41	-13.42	-27.81	-27.87
$\dot{X}_{ia}$	-2.22	-2.22	-0.86	-0.85	5.47	5.56
$\dot{X}_{2a}$	2.22	2.22	0.86	0.85	9.81	10.03
$\dot{X}_{1b}$	-3.96	-3.96	-1.53	-1.53	3.73	3.80
$\dot{X}_{2b}$	3.96	3.96	1.53	1.53	11.66	11.78
$\dot{Z}_{1a}$	-20.74	-20.77	-8.02	-8.03	-13.09	-13.10
$\dot{Z}_{2a}$	20.74	20.77	8.02	8.03	28.48	28.69
X_{max}	-16.67, 16.67	-16.72, 16.72	-5.18, 5.18	-5.16, 5.16	-15.17, 14.77	-15.32, 13.79
Modulus of eigenvalues of [P]	3.83	4.02	12.08	12.15	0.93	0.93
	0.95	0.77	0.99	0.69	0.93	0.93
	0.95	0.52	0.99	0.43	0.58	0.58
	0.09	0.03	0.25	0.01	0.58	0.58
Stability	Unstable	Unstable	Unstable	Unstable	Stable	Stable

[+]Impacts/cycle is implied.

Table 3.1. A numerical comparison of previous [59] and present theoretical results for two equispaced and two unequispaced impacts/cycle.

between results from the general theory and those of Masri [54] are indicated in Figure 3.3 by the relatively small hatched region abc and a'b'c'. Region abc is replaced by region a'b'c' and other areas are slightly affected when the general theory is applied. A close examination of Masri's theoretical development revealed that this slight discrepancy is caused largely by an algebraic mistake which is explained in Appendix A3. Similar differences exist in the stability governing eigenvalue modulii of the analogous two equispaced impacts/cycle cases presented in Table 3.1. They are eliminated correctly however in the two unequispaced impacts/cycle situation indicated in this table because the mistake does not then apply. The sole major fluctuation in this instance, the change in the otherwise strongly tallying X_{max}, is most probably a printing error in the 13.79. Finally the initial four columns of Table 3.1 suggest that although the values of α_2/π, $\Omega t_1/\pi$,---- and X_{max} may be very close, significant differences can arise in the stability eigenvalues. Therefore it is quite feasible that subtle variations stemming from the use of either single or double precision arithmetic, say, may lead to opposite conclusions regarding stability. The latter situation is most likely to arise when the true maximum eigenvalue modulus is near unity or, in other words, at a position close to a stability boundary. This point will be expanded later.

An additional comparison is given in Figure 3.4 of the results from the degeneration of the general theory into two unequispaced

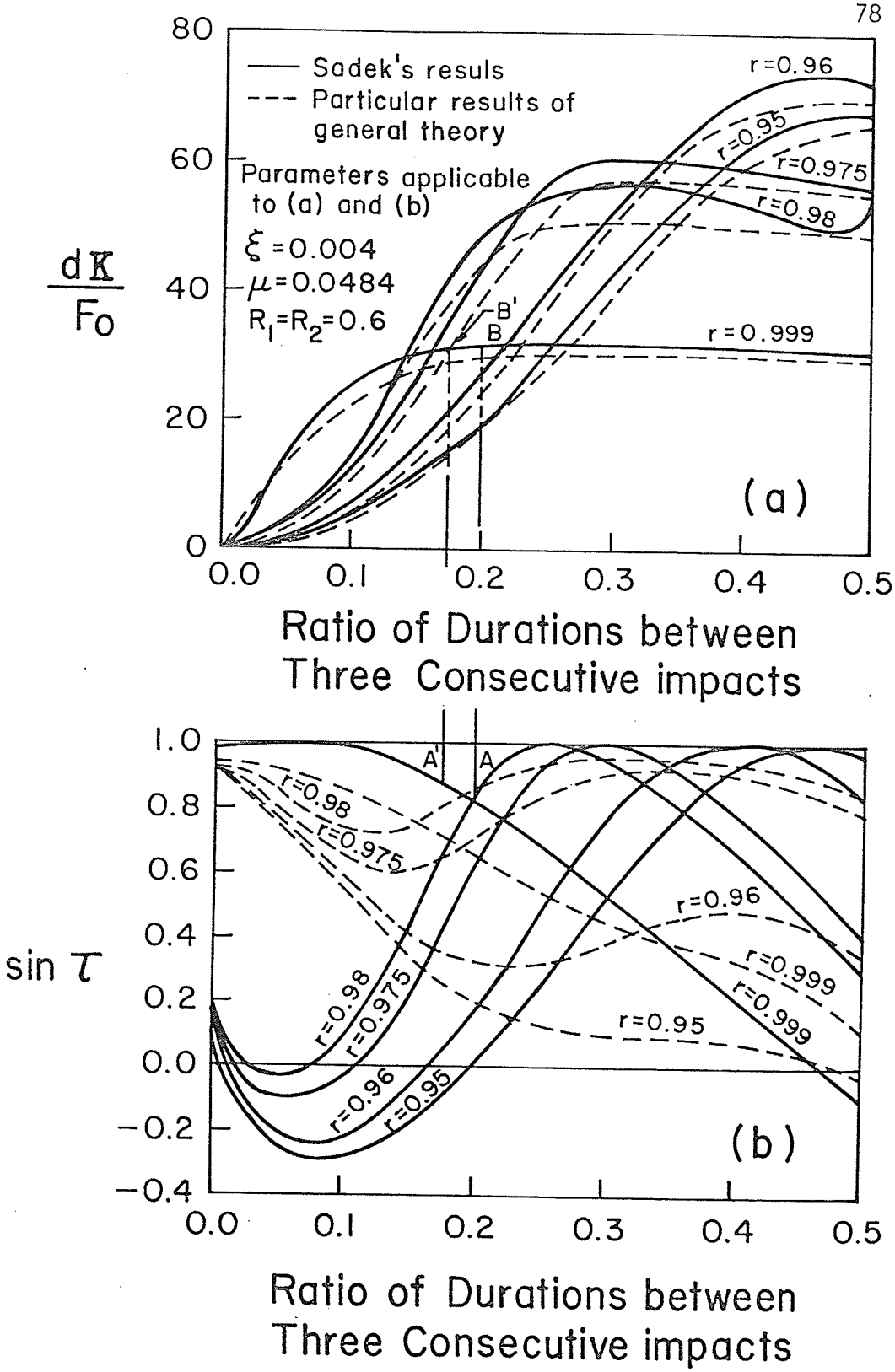

Figure 3.4. Comparison of two unequispaced impacts/cycle theoretical results with those of Sadek [57]. Both data sets were computed without regard for stability.

impacts/cycle and those from a Fourier series approach proposed by Sadek [57]. Sadek disregarded the question of stability so that the information is presented without such a determination. Figure 3.4(a) indicates that values of $d/(F_o/K)$ correlate closely whereas large differences occur generally in Figure 3.4(b) for $\sin\tau$ at frequency ratios, r, near one. These particular differences are not surprising in view of the demonstrated substantial agreement with the work of Masri who, in an unresolved dispute, questioned the validity of Sakek's results [59]. A detailed examination of Sadek's theory indicates that the velocity discontinuity of the primary mass at an impact is treated improperly. Consequently equation (13) of reference 57 implies that the phase angle τ is independent of the amplitude F_o of the external force. This assertion is refuted clearly by Sadek's own evidence presented unadulterated as the solid curves of Figure 3.4. An independent increase in F_o reduces $d/(F_o/K)$ but the frequency ratio, r, remains unaltered at a value, for example, of 0.999. Consequently point B is transposed leftward along the dashed curve $r = 0.999$ to position B' say if the periodic motion, despite a change in the ratio of durations, is still to consist of two unequispaced impacts/cycle. Points B and B' respectively correspond to points A and A' in Figure 3.4(b) which obviously relate to different τ.

The only previous example of three impacts/cycle stable periodic motion [59] is presented as point 'a' in Figure 3.5. Masri also illustrated for the particular damper indicated special cases of the

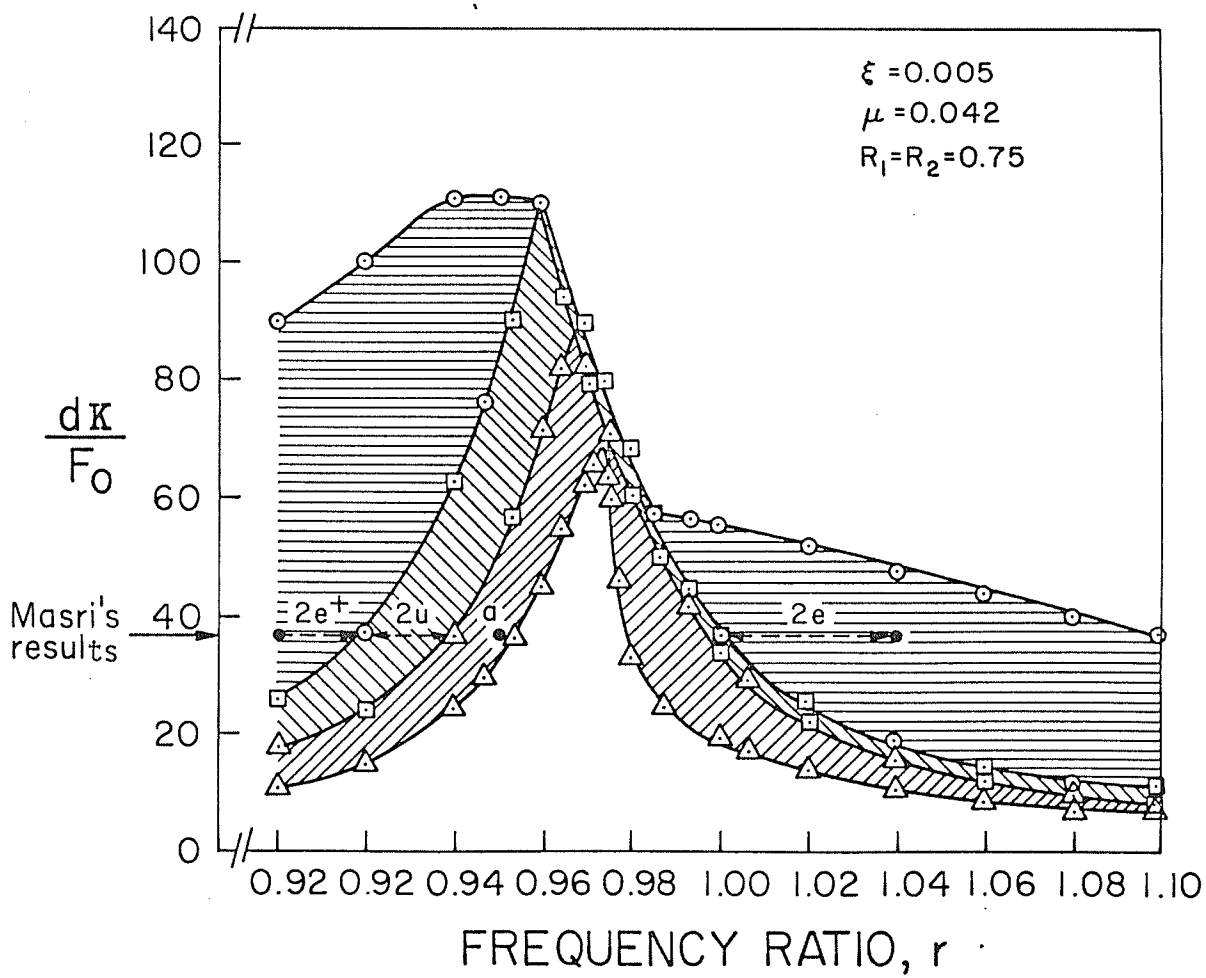

Figure 3.5. Comparison of predicted two equispaced, two unequispaced and three impacts/cycle stability zones with the previously most comprehensive results at d = 37 (F_o/K) alone. ... Masri's results [59] otherwise usual notation is employed for general theory.

+Implies equispaced, e, or unequispaced, u, impacts/cycle.

stability of two equispaced and two unequispaced impacts/cycle. His results therefore correspond to the single point 'a' and the dashed lines along $dK/F_0 = 37$. The much more comprehensive continuous curves in this figure emanate from analogous computations based upon the general theory. These two sets of results agree completely along $dK/F_0 = 37$ except in the very narrow two unequispaced impacts/cycle zone near $r = 1$ and the two equispaced impact/cycle zone but only when r is greater than 1.04. The disagreement in the equispaced zone, occurring as in Figure 3.3 when $r > 1$, likely stems again from the discrepancy discussed in Appendix A3. The complete omission by Masri of the two unequispaced impacts/cycle zone on the other hand arises most probably from slightly less accurate computations. Similar small differences have been seen previously to produce opposite views of stability when, as here, stability boundaries are extremely close. Finally, it should be observed that point 'a', the sole three impacts/cycle example, certainly falls within the corresponding stability zone obtained from the general theory.

In summary, the general theory has been shown to agree quite well with the sparse theoretical results of Masri. The reasons for discrepancies with Masri's as well as Sadek's work have been given However, the incongruences are disturbing so that further verification was considered prudent. Consequently, additional comparisons were sought with experimental data. This entailed the building of mechanical systems to simulate as far as possible the idealised model shown in

Figure 3.1. Precautions taken to ensure a reasonable simulation are described in the following section.

3.4 Details of the Experiment

The experimental model and measuring equipment are displayed in Figure 3.6 with additional details shown in Figure 3.7. The primary system consists of the previous, rigid slotted mass cantilevered from essentially the concrete base rather than the shaker. Two cantilivers were composed of two flexible, spring steel strips interposed by a very still but light hollow beam. Tightened screws and bolts were used to connect structural components to ensure, as far as possible, that the primary system moved integrally. It is practically impossible to prevent all such relative motions, however some friction developed at the joints. The ensuing dissipation was found from conventional free decay and sinusoidal resonance tests [5] to be equivalent to a viscous damping ratio, ξ, of 0.0114 ± 0.0005. The first and second natural frequencies of the primary system alone were found to be 19.87 ± 0.03 Hz. and 430 ± 2 Hs. from solely the resonance tests. Standard checks of the amplitude and phase of the displacement of the primary system to those contemplated for the external sinusoidal force indicated good linearity. Therefore this system fairly represents a linear oscillator over the limited frequency range of 10 to 50 Hz. employed in the vibroimpact experiments. Also, the length 12.0 ± 0.8 in. of the vertical supports ensured that the primary mass, in conjunction

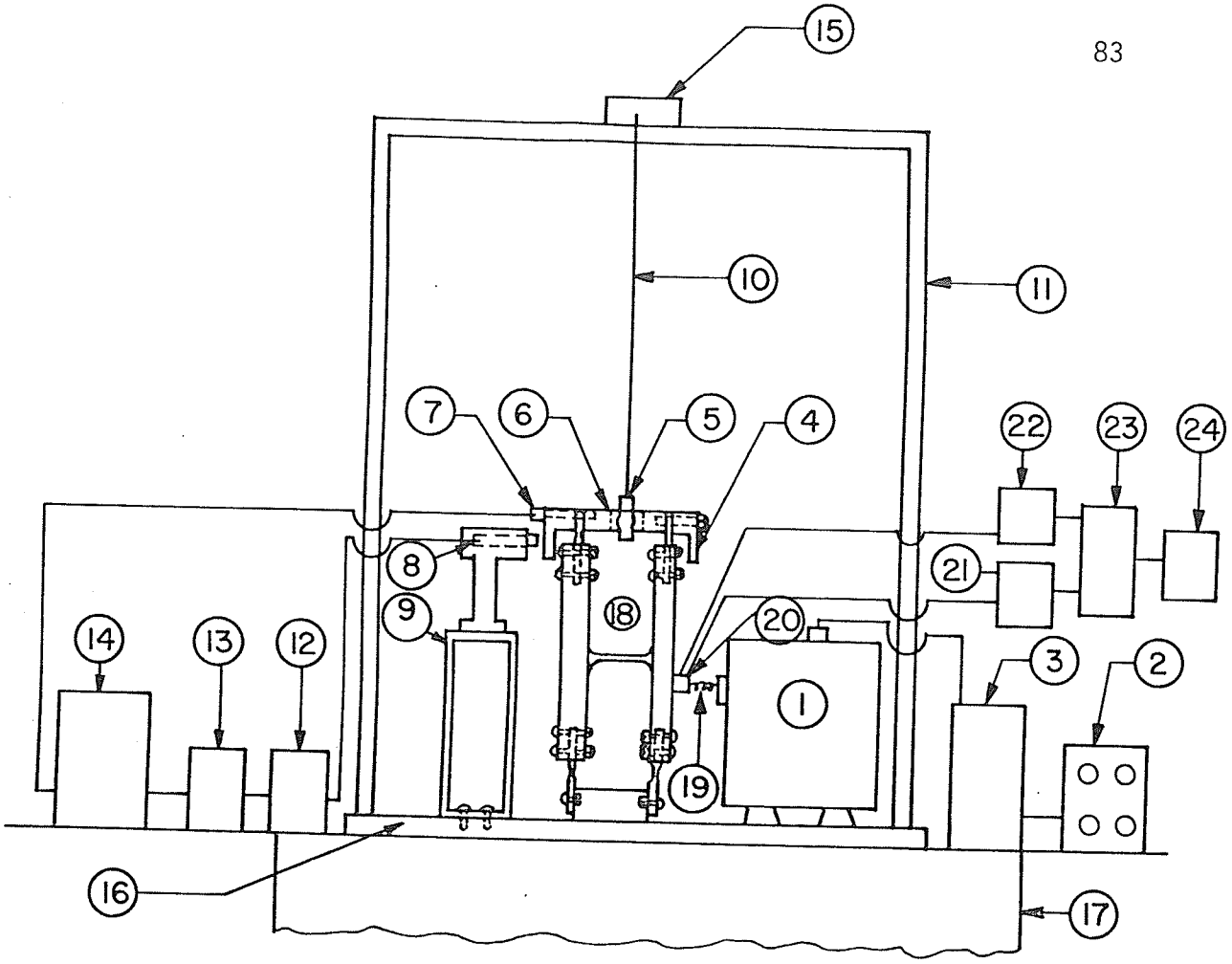

Figure 3.6. Details of the experimental apparatus and instrumentation.

Key:

(1) Electromagnetic shaker, Ling Model 400. Series 192

(2) Hewlett-Packard Function Generator 3110B

(3) Amplifier Ling Model PA300

(4) Aluminum adapter

(5) Secondary mass made from either steel or brass

(6) Slotted primary mass of die tool steel

(7) Bruel & Kjaer accelerometer Type 4333.

(8) Wayne Kerr capacitance transducer

(9) Support for capacitance probe

(10) Two-light cotton threads

(11) Solid frame

(12) Wayne-Kerr feedback amplifier TE MK II

(13) Hewlett-Packard multimeter 5306A

(14) Tektronix double beam storage oscilloscope 7313

(15) Adjusting mechanism

(16) Cold rolled plate

(17) Heavy concrete block

(18) Hollow beams

(19) Weak spring

(20) Bruel & Kjaer Impedance Head, Type 8000

(21) Bruel & Kjaer mass compensation unit Type 5565

(22) Bruel & Kjaer conditioning amplifier Type 2626

(23) Bruel & Kjaer mass compensation unit Type 5565

(24) Hewlett-Packard multimeter 5306A

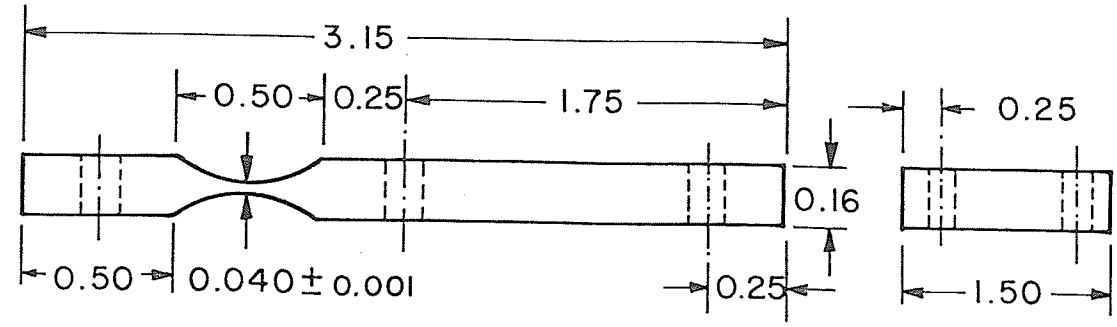

(a) Spring steel strip

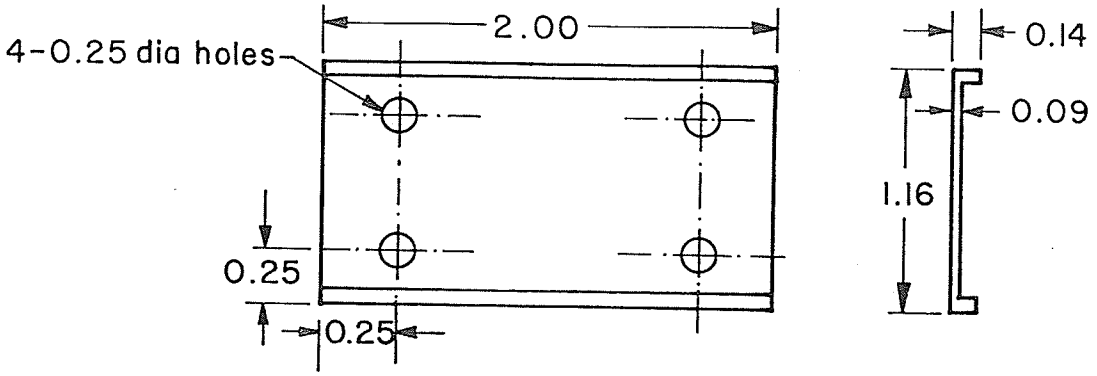

(b) Spacer

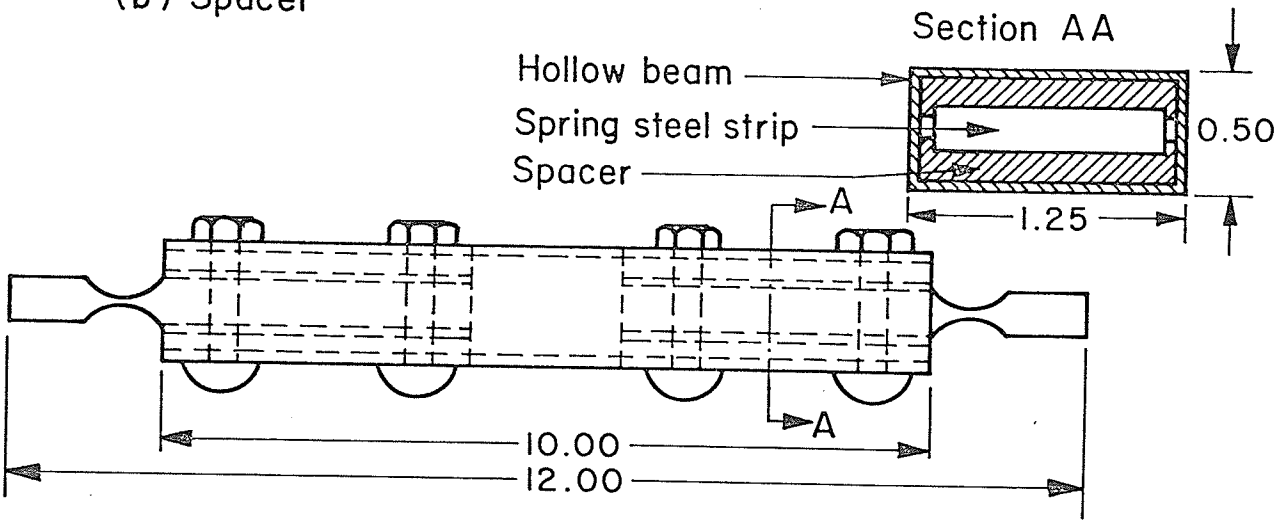

(c) Hollow beam

All dimensions are in inches and those tolerances not specified are ± 0.01 inches.

Figure 3.7. Details of spring steel strip, spacer and hollow beam.

with the secondary, never moved more than 0.38° ± 0.05° from the vertical. Consequently gravitational effects were neglected. These same supports were also much stiffer in torsion than flexure so that the experimental primary mass should travel unidirectionally like the theoretical model. Secondary masses, described already in Section 2.3, have been shown previously to move virtually freely and unidirectionally too.

The primary system was connected as shown in Figure 3.6 through an impedance head and spring to the electromagnetic shaker. This spring was much weaker than the primary system's effective stiffness so that a force rather than a displacement-like input was obtained. The sinusoidally time varying input, generated to within 2% of the nominal amplitude, was monitored with the aid of the directly coupled impedance head. Compensation for the extraneous mass of this head was achieved by employing the electrical compensation circuit recommended by its manufacturer [83]. Precautions taken to avoid disturbances from building vibrations have been explained in Chapter 2. The absolute displacement and acceleration were measured as before at essentially the "free" end of the cantilevered primary system. Displacements were determined relative to a light aluminium bracket attached rigidly to the slotted mass. An identical bracket was fixed similarly to the other side of this mass to maintain symmetry and prevent unbalance. Measurement procedures were the same as in Chapter 3. However the evaluation of the stability zones of the damper with high

periodic impact numbers was restricted by the limited force capability of the shaker [84]. Only those experimental results will be presented for which the mechancial model was deemed a reasonable representation of the idealised vibroimpact damper.

3.5 Comparison of Experimental and Theoretical Results

Experimental and theoretical results are reported in Figure 3.8 through 3.11 and also in Figure 3.12 and 3.13 for impact dampers with equal and unequal coefficients of restitution respectively. The format used in these figures is similar to that employed previously for an Impact-Pair. The major difference is that the 2A in the former 2A/d stability ordinate is replaced by the standard "static" deflection of the primary system, F_o/K. Frequency and the conventional frequency ratio Ω/ω, or r, form basically the same stability abscissa because ω was taken as a constant 19.87 Hz. Data is given only for a sinusoidal loading frequency Ω of 12 to 27 Hz. This range adequately encompasses the primary interest of the damper's behaviour at the natural frequency, ω, of the primary system alone. Nomenclature, symbols and the lettering notation used to relate time histories to corresponding points of a stability chart are identical to before. Parameters employed theoretically are given specificially at the top of a pertinent figure.

The mature stainless steel secondary mass solely was employed experimentally. Unequal coefficients of restitution were obtained as before by taping one impact surface of the otherwise invariant stainless steel primary mass. Computations were performed by utilising measured values for all passive components and the dynamic characteristics of the sinusoidal loading. The method of determining the passive components of that equivalent oscillator which fairly describes the

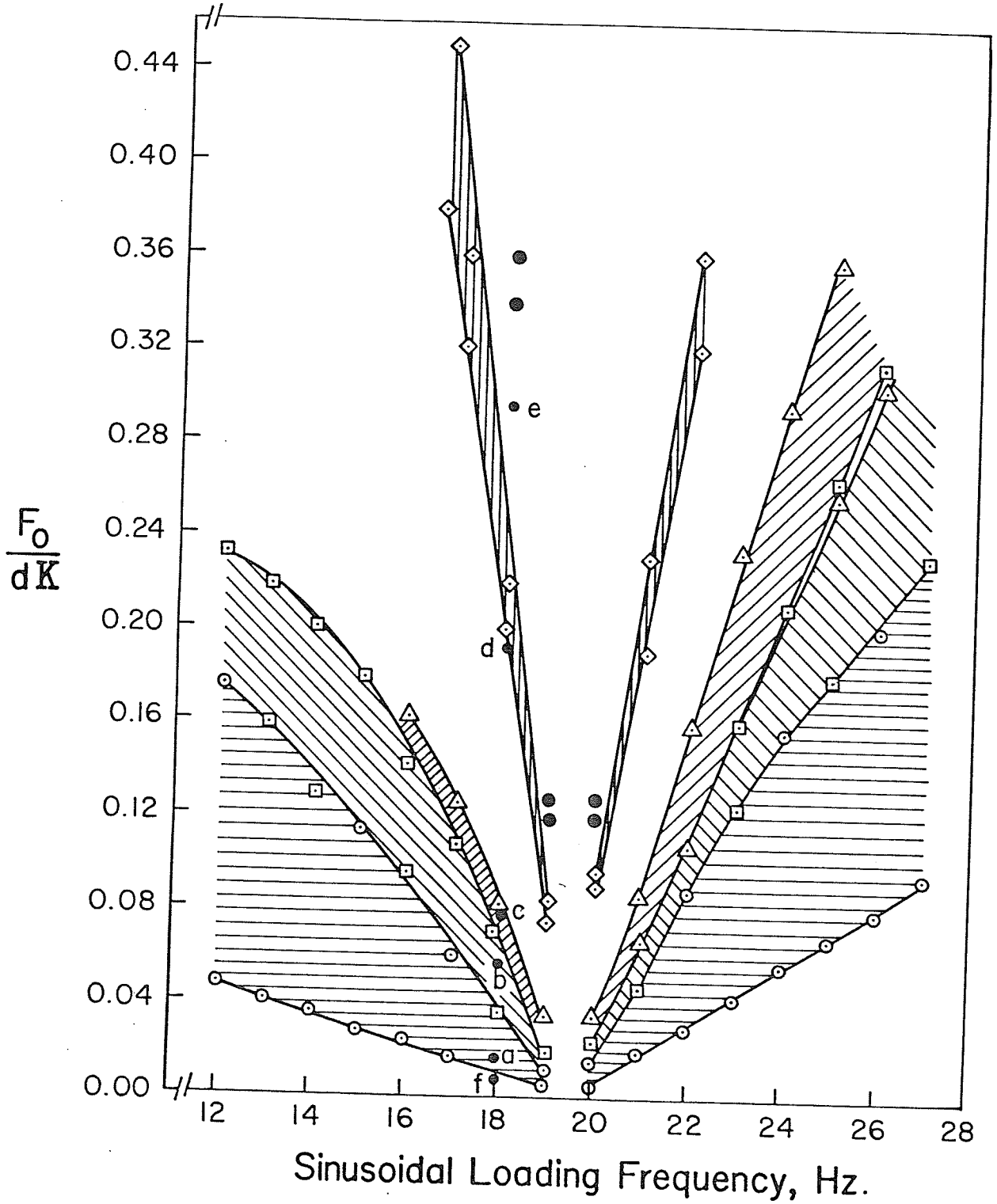

Figure 3.8. Stability zones of experimental periodic motions with identical coefficients of restitution. Gap size is 0.0105 $\pm$ 0.0005 in.

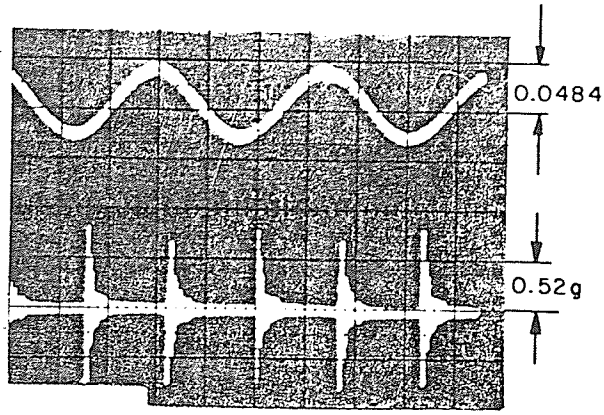

(a) Two equispaced impacts/cycle

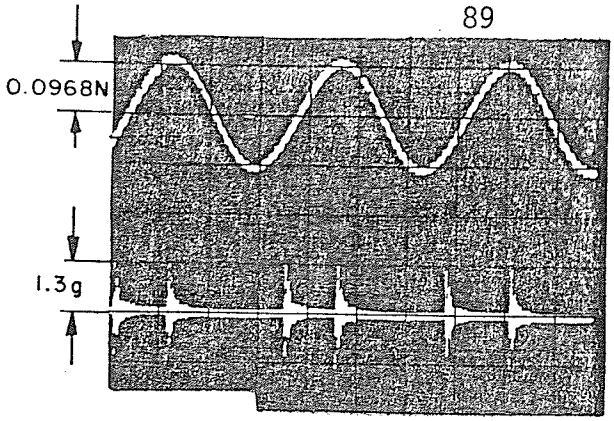

(b) Two unequispaced impacts/cycle

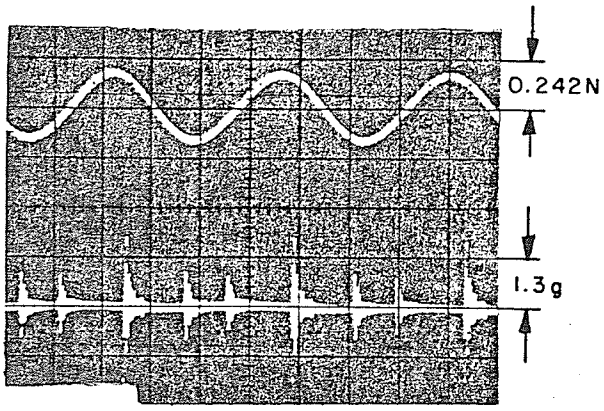

(c) Three impacts/cycle

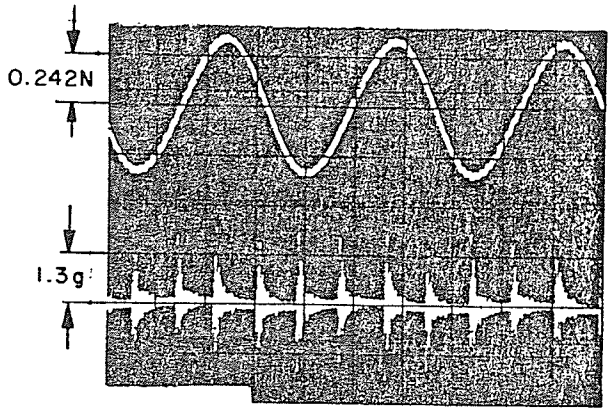

(d) Four impacts/cycle

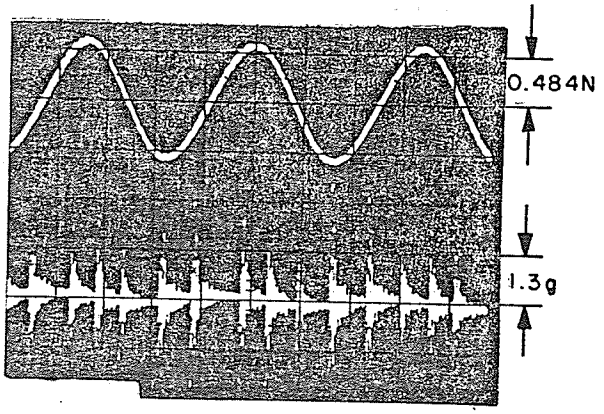

(e) Five impacts/cycle

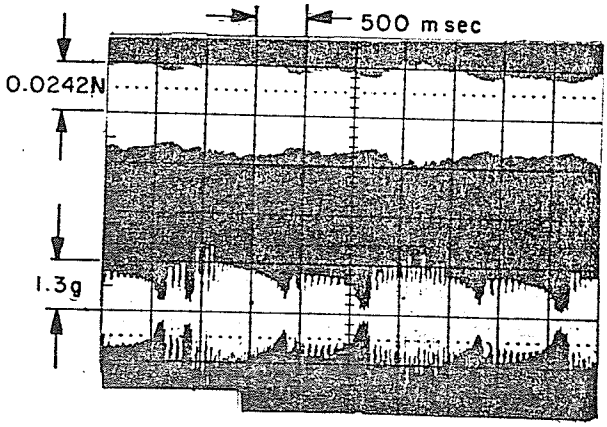

(f) Beating motion

Horizontal time scale is 16.7 msec./division

Figure 3.9. Typical experimental motions of the primary mass when the impact damper has equal coefficients of restitution. Top and bottom traces in all figures represent prescribed force and absolute acceleration of primary mass, respectively.

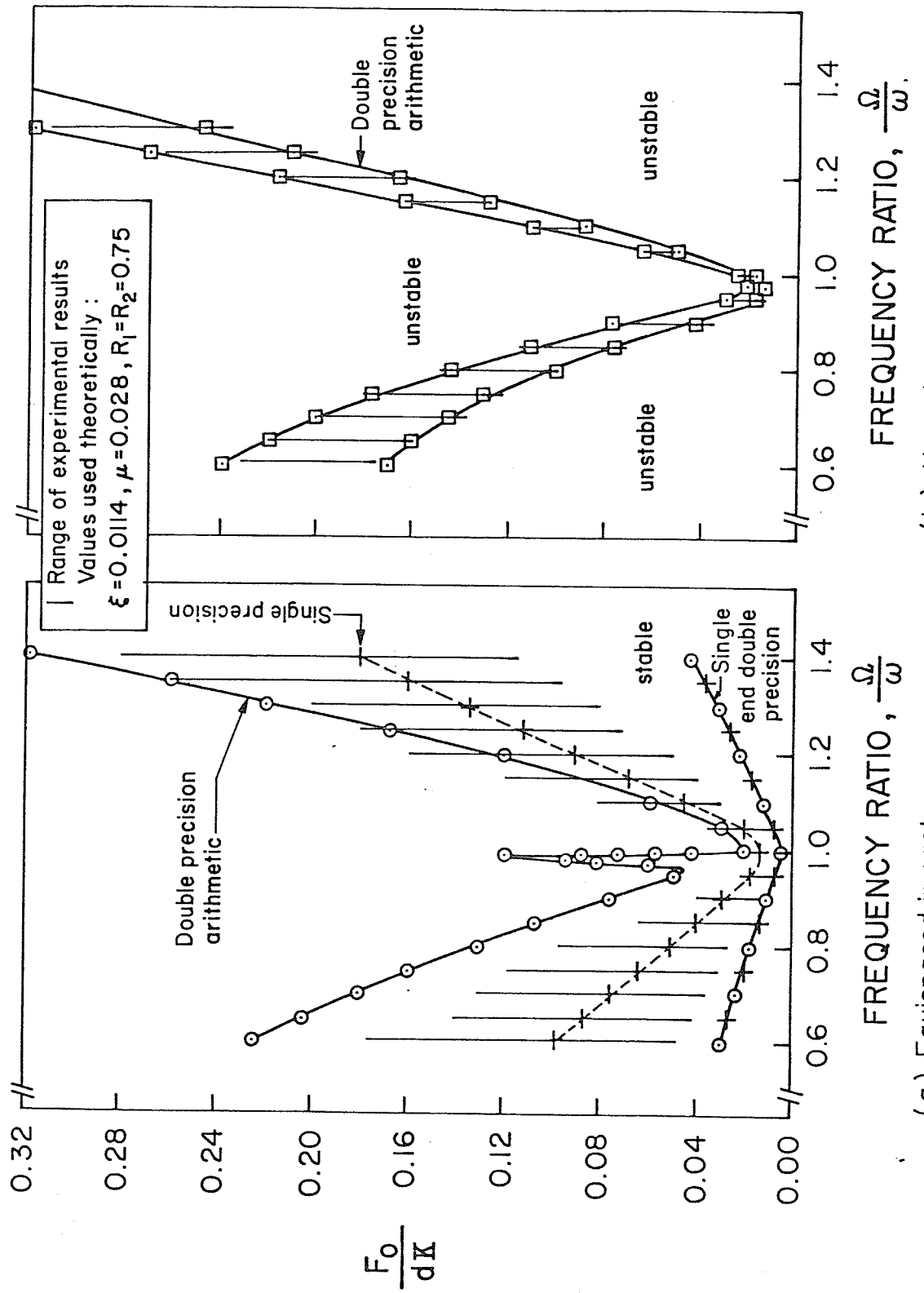

Figure 3.10. Comparison of experimental and theoretical stability zones for two impacts/cycle with identical coefficients of restitution. Gap size is 0.0105 ± 0.0005 in.

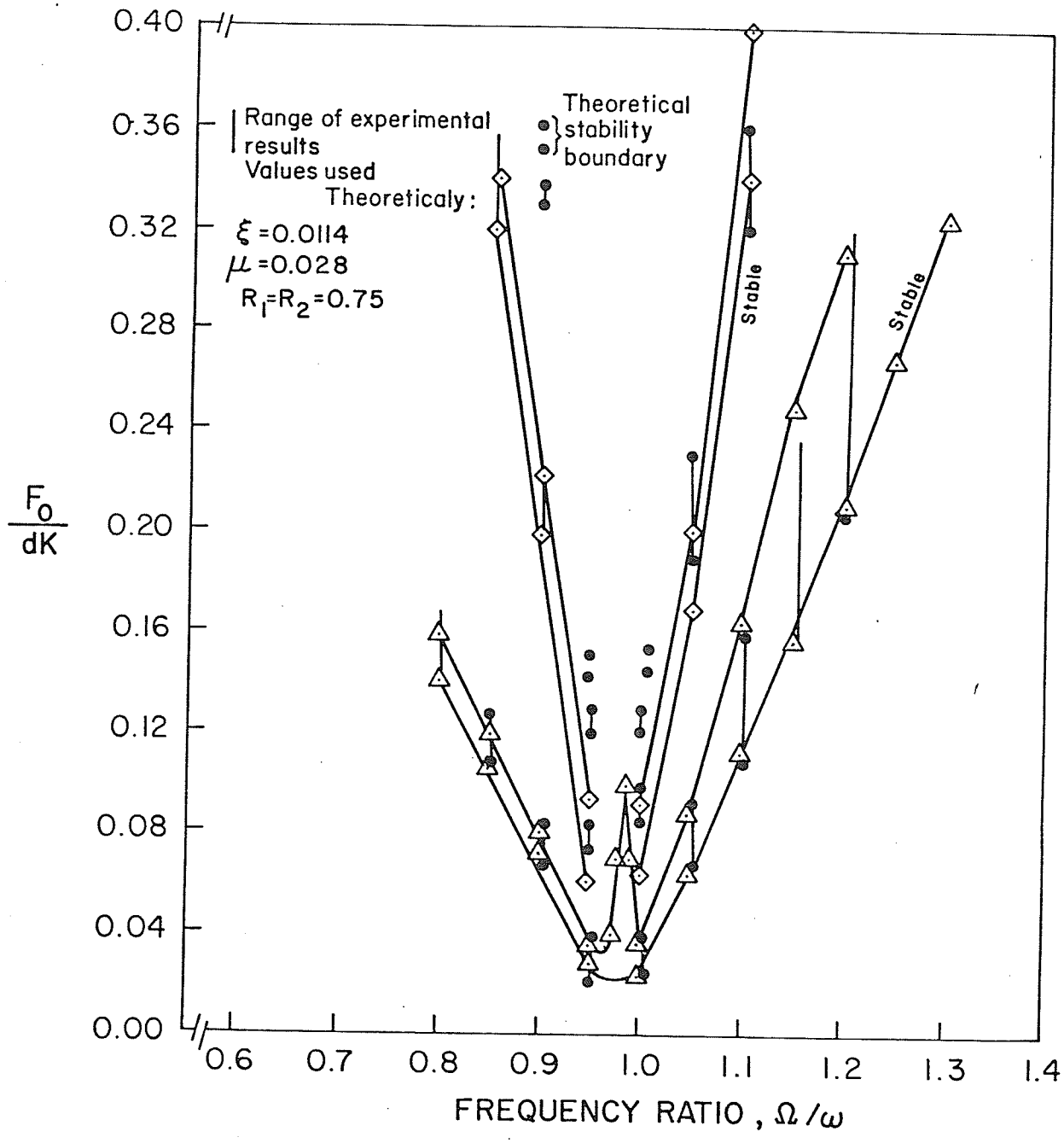

Figure 3.11. Comparision of experimental and theoretical stability zones for three, four and five impacts/cycle with identical coefficients of restitution. Gap size is 0.0105 $\pm$ 0.0005 in.

basic nature of the primary system is given in Appendix A5. Any one coefficient of restitution was assumed constant and identical again to the arithmetically averaged extremes of the observed values. This procedure generally produced reasonable stability correlations for the seasoned stainless steel Impact-Pair.

3.5.1 Identical Coefficients of Restitution

The impact damper's experimentally determined stability zones in Figure 3.8 are much more sensitive to variations in the driving frequency than the comparable zones of an Impact-Pair. This sensitivity seemed particularly keen around the natural frequency 19.87 Hz. of the primary system acting alone. The complementary narrowing of all stability zones around this frequency made the correspondingly required finer control of the amplitude of the prescribed force. Consequently, no experimental data could be given in this narrow but crucial region. Similar difficulties have been encountered previously in the study of two impacts/cycle stability zones [51].

Time histories at the points designated by the letters in Figure 3.8 are displayed correspondingly in Figure 3.9. Except for the beating motion of Figure 3.9(f), the time displays are similar to those of the analogous Impact-Pair. The beating can be seen from Figure 3.9 to occur when the frequency of the sinusoidal loading

differed slightly from the natural frequency of the primary system acting alone.

Theoretical results are presented as continuous curves in Figure 3.10 and 3.11 whereas the vertical lines correspond to the experimental data of Figure 3.8. Stability zones for two impacts/cycle are separated to improve clarity. Experimental determination of the stable five impacts/cycle boundaries was impaired by the restricted forcing amplitude of the electromagnetic shaker. Consequently these experimental data points, shown in this instance alone as vertical lines with end dots, are few in number.

Figures 3.10 and 3.11 indicate that the experimental and theoretical results generally agree well. The largest differences seem to occur in the two highest numbered, four and five impacts/cycle, stability zones again and, somewhat surprisingly, in the case of two equispaced impacts/cycle. A closer inspection of the latter stability zone revealed that the maximum absolute eigenvalue of [P] in equation (3.20b) varied between 0.996 and 0.999 in this zone. It has been seen already from Table 3.1 that minor differences in the computation of a periodic motion may substantially alter the eigenvalues. Even a slight change in this instance may change the conclusion regarding stability. Computations were repeated by using single rather than the otherwise employed double precision arithmetic to illustrate this particular point. The resulting clear

differences which happen in the upper two equispaced impacts/cycle stability boundary alone are displayed in Figure 3.10(a). Double precision arithmetic produces values which seem to correlate better generally with the upper experimental stability boundary. However it also gives an unusually substantial and inexplicable blip around Ω/ω of one. Further investigations are needed to experimentally verify this observation and to assess the accumulated error in the maximum absolute eigenvalue stemming from the propagation of small computational inaccuracies.

Sources of experimental error additional to those described for the Impact-Pair are the extra weak spring coupling and the possible excitation of more than one structural mode of the primary system. The probable non-linearity of the spring at the largest forcing amplitudes may affect somewhat the highest numbered impact zones. At the smallest forcing amplitudes conversely, the coupling between shaker and primary system became more noticeable. Consequently it was more difficult to control the forcing amplitude particularly close to a Ω/ω of one. Problems of interactions between different modes of the primary system should be ameliorated by the more restricted frequency span than that covered for the Impact-Pair. The uppermost frequency of 27 Hz. was much smaller than the frequency of about 430 Hz. for the second, lightly damped mode. Therefore none of these additional factors should be expected to degrade seriously the

cumulative error observed for the seasoned Impact-Pair. Consequently the generally comparable experimental and theoretical differences to those noted for the Impact-Pair should not be surprising. The most major discrepancies in the four and five impacts/cycle stability zones were probably still largely caused by superfluous lifting of the secondary mass.

3.5.2 Unequal Coefficients of Restitution

Experimental and theoretical stability zones for unequal rather than equal coefficients of restitution are displayed in Figure 3.12(a). Figure 3.12(b) presents those experimental zones involving many rapid impacts on the tape. They are analogous to the sliding-like cases observed for the Impact-Pair with unequal restitution coefficients. Consequently the presently developed theory is inapplicable. Otherwise the agreement between experiment and theory appears reasonable although somewhat poorer than for equal coefficients. Stable equispaced impacts were,predictably, not found.

3.5.3 Performance of an Impact Damper

Selective,stable,periodic motions shown previously are presented again in Figure 3.14. The form of this figure is more amenable to the assessment of the practically important, impact damper's ability to attenuate the displacement amplitude at frequencies near

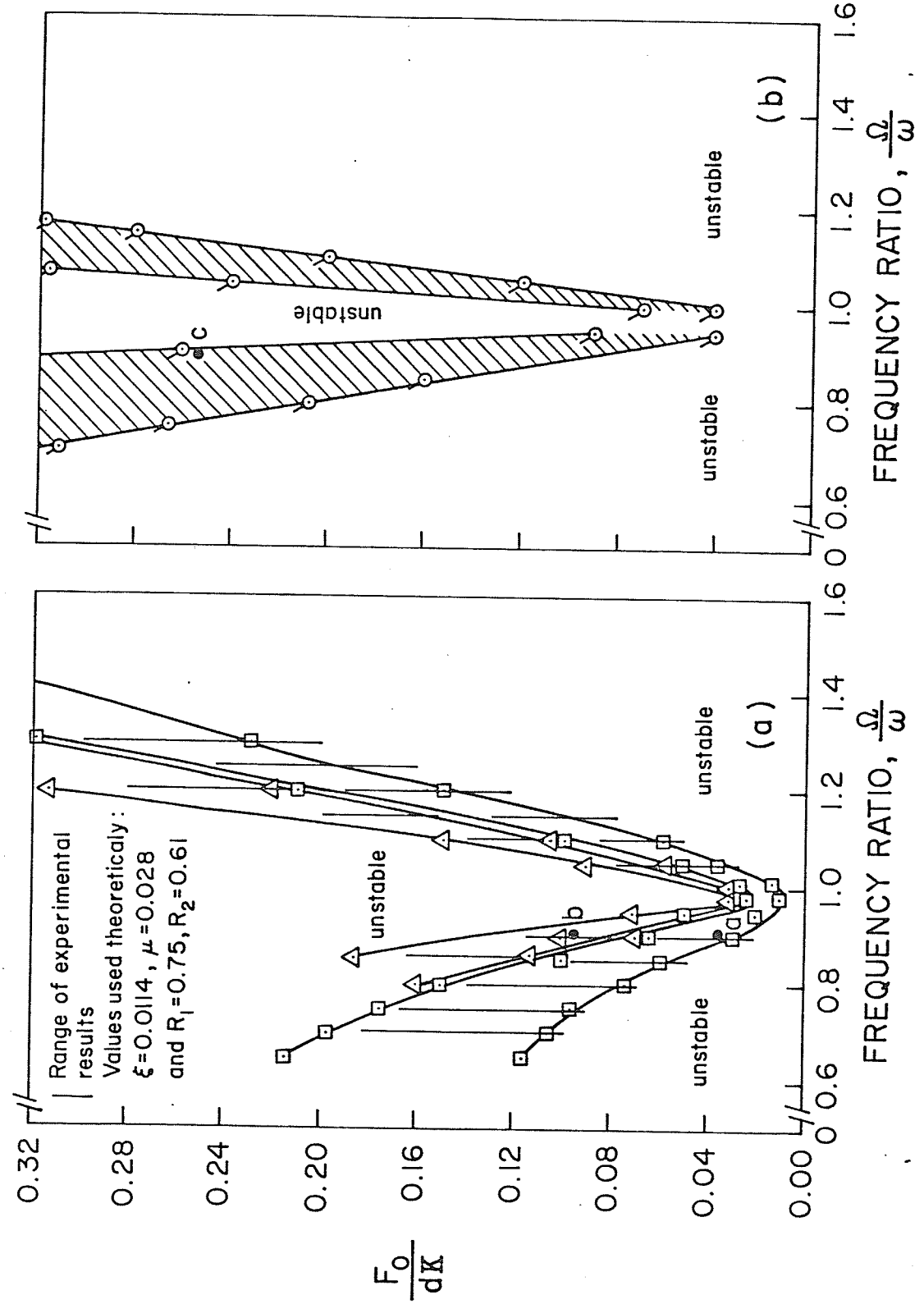

Figure 3.12. Comparison of (a) experimental and theoretical stability zones for (a) two and three impacts/cycle and (b) experimental stability zone of sliding-like phenomenon. Coefficients of restitution are unequal and the gap size is 0.0081 ± 0.0005 in.

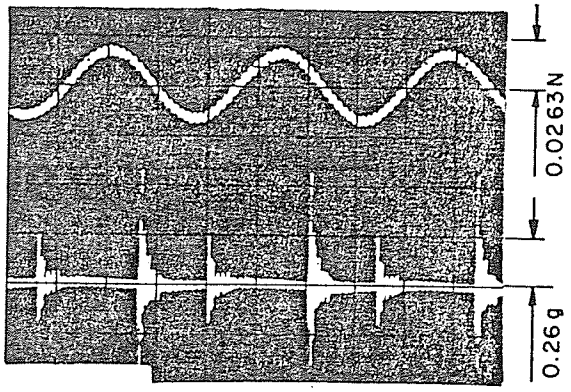

(a) Two unequispaced impacts/cycle with one impact on steel and one on tape

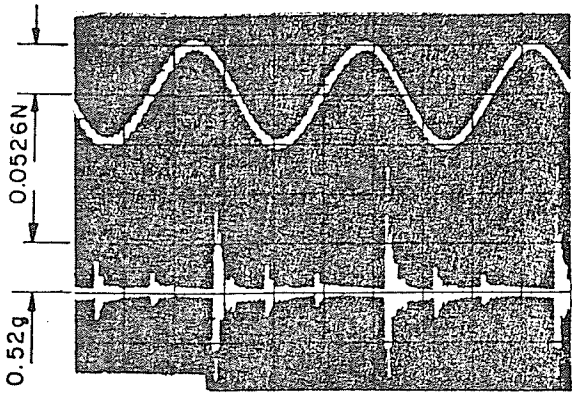

(b) Three impacts/cycle with one impact on steel and two on tape

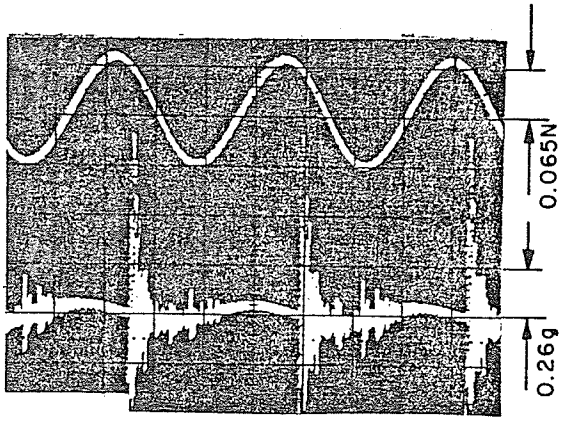

(c) One impact on steel and many on tape

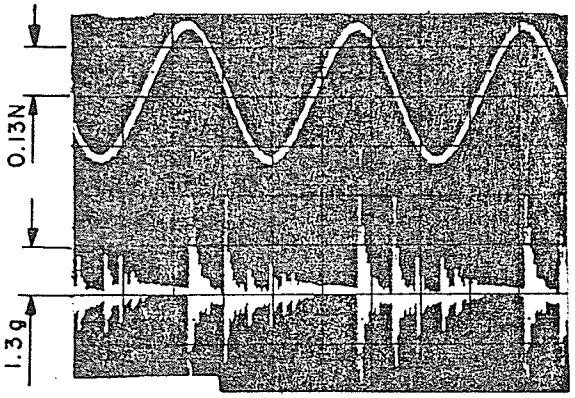

(d) Two impacts on steel and many on tape

Horizontal time scale is 16.7 msec./division

Figure 3.13. Typical experimental motions of primary mass when the impact damper has unequal coefficients of restitution. Top and bottom trace in all figures represent prescribed force and absolute acceleration of primary mass, respectively.

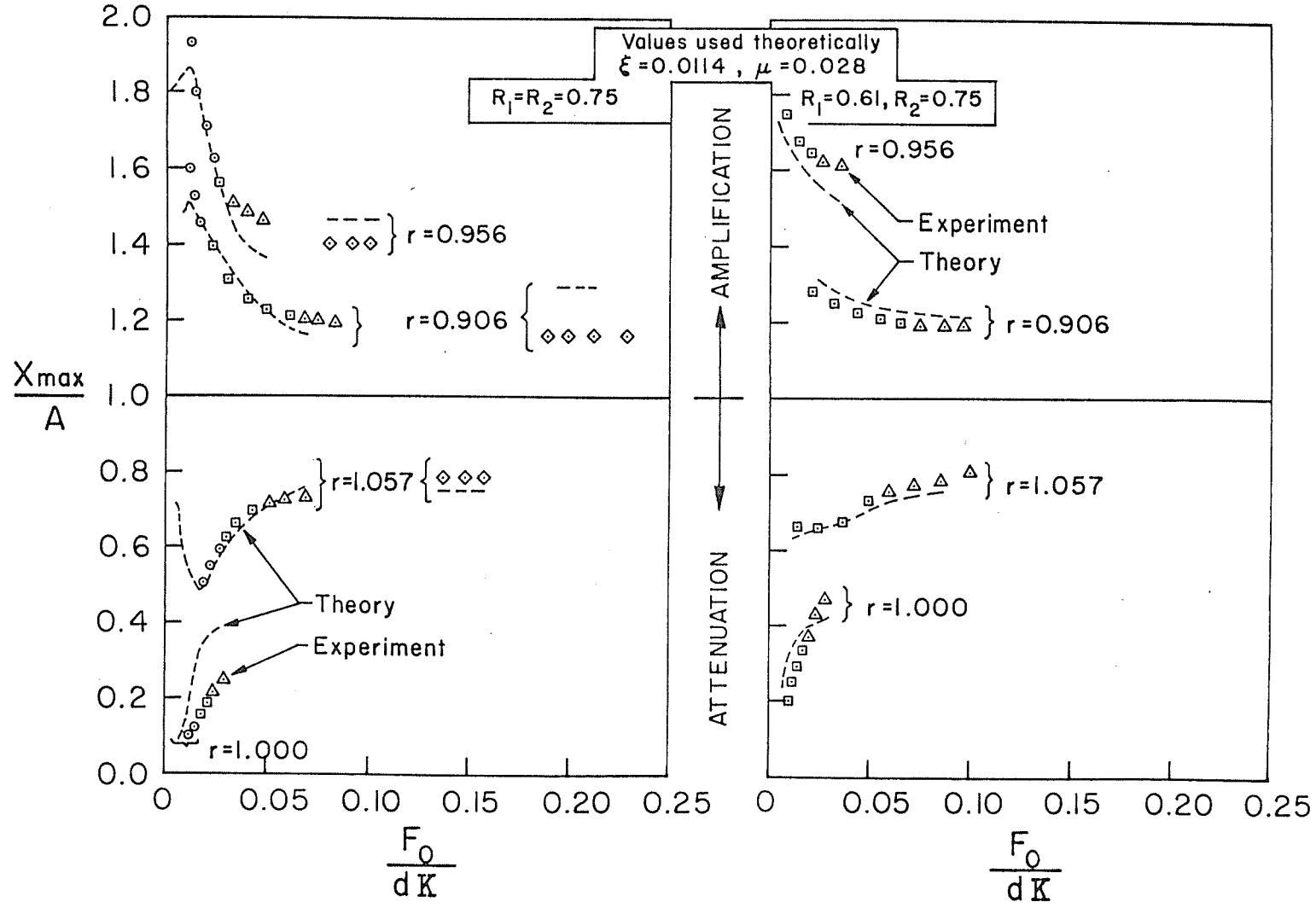

Figure 3.14. Comparision of the theoretical and experimental displacement performance of an impact damper with (a) identical coefficients and (b) different coefficients of restitution.

the resonant frequency, ω, of the single primary system. Attenuations happen when X_{max}/A, the ratio of the maximum deflection of the primary system with and without the damper, is less than unity. Amplification occurs conversely when this ratio is greater than one which is generally considered detrimental. Both experimental and theoretical data is shown for which the two coefficients of restitution are either equal or have the largest observed difference. Results are limited to those experimental frequency ratios r (Ω/ω) closest to one.

Figure 3.14 indicates that the impact dampers considered invariably attenuate the maximum deflection of the primary system most at the initial resonant frequency ω or when r equals one. It then seems beneficial to have equal coefficients of restitution to ensure two equispaced impacts/cycle. The attenuation at a given F_o/dK diminishes for a slight increase in r but, more importantly, amplifications always happen and may even be large for a small decrease in r. Therefore the traditional impact damper design based upon two equispaced impacts/cycle [53, 68] seems reasonable in this instance. However its performance may deteriorate even more than that of a conventional vibration neutraliser [6, 90] if fluctuations in Ω produce r less than one in practice.

3.6 Conclusions

A general theory has been developed for an impact damper to accommodate any number of impacts in some repetitive cycle. The theory agrees on the whole with previous, more restrictive and sparser predictions. The credibility of the general theory is enhanced greatly by the close correlation demonstrated between it and comprehensive experimental results. The recommended procedure for designing impact dampers is seen to be reasonable for one example of a lightly damped primary system with external sinusoidal loading. This particular example, however, suggests that the operation of the primary system should be maintained at or slightly above its fundamental resonance.

CHAPTER 4

SIMILARITIES BETWEEN VARIOUS VIBROIMPACT SYSTEMS

4.1 Introduction

Vibroimpact systems are nonlinear essentially because of the discontinuous velocities at impacts. Nonlinear, unlike linear systems cannot be generally solved universally by using, say, the principle of superposition. Consequently nonlinear systems are often studied individually which can be tedious [1, 2]. It would be beneficial therefore if the particular solution of a given vibroimpact system could be derived under certain specified conditions from a similar known solution. Solutions will be considered similar if they stem under specific conditions from the same equation and if they additionally involved identical impacts in a repetitive cycle.

The solution developed in the previous chapter for the sinusoidally forced vibroimpact damper will form the basis of those similar solutions appropriate to the idealisations of Figure 4.1. This figure also shows the connection between the idealisations and the conditions required for possible similar solutions. Kobrinskii [2] has noted already the general similarity between case (a) and (b.1) of Figure 4.1. Also, by using the approximations indicated, Dubowsky [10] has demonstrated the general similarity of case (b.1) and (b.3)

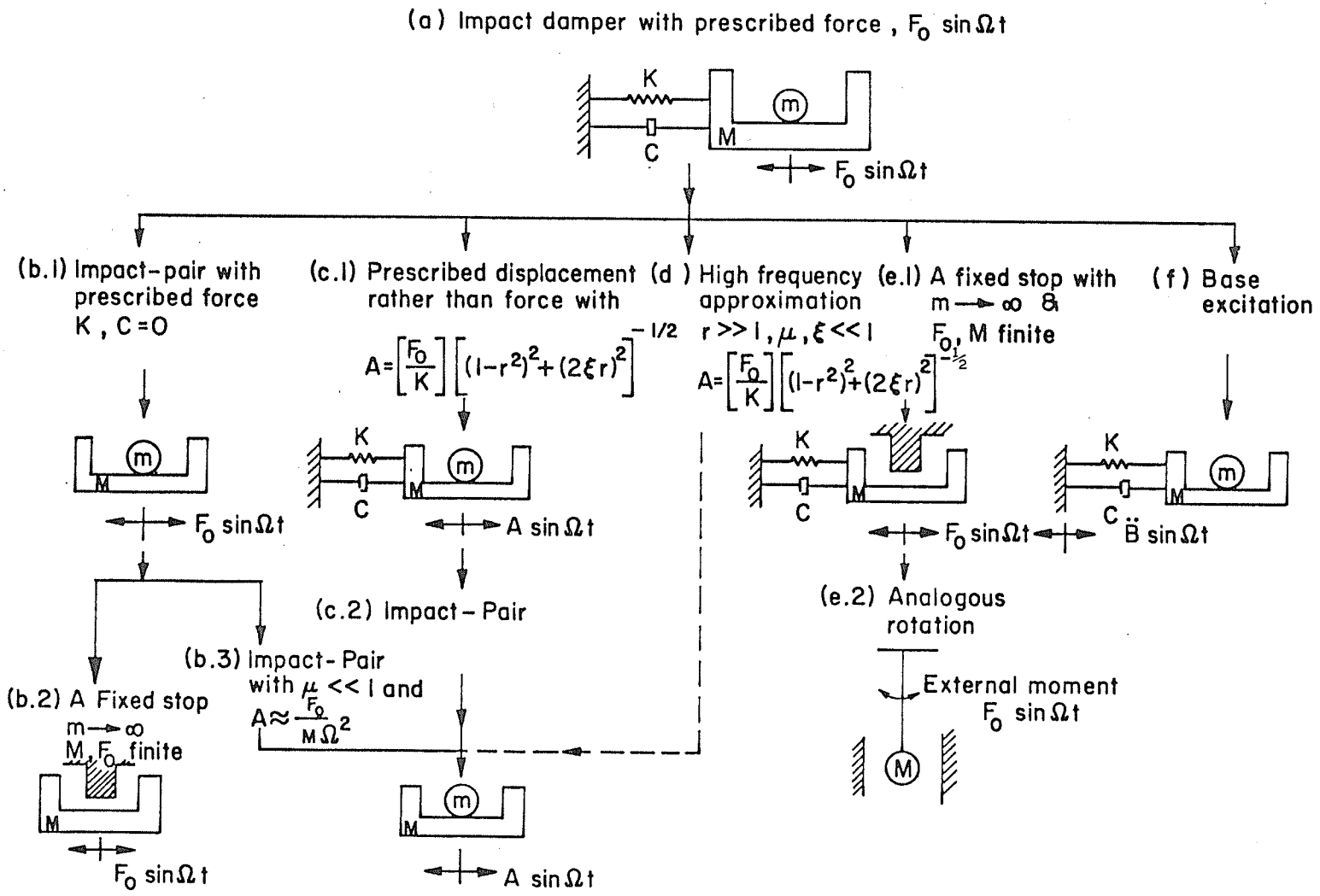

Figure 4.1. Relationship between various vibroimpact systems. F_0, A and $\ddot{B}$ symbolize the amplitude of a prescribed force or moment, displacement and acceleration respectively.

when the primary mass M does not drift radically to one side. Like similarities will be shown exactly for case (a), (c.1) and (c.2) or (b.3). The connection between the high frequency approximation (d) with (b.3) or (c.2) will be only suggested at this time for two impacts/cycle by employing several numerical illustrations. On the other hand case (b.1) and (b.2) are compatible physically only if M does not drift at all sideways. Drifting does not happen in situation (b.1) for two equispaced impacts/cycle when these two cases will be demonstrated similar. A comparable relationship will be drawn between situation (a) and (e.1) where drifting obviously cannot occur. Case (e.1) has been applied commonly to piping, heat exchanger tubes and PWR assemblies [78, 85-87]. It has been shown previously to be like the rotating system of (e.2) [2]. An analogous situation exists too between a sinusoidal load applied to the primary mass of the impact damper and the base acceleration indicated in case (f) [53, 89]. The amplitude of the external load F_o is replaced merely by the inertial amplitude $M\ddot{B}$.

These similarities not demonstrated before will be considered along with appropriate conditions in the order suggested by Figure 4.1.

4.2.1 Similarities Between Case (a), (c.1) and (c.2) of Figure 4.1

The displacement amplitude of M is simply A between consecutive impacts in both case (a) and (c.1) of Figure 4.1 if the F_o in (a) is tuned to

$$F_o = A K[(1 - r^2)^2 + (2 \xi r)^2]^{\frac{1}{2}} \qquad (4.1)$$

Then the motions of m must be identical for a given periodic impact sequence in these two cases because all other corresponding variables are equal. Consequently the two idealisations are similar providing equation (4.1) holds. The similarity of case (c.1) to (c.2) will be proved next for any periodic repetition of impacts providing the condition

$$\mu << 1 \qquad (4.2)$$

applied often in practice, is valid. Equations developed in Chapter 3 for the forced impact damper generally remain true providing the amplitude, F_o, of the external force is transformed by using equation (4.1) to an equivalent prescribed displacement amplitude, A. It remains to be shown that the general equations of motion of the impact damper and Impact-Pair, both having the identical prescribed displacements

$$X(t) = A \sin(\Omega t + \tau) , \qquad (4.3)$$

are common when condition (4.1) and (4.2) hold. The essentially immaterial phase τ has been reintroduced into equation (4.3) for convenience.

A comparison of equation (4.3) with equation (3.6a) of Chapter 3 indicates that

$$a_i = 0 = b_i \qquad i = 1, 2\text{----}N \tag{4.4}$$

for usually non-zero ξ, r, η, Ω and α_i. The a_i and b_i are given alternatively by equation (3.5a) and (3.5b) which, when combined with requirement (4.4), produce

$$X_i = A \sin\theta_i = A \sin(\tau + \alpha_i), \; i = 1, 2\text{----}N \tag{4.5}$$

and

$$\dot{X}_{ia} = Ar\omega\cos\theta_i = A\Omega\cos(\tau + \alpha_i), \; i = 1, 2\text{----}N \tag{4.6}$$

when r and θ_i are obtained from equation (3.3) and (3.6b). However $\dot{X}_{ia}$ is given also by equation (3.12b) so that

$$A\Omega\cos(\tau + \alpha_i) = k_{9i} V_{ib} + k_{10i} V_{ia}, \; i = 1, 2\text{----}N \; . \tag{4.7}$$

Coefficients k_{9i} and k_{10i} in the last expression may be obtained from equation (A2.11a) and (A2.11b) of Appendix A2 as

$$k_{9i} = \frac{(1 + \mu)R_i}{1 + R_i} \quad \text{and} \quad k_{10i} = \frac{1 - \mu R_i}{1 + R_i}, \; i = 1, 2\text{----}N \; .$$

These last relationships take the simpler approximation

$$k_{9i} = \frac{R_i}{1 + R_i} \quad \text{and} \quad k_{10i} = \frac{1}{1 + R_i}, \; i = 1, 2\text{----}N \tag{4.8}$$

when condition (4.2) is applied in conjunction with the usual practical requirement of $0 < R_i \leq 1$, $i = 1, 2\text{----}N$. Substituting equation (4.8) and variables V_{ia} and V_{ib} from equation (3.14) and (3.15) directly into equation (4.7) leads to

$$A\Omega\cos(\tau+\alpha_i) = \left(\frac{R_i}{1+R_i}\right)\left[\frac{\Omega\{X_{(i+N)} + Y_{(i+N)} - X_{(i+N-1)} - Y_{(i+n-1)}\}}{\alpha_{(i+N)} - \alpha_{(i+N-1)}}\right.$$

$$+ \left(\frac{1}{1+R_i}\right)\left[\frac{\Omega\{X_{(i+1)} + Y_{(i+1)} - X_i - Y_i\}}{\alpha_{(i+1)} - \alpha_i}\right] , \quad i = 1,2\text{----}N. \quad (4.9)$$

Expansion of the trigonometric terms in equation (4.5) and (4.9) immediately gives equation (2.14) and (2.15), the general equations of motion of the Impact-Pair.

4.2.2 Correspondence Between Case (d) and (b.3) or (c.2)

The relationship between the practically important two impacts/cycle stability zones of certain externally loaded impact dampers and an Impact-Pair with prescribed displacement in case (b.3) or (c.2) is illustrated in Figure 4.2. Numerical computations were performed for the damper by using the invariable light damping ratio ξ of 0.05 and the various μ and r given in the figure. Values were selected generally to obey the restrictions

$$r \gg 1, \quad \mu \ll 1 \text{ and } \xi \ll 1 \quad (4.10)$$

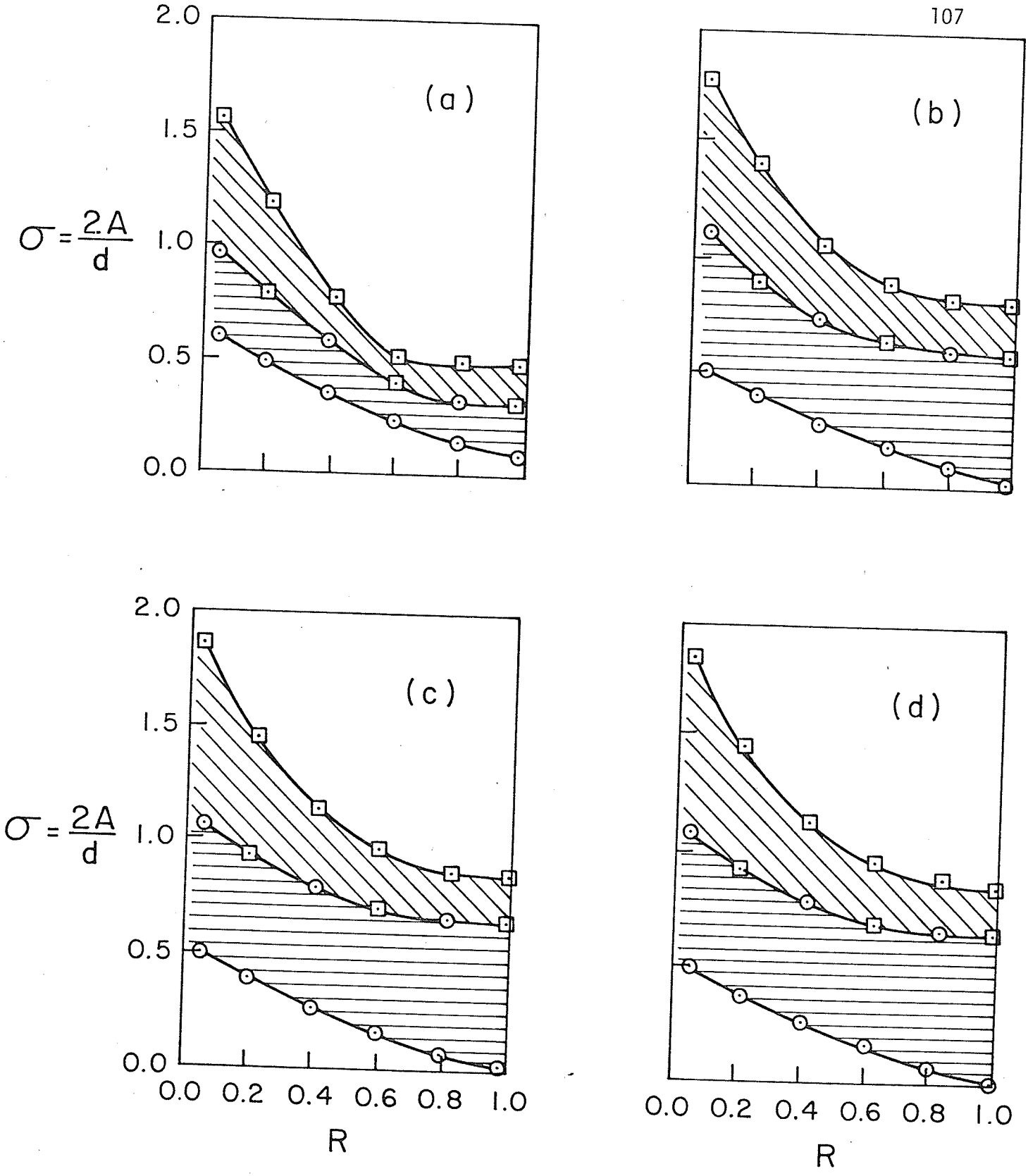

Figure 4.2. Comparison between the two impacts/cycle stability zones of particular impact dampers (a), (b) and (c) and (d) an Impact-Pair. Dampers have a constant ξ of 0.05 but other values are (a) μ = 0.5, r = 6; (b) μ = 0.05, r = 6; and (c) μ = 0.01, r - 12. Coefficients of restitution take identical value R.

typical of the high frequency behaviour of a realistic damper. Stability zones were plotted in the standard format of Figure 2.5. This procedure entailed the conversion of the external load's amplitude F_o by using equation (3.3) of Chapter 3 to an equivalent displacement amplitude A of the primary mass. The equivalence, written explicitly again in case (d) of Figure 4.1, is invariant for constant passive components and a given frequency ratio. It is understood however that the repetitive period may reference the (identical) cyclical behaviour of the external load or, as appropriate, the prescribed displacement.

A comparison of the dampers' stability zones in Figure 4.2 suggests that their correspondence with those of the Impact-Pair improves as restrictions (4.10) are satisfied better. For example, both two impacts/cycle stability zones of the damper with the largest r and smallest μ and the Impact-Pair virtually coincide. Consequently case (d) of Figure 4.1 appears to be similar to (b.3) or (c.2) under the restrictions listed in the inequalities designated by (4.10). Hence further investigations of a more theoretical nature seem justified.

4.2.3 Similarity of Case (a) and (e.1)

The similarity of case (a) and (e.1) shown in Figure 4.1 will be proved in this section for two equispaced impacts/cycle of the external load $F_o \sin\Omega t$. An essential condition is for the

secondary mass m to be infinitely larger than the primary M. The M and F_o should be finite to ensure that the strength of the impacts remains bounded [17]. Then the velocity of m will be virtually zero after an impact or essentially fixed as in case (e.1).

The equations of motion (3.19a) and (3.19b) developed generally in Chapter 3 for impact damper (a) simplify to

$$2 \sin\tau + H \cos\tau = - \rho \tag{4.10a}$$

where

$$H = 2\Omega \left[\frac{[(\sigma_2-\sigma_1) + \sigma_1\sigma_2 (\xi\omega-\phi_2)]h_1 + [1+h_2][\sigma_1\sigma_2(\phi_1 + \eta\omega)]}{(\xi\omega\sigma_2-\sigma_1\phi_2)h_1 + (1+h_2)[\sigma_1\phi_1+\eta\sigma_2\omega]} \right] \tag{4.10b}$$

and

$$\rho = \frac{d\,[(1-r^2)^2 + (2\xi r)^2]^{\frac{1}{2}}}{F_o/K} \tag{4.10c}$$

for two equispaced impacts/cycle with R_1, R_2 both equal to R and a given F_o expressed in terms of a corresponding constant A by equation (3.3). The above particular equations were given originally in reference 53. Variables h_1, h_2, ϕ_1, ϕ_2, σ_1 and σ_2 are defined explicitly in Appendix A3 where it is shown that

$$\lim_{\mu\to\infty} \sigma_1 \to 0, \quad \lim_{\mu\to\infty} \sigma_2 \to 0 \tag{4.11a}$$

but

$$\lim_{\mu\to\infty} \frac{\sigma_1}{\sigma_2} \to - R \ . \tag{4.11b}$$

The mass ratio μ tends to infinity in the limit when m is very much larger than a finite M. Then by employing tendencies (4.11a) and (4.11b) in equation (4.10b), it can be demonstrated that

$$\lim_{\mu\to\infty} H \to 2\Omega \frac{(1 + R)h_1}{(\xi\omega + R\phi_2)\, h_1 + (\eta\omega - R\phi_1)(1 + h_2)} \cdot \qquad (4.12)$$

If the last relationship is substituted into equation (4.10a), the resulting equation is identical to the one developed in Reference 2 and 29 specifically for case (e.1). Therefore the solutions of case (a) and (e.1) are similar for the outlined conditions.

4.2.4 Similarity of Case (b.2) and (b.1)

The similarity between case (b.1) and (b.2) is demonstrated more easily by first considering the idealisation of (b.2) in Figure 4.1. Rigid mass M totally clears the fixed stop by a non-zero distance d. It collides with the stop twice after the establishment of periodic motion for every cycle of the external load $F_o \sin \Omega t$. Durations between consecutive collisions are assumed identical and, hence, equal π/Ω. Any impact in the periodic motion may be designated arbitrarily as the first. This first impact is assumed for convenience to occur at time zero on the left side of M in Figure 4.1. Therefore the absolute displacement of M, X, is known to be

$$\left.\begin{aligned} X &= +\,d/2 \qquad \text{at} \qquad t = 0 \\ \text{and} \qquad & \\ X &= -\,d/2 \qquad \text{at} \qquad t = \pi/\Omega \end{aligned}\right\} \tag{4.13}$$

On the other hand the equation of motion of M is

$$M\ddot{X} = F_o \sin\Omega t \tag{4.14}$$

between impacts. The solution of this second order ordinary differential equation is given straightforwardly by

$$X = A \sin(\Omega t+\tau) + C_1 t + C_2 \tag{4.15}$$

where

$$A = F_o/(M\Omega^2) \tag{4.16}$$

and C_1 and C_2 are arbitrary constants. Equation (4.15) has to satisfy the two conditions numbered (4.13) so that

$$+\frac{d}{2} = A\sin\tau + C_2 \tag{4.17a}$$

and

$$-\frac{d}{2} = -A\sin\tau + C_1 \cdot \frac{\pi}{\Omega} + C_2 \quad . \tag{4.17b}$$

Adding equation (4.17b) to (4.17a) and rearranging gives

$$C_2 = -\frac{\pi}{2\Omega} C_1 \quad . \tag{4.18}$$

The velocity of M immediately after the first impact, $\dot{X}_{1a}$, is obtained by differentiating equation (4.15) and substituting 0_+ for t. This produces

$$\dot{X}_{1a} = A\Omega\cos\tau + C_1 \quad . \tag{4.19}$$

Similarly the velocity of M just before the second impact, $\dot{X}_{2b}$, at $(\pi/\Omega)_-$ is

$$\dot{X}_{2b} = -A\Omega\cos\tau + C_1 \quad . \tag{4.20}$$

However $\dot{X}_{2b}$ is merely in the opposite direction to $\dot{X}_{1b}$ due to the symmetry of the periodic motion [1]. Mathematically

$$\dot{X}_{1b} = - \dot{X}_{2b}$$

or, from equation (4.20),

$$\dot{X}_{1b} = A\Omega\cos\tau - C_1 \quad . \tag{4.21}$$

Now $\dot{X}_{1b}$ and $\dot{X}_{1a}$ are related through the coefficient of restitution, R, by

$$\dot{X}_{1a} = - R \dot{X}_{1b} \quad . \tag{4.22}$$

Substituting equation (4.19) and (4.21) into equation (4.22) gives

$$A\Omega\cos\tau + C_1 = - R (A\Omega\cos\tau - C_1)$$

or

$$C_1 = - A\Omega \left(\frac{1 + R}{1 - R}\right) \cos\tau \quad . \tag{4.23}$$

Combining equation (4.18) and (4.23) leads to

$$C_2 = A \frac{\pi}{2} \left(\frac{1 + R}{1 - R}\right) \cos\tau \quad . \tag{4.24}$$

Equation (4.24) can be substituted in equation (4.17a) to produce

$$\sin\tau + \frac{\pi}{2} \left(\frac{1 + R}{1 - R}\right) \cos\tau = \frac{d}{2A} \tag{4.25}$$

after division by A. The last equation is identical to that given in Reference 2 for the system shown in case (b.1). Therefore the two systems are similar for periodic motion involving two symmetrical impacts per cycle of the external load.

4.3 Conclusions

Relationships between existing similar solutions have been placed into better perspective. They have been complemented by several new and practically relevant examples. Similarity relationships do provide a useful means of extending and checking various idealisations even though a completely general set relationships cannot be provided.

CHAPTER 5

CONCLUSIONS AND RECOMMENDATIONS FOR FUTURE WORK

A theory is developed to predict general stable periodic motions of an Impact-Pair and impact damper when subjected to a prescribed, sinusoidally time varying external load or displacement. Any one impact is considered instantaneous and representable by the macroscopic coefficient of restitution. Times between individual impacts and the overall periodicity are presumed known. Ensuing predictions are compared with previous but, sparse, theoretical results and more comprehensively with new experimental data. Agreement between theories is fairly good generally but several incongruences, although explainable, remain in the case of the impact damper. Credibility is increased therefore by the close correlations demonstrated between general theory and experiments involving widely different conditions. Minor discrepancies arise, however, due primarily to imperfect experimental simulations of single direction motions and supposedly plane surfaces which change slightly after many contacts. The latter variations seem to become progressively less pronounced after an initial work-hardening phase. If such behaviour is general, a proposal to simply determine the clearance without dismantling an Impact-Pair would be useful.

Impact dampers are currently designed assuming stable periodic motion comprising two equispaced impacts. The validity of this

assumption is certainly questionable when the external load, say, is so transient that periodic motion cannot even be established. It has also been demonstrated that even with stable periodic motions, equispaced impacts happen strictly only when consecutive collisions involve identical coefficients of restitution. However, extrapolation from the corresponding Impact-Pair investigation suggests that differences less than about 5% are not likely to be practically significant. On the other hand uncontrolled fluctuations in the frequency of a sustained sinusoidal loading of a lightly damped primary system could seriously degrade the impact damper's performance. The damper will amplify rather than attenuate the primary's maximum deflection for large fluctuations which drive the forcing frequency even slightly below its own fundamental natural frequency. Optimal deflection reductions are produced in these circumstances when the primary system alone is resonant and the damper generates exactly equispaced, two impacts/cycle of the sinusoidal load. In other words, the present design philosophy concerning impact dampers is, then, certainly appropriate.

The solution of any one particular problem becomes increasingly useful as its applicability is demonstrated more universally. This is generally not a straightforward procedure in vibroimpact problems because the principle of superposition is invalid. However, similarities have been shown to exist under certain conditions between various Impact-Paris and impact dampers. Work is needed to generalize the

concept and place it on a more rigorous foundation. Other major questions requiring theoretical answers relate to:

1) The conditions needed for a stable periodic motion to be unique;
2) the least time taken for a stable periodic motion to revert back to its form after the application of a small perturbation;
3) the effect of numerical errors when absolute eigenvalues are near one.

Of these the first two offer most promise of furthering our understanding of vibroimpact systems. Further experimentation should be performed to investigate the possibility of optimizing the number and timing of impacts produced by a damper under earthquake-like loading. Such loads could encompass a wide range of amplitudes and, unlike the present sinusoidal force, simultaneously applied frequencies which could be non-stationary. Then, many different secondary systems may be needed or, alternatively, feedback may be introduced to continuously adjust the character of the single unit damper.

REFERENCES

1. A. Ye. Kobrinskiy 1969 Mechanisms with elastic couplings, Dynamics and Stability. NASA Technical Translation TTF-534.

2. A.E. Kobrinskii and A.A. Kobrinskii 1973 Vibroimpact System. Moscow: Nauka Press (in Russian).

3. V.I. Babitskii 1978 Theory of Vibroimpact Systems. Moscow: Nauka Press (in Russian).

4. I.I. Bykhovsky 1980 Fundamentals of Vibration Engineering. New York: Robert E. Krieger Publishing Company.

5. W.T. Thomson 1965 Vibration Theory and Applications. New Jersey: Prentice Hall, Inc.

6. J.B. Hunt 1979 Dynamic Vibration Absorbers. Letchworth: The Garden City Press Limited.

7. C. Lawson and R. Hanson 1974 Solving Least Square Problems. New Jersey: Prentice-Hall, Inc.

8. J. H. Wilkinson 1969 The Algebric Eigenvalue Problem. Oxford, Clarendon Press.

9. T.D. Goodman 1963 Machine Design May 23, 150-157. Dynamic effects of backlash.

10. S. Dubowsky and F. Freudenstein 1971 Journal of Engineering for Industry, Transactions of the American Society of Mechanical Engineers 93B, 305-316. Dynamic analysis of mechanical systems with clearances. Part 1. Formation of dynamic model, Part 2. Dynamic response.

11. S. Dubowsky 1974 Journal of Engineering for Industry, Transaction of the American Society of Mechanical Engineers 96B, 317-323. On predicting the dynamic effects of clearances in planer mechanisms.

12. S. J. Grant and J. N. Fawcett 1979 Mechanism and Machine Theory 14, 99-110. Effects of clearance at the coupler-rocket bearing of a 4-bar linkage.

13. R. Wilson and J.N. Fawcett 1974 Mechanism and Machine Theory 9, 61-80. Dynamics of the slider-crank mechanism with clearance in the sliding bearing.

14. R.S. Haines 1980 Mechanism and Machine Theory 15, 361-370. Survey: 2-dimensional motion and impact at revolute joints.

15. C.C. Wang 1978 Journal of Mechanical Design, Transactions of the American Society of Mechanical Engineers 100, 363-373. Rotational vibration with backlash-Part 1.

16. C.C. Wang 1981 Journal of Mechanical Design, Transactions of the American Society of Mechanical Engineers 103, 387-397. Rotational vibration with backlash-Part 2.

17. A.A. Zevin 1973 Mechanics of Solids, 8, 5, 23-29. Upper bounds for impulse values in vibration-impact systems.

18. M.F. Ranky 1978 Institute of Sound and Vibration Research. Technical Report No.100. Diagnostics of gear assembly, a new approach using impact analysis.

19. M.A. Veluswami and F.R.E. Crossley 1975 Journal of Engineering for Industry, Transactions of the American Society of Mechanical Engineering 97, 820-227. Multiple impacts of a ball between two plates, Part 1: Some experimental observations.

20. M.A. Veluswami, F.R.E. Crossley and G. Horvey 1975 Journal of Engineering for Industry, Transactions of the American Society of Mechanical Engineers 97, 828-835. Multiple impacts of a ball between two plates, Part 2: Mathematical modelling.

21. C. Cempel 1978 Journal of Sound and Vibration 60, 411-416. Detection of clearances in machine kinematic pairs by coherence method.

22. R.I. Kutchev and A.G. Pavlov 1973 Russian Engineering Journal 53, 32-35. Influence of roller-bearing clearance on vibration.

23. J.W. Kannel and D.K. Snediker 1977 Machine Design 49-8, 78-82. The hidden cause of bearing failure.

24. P.A. Engel 1977 Machine Design 49-12, 100-105. Predicting impact wear.

25. E.E. Ungar and D. Ross 1965 Journal of Sound and Vibrations 2, 132-145. Vibration and noise due to piston-slap in reciprocating machinery.

26. A. Simpson and W.R. Reynolds 1977 Journal of Sound and Vibration 55, 109-133. The effect of vibration on an aircraft fuel density meter.

27. D.A. Conrad and D.G. Shellhorn 1962 Ingenieur Archiv 31, 444-452. Zero-shift in galvanometers subjected to mechanical vibration.

28. V.I. Babitskii and A.N. Tresvyatskii 1975 Mechanics of Solids 10, 18-23. One case of loss of stability by a mechanism having forced closure.

29. V.I. Babitskii 1966 Mashinoved 1, 22-26. Existence of high frequency oscillations of large amplitude in linear system with limiters (in Russian).

30. V.I. Babitskii, R.E. Brunshtein and A.E. Kobrinskii 1965. Teoriya Mashin i Mekhanizmov 105/106, 122-134. Dynamics and stability of elastic systems with backlash (in Russian).

31. R.E. Brushtein and A.E. Kobrinskii 1959 Mekh. i Mash., Izv. Akad. Nauk SSSR, Otd. Telsh. Nauk 1, 10-21. Periodic motion of a system consisting of a small pellet in a hallow cavity (in Russian).

32. R.E. Brushtein and A.E. Kobrinskii 1961 Thudi Inst. Mashinoved., Akad. Nauk SSSR 21, 83/84, 46-54. Investigation of the dynamics and stability of vibrating systems (in Russian).

33. Yu. A. Stepanenko 1964 Mekhanika Mashin (Moscow) 7-8, 111-118. Dynamics of nonlinear components with breaks in the kinematic linkage (in Russian)

34. W. Goldsmith 1960 Impact. Edward Arnold Ltd., London.

35. T. Fujita and S. Hattori 1980 Bulletin of Japan Society of Mechanical Engineers 23, 409-418. Periodic vibrations and impact characteristics of a nonlinear system with collision.

36. A.D. Bernstein 1977 American Journal of Physics 45, 41-44. Listening to the coefficient of restitution.

37. H.P. Kirchner and R.M. Gruver 1978 Materials Science and Engineering 33, 101-106. The effect of Localized damage on energy losses during impact.

38. G. Poletti and F. Rossitto 1978 Journal of the British Interplanetary Society, 31, 267-270. Dynamic experiment on the adhesion of metals.

39. C. Texier 1978 Revue de physique appliquee 13, 13-22. Decharges electriques dans Le vide: impact de microparticules sphereques de fer de la taille du micron sur des electrodes polies mecaniquement I: effects mecaniques du choc (in French).

40. K.H. Hunt and F.R.E. Crossley 1975 Journal of Applied Mechanics, Transactions of the American Society of Mechanical Engineers 42, 440-445. Coefficient of restitution interpreted as damping in vibroimpact.

41. Y. Tatara 1977 Journal of Applied Mechanics, Transactions of the American Society of Mechanical Engineers 44, 773-774. Effect of external force on contacting times and coefficient of restitution in a periodic collision.

42. B.N. Cole 1979 International Journal of Mechanical Engineering Education 7, 91-97. Impact, stress waves and rebound.

43. M. Endo, S. Nishi, M. Nakawaga and M. Sakata 1981 Journal of Sound and Vibration 75, 285-302. Sound radiation from a circular cylinder subjected to elastic collision by a sphere.

44. S. Dubowsky 1980 Journal of Acoustical Society of America 67, 551-563. Analytical method to predict noise radiation from machine systems.

45. IMSL Library 0007 1979 International Mathematics and Statistical Library, Inc.

46. F. Peterka 1978 Mechanism and Machine Theory 13, 75-83. Existence and stability of self-excited vibrations with impacts.

47. Iu. S. Fedosenko and M.I. Feigin 1971 PMM Journal of Applied Mathematics and Mechanics 35, 844-850. Periodic motions of a vibrating striker including a slippage region.

48. Iu. S. Fedosenko 1973 PMM Journal of Applied Mathematics and Mechanics 37, 949-956. Forced oscillations with a sliding regime range of a two-mass system interacting a fixed stop.

49. P. Lieber and D.P. Jensen 1945 Transaction of the American Society of Mechanical Engineers 67, 523-530. An acceleration damper: development, design and some applications.

50. C. Grubin 1956 Journal of Applied Mechanics, Transaction of the American Society of Mechanical Engineers 78, 373-378. On the theory of the acceleration damper

51. R.N. Arnold 1956 Proceedings of International Congress of Applied Mechanics 9, 407-418. Response of an impact vibration absorber to forced vibration.

52. G.B. Warburton 1957 Journal of Applied Mechanics, Transactions of the American Society of Mechanical Engineers 79, 322-324. On the theory of the acceleration damper.

53. S.F. Masri 1965 Ph.D. Thesis, California Institute of Technology. Analytical and experimental studies of impact dampers.

54. S.F. Masri and T.K. Caughey 1966 Journal of Applied Mechanics, Transactions of the American Society of Mechanical Engineers 33, 586-592. On the stability of the impact damper.

55. D.M. Egle 1967 Journal of Engineering for Industry, Transactions of the American society of Mechanical Engineers 89, 653-661. An investigation of an impact vibration absorber.

56. M.I. Feigin 1967 Journal of Applied Mathematics and Mechanics 31, 166-171. Dynamic theory of a controlled vibration damping model.

57. M.M. Sadek 1965-66 Proceedings of the Institution of Mechanical Engineers 180, 895-906. The behavior of the impact damper.

58. H. Dittrich 1966 Ingenieur-Archiv 35, 150-171. Study of a discontinuous working vibration damper (in German).

59. S.F. Masri 1970 The Journal of the Acoustical Society of America 47, 229-237. General motion of an impact dampers.

60. S.F. Masri 1968 The Journal of the Acoustical Scoiety of America 45, 1111-1117. Analytical and experimental studies of multi-unit impact dampers.

61. V.I. Babitskii and M.Z. Kolovskii 1970 Mashinovedenie 2, 16-24. On the dynamics of a system with an impact vibration absorber (in Russian).

62. W.M. Mansour and D.R.T. Filho 1974 Journal of Sound and Vibration 33, 247-265. Impact dampers with Coulomb friction.

63. C. Cempel 1974 Journal of Sound and Vibration 34, 199-209. The multi-unit impact damper: Equivalent continuous force approach.

64. C. Cempel 1975 Journal of Sound and Vibration 40, 249-266. Receptance model of the multi-unit vibration impact neutralizer- "MUVIN".

65. S.F. Masri and K. Kahyai 1974 International Journal of Non-linear Mechanics 9, 451-462. Steady-state motion of a plate with a discontinuous mass.

66. R.K. Roy, R.D. Rocke and J.E. Foster 1975 Journal of Engineering for Industry, Transactions of the American Society of Mechanical Engineers 97, 1317-1324. The application of impact dampers to continuous systems.

67. S.F. Masri 1973 Journal of the Engineering Mechanics Division, Proceedings of the American Society of Civil Engineers 99, 669-683. Forced vibration of class of nonlinear dissipative beams.

68. E. Skipor and L.J. Bain 1980 Journal of Mechanical Design, Transactions of the ASME 102, 338-343. Application of impact damping to rotary printing equipment.

69. J. Inoue, S. Miyaura and Akito Nishiyama 1968 Bulletin of Japan Society of Mechanical Engineers 11, 102-106. On the vibrotransport-ation and Vibroseparation* (Part 1. On the stability for the periodic motion of the jumping granular solid).

70. C.C. Fu and B. Paul 1968 International Journal of Solids and Structures 4, 897-905. Stability of motion of Impact tools.

71. C.C. Fu 1969 Journal of Applied Mechanics, Transcations of the American Society of Mechanical Engineers 91, 743-749. Dynamic stability of an impact system connected with rock drilling.

72. D.L. Sikarskie and B. Paul 1969 Journal of Engineering for Industry, Transactions of the American Society of Mechanical Engineering 91, 931-938. Periodic motions of a two body system subjected to repetitive impact.

73. M. Senator 1970 The Journal of the Acoustical Society of America 47, 1390-1397. Existence and stability of periodic motions of a harmonically forced impacting system.

74. G.M.L. Gladwell and W.M. Mansour 1971 Journal of Sound and Vibrations 15, 495-507. The analysis of some intermittent contact devices.

75. M.A. Parameswaran and S. Ganapathy 1979 Mechanism and Machine Theory 14, 89-97. Vibratory conveying-analysis and design: A review.

76. H.G. Davies 1980 Journal of Sound and Vibration 68, 479-487. Random vibration of a beam impacting stops.

77. G.S. Whiston 1979 Journal of Sound and Vibrations 67, 179-186. Impacting under harmonic excitation.

78. H. Nuno, M. Mizuta, K. Kitade, I. Saruyama 1973 Preprints 2nd International Conference on Structural Mechanics in Reactor Technology 4, Paper K 6/10, 12. A method of colliding vibration analysis of PWR fuel assemblies under seismic condition.

79. V.F. Zhuravlev 1976 Mechanics of Solids 11, 23-27. A method of analyzing vibration-impact systems by means of special functions.

80. V.F. Zhuravlev 1977 Mechanics of Solids 12, 14-18. Investigation of certain vibration-impact systems by the method of nonsmooth transformations.

81. L.V. Baspalova, Yu. I. Neimark and M.I. Feigin 1966 Inzhenernyi Zhurnal Mekhanika Tverdogo Tela 1, 151-159. Dynamic systems with impact interactions and theory of nonlinear oscillations. (in Russian).

82. C.N. Bapat 1981 Department of Mechanical Engineering, Departmental Memo, University of Manitoba. Computer programs to develop stability charts of vibroimpact systems.

83. Instructions and applications manual for Impedance heads Type 8000 and 8001, 1971. Copenhagen. Brüel & Kjaer.

84. Instruction manual for 400 series vibrator and amplifier model PA300. 1972 Hertfordshire, England. Ling Dynamic Systems Limited

85. R.J. Rogers and R.J. Pick 1976 Nuclear Engineering and Design 36, 81-90. On the dynamic spatial response of a heat exchanger tube with intermittent baffle contacts.

86. R.J. Rogers and R.J. Pick 1977 Nuclear Engineering and Design 44, 247-253. Factors associated with support plate forces due to heat-exchanger tube vibratory contact.

87. R.D. Blevins 1975 Journal of Engineering for industry, Transactions of the American Society of Mechanical Engineers 97, 1301-1304. Vibration of a loosely held tube.

88 Y. Muzyka 1981 B.Sc. (Engineering) Thesis, Department of Mechanical Engineering, University of Manitoba. An experimental investigation of multiple unit impact dampers.

89. P.L. Gould and S.H. Abu-Sitta 1980 Dynamic Response of Structures to Wind and Earthquake Loading. New York - Toronto: John Wiley & Sons.

90. M.I. Feigin 1966 PMM Journal of Applied Mathematics and Mechanics 30, 1118-1123. Resonance behaviour of a dynamical system with collisions.

91. C.C. Kennedy and C.D.P. Pancu 1947 Journal of the Aeronautical Sciences 14, 603-625. Use of vectors in vibration measurement and analysis.

92. Instruction manual for Action Master 500, Photosonic Ltd.

APPENDIX A1

It is required to show that a necessary condition for two equispaced impacts/k cycles (k = 1, 3, 5,---) to occur in an Impact-Pair is for R_1 to equal R_2. Equations (2.17) through (2.21) of the main text hold generally and certainly for the special periodicity condition

$$\alpha_2 = \pi k \tag{A1.1}$$

associated with two equispaced impacts/k cycles. Substituting equation (A1.1) into these general equations leads to

$$L_2 = \frac{(1 - R_2)}{\pi k} = \left(\frac{1 - R_2}{R_1 - 1}\right) L_1, \quad 0 < R_1 < 1 \tag{A1.2}$$

and, from equation (2.19),

$$x_1 = A \sin\tau = - x_2 \quad . \tag{A1.3}$$

Then by using equation (A1.1) through (A1.3), the two equations numbered (2.20) respectively become

$$2L_1.A\sin\tau - (1 + R_1).A\cos\tau = dL_1 \tag{A1.4}$$

and, after some simple algebraic manipulation,

$$2L_1.A\sin\tau + \frac{(1 + R_2)(R_1 - 1)}{(1 - R_2)}.A\cos\tau = dL_1 \quad . \tag{A1.5}$$

Consequently

$$-(1 + R_1) = \frac{(1 + R_2)(R_1 - 1)}{(1 - R_2)} \qquad \text{(A1.6)}$$

by inspecting equation (A1.4) and (A1.5). After cross-multiplication and cancellation of common terms, equation (A1.6) gives the required result that

$$R_1 = R_2 \quad , \quad 0 < R_1 < 1 \quad , \qquad \text{(A1.7)}$$

for two equispaced impacts/k cycles.

APPENDIX A2

DERIVATION OF GENERAL EQUATIONS OF AN IMPACT DAMPER

The general equation (3.19a) and (3.19b) of Chapter 3 will be derived. Components of the 4 x 4 matrix $[P_i]$ will be given subsequently because they involve variables which are defined here.

The absolute displacement of the primary system at the (i+1)th impact, $X_{(i+1)}$, is obtained by substituting the contact instant $t_{(i+1)}$ in equation (3.6a). Then by using equation (3.4) to write $\alpha_{(i+1)}$ instead of $\Omega t_{(i+1)}$, $X_{(i+1)}$ can be shown to be

$$X_{(i+1)} = \exp\left[-\frac{\xi}{r}(\alpha_{(i+1)} - \alpha_i)\right]\left[a_i \sin\frac{\eta}{r}(\alpha_{(i+1)} - \alpha_i) + b_i \cos\frac{\eta}{r}(\alpha_{(i+1)} - \alpha_i)\right] + A \sin(\alpha_{(i+1)} + \tau), \quad i = 1, 2\text{----}N \quad . \tag{A2.1}$$

The velocity of the primary mass just before the (i+1)th impact, $\dot{X}_{(i+1)b}$, is simply the time derivative of equation (3.6a) at time $t_{(i+1)-}$, or

$$\dot{X}_{(i+1)b} = \begin{cases} \exp[-\frac{\xi}{r}(\alpha_{(i+1)} - \alpha_i)][\{a_i \cos\frac{\eta}{r}(\alpha_{(i+1)} - \alpha_i) \\ \qquad - b_i \sin\frac{\eta}{r}(\alpha_{(i+1)} - \alpha_i)\} \frac{\eta\Omega}{r} \\ -\frac{\xi}{r}\Omega\{a_i \sin\frac{\eta}{r}(\alpha_{(i+1)} - \alpha_i) + b_i \cos\frac{\eta}{r} \cdot \\ \qquad (\alpha_{(i+1)} - \alpha_i)\}] + A\Omega\cos(\alpha_{(i+1)} + \tau), \\ \qquad i = 1, 2\text{----}N \quad . \end{cases} \tag{A2.2}$$

Let

$$\left.\begin{aligned} E_i &= \exp\left[-\frac{\xi}{r}(\alpha_{(i+1)} - \alpha_i)\right], \quad \phi_i = \frac{\eta}{r}(\alpha_{(i+1)} - \alpha_i) \\ &\text{and} \\ C_{9i} &= E_i \sin\phi_i, \quad C_{10i} = E_i \cos\phi_i \end{aligned}\right\} \tag{A2.3}$$

so that equation (A2.1) and (A2.2) may be expressed more succinctly as

$$X_{(i+1)} = C_{9i}\, a_i + C_{10i}\, b_i + A \sin(\alpha_{(i+1)} + \tau), \quad i = 1, 2\text{----}N \tag{A2.4}$$

and

$$\dot{X}_{(i+1)b} = \begin{cases} [(C_{10i}a_i - C_{9i}b_i]\,\eta\omega - \xi\omega\,[C_{9i}a_i + C_{10i}b_i] \\ + A\Omega\cos(\alpha_{(i+1)} + \tau) \quad , \; i = 1, 2\text{----}N \; . \end{cases} \tag{A2.5}$$

Equation (A2.5) can be simplified to

$$\dot{X}_{(i+1)b} = \begin{cases} a_i\,[(\eta C_{10i} - \xi C_{9i})\omega] + b_i[(-\eta C_{9i} - \xi C_{10i})\omega] \\ + A\Omega\cos(\alpha_{(i+1)} + \tau),\ i = 1,2\text{---}N \end{cases} \tag{A2.6}$$

by collecting terms involving a_i and b_i. If

$$C_{11i} = \omega(\eta C_{10i} - \xi C_{9i}) \quad \text{and} \quad C_{12i} = -\ \omega(\eta C_{9i} + \xi C_{10i}),$$

$$i = 1,\ 2\text{----}N \tag{A2.7}$$

then equation (A2.6) can be rewritten as

$$\dot{X}_{(i+1)b} = C_{11i}a_i + C_{12i}b_i + A\Omega\cos(\alpha_{(i+1)} + \tau),\ i = 1,\ 2\text{---}N \tag{A2.8}$$

The N constituent relations implicit to both equation (A2.4) and (A2.8) form the basis of the 2N equations to be developed. Coefficients C_{9i} through C_{12i} can be enumerated from the known frequencies Ω and ω, the given passive components and the assumed impact sequence and periodicity. The a_i and b_i can be expressed in terms of the unknowns A, τ and all X_i by using equation (3.5a) separately and, together with equation (3.6b) and (3.7), in conjunction with equation (3.18). The only remaining determinable variable on the right of equation (A2.4) and (A2.8) is the $\alpha_{(i+1)}$, which can be obtained from equation (2.13) by using the assumed sequence and

periodicity of impacts. Also the $\dot{X}_{(i+1)b}$ on the left of equation (A2.8) may be found in terms of the X_i by employing equation (2.13) again and replacing subscript i in equation (3.16) with (i+1). These procedures will be shown next to produce the final 2N linear simultaneous equations required in Chapter 3 which involve the (N+2) unknowns of X_i, i = 1, 2, ----N, A and τ.

Equation (A2.4) and (A2.8) become

$$X_{(i+1)} = C_{9i}\left[\frac{1}{\eta}\left\{\frac{1}{\omega}\left[\frac{k_{9i}(X_i+Y_i - X_{(i-1)}-Y_{(i-1)})}{\alpha_i - \alpha_{(i-1)}} + \frac{k_{10i}\,(X_{(i+1)}+Y_{(i+1)} - X_i-Y_i)}{\alpha_{(i+1)} - \alpha_i}\right]\Omega - \text{Arcos}(\alpha_i + \tau) + \xi\,[X_i - A\sin(\alpha_i + \tau)]\right\}\right] + C_{10i}\,[X_i - A\sin(\alpha_i + \tau)] + A\sin(\alpha_{(i+1)} + \tau),$$

$$i = 1, 2---N \qquad \text{(A2.9)}$$

and

$$\frac{k_{7(i+1)}[X_{(i+1)}+Y_{(i+1)}-X_i-Y_i]\Omega}{\alpha_{(i+1)} - \alpha_i} + \frac{k_{8(i+1)}[X_{(i+2)}+Y_{(i+2)}-X_{(i+1)}-Y_{(i+1)}]\Omega}{\alpha_{(i+2)} - \alpha_{(i+1)}}$$
$$= C_{11i}\left[\frac{1}{\eta}\left\{\frac{1}{\omega}\left[\frac{k_{9i}\{X_i+Y_i - X_{(i-1)}-Y_{(i-1)}\}\Omega}{\alpha_i - \alpha_{(i-1)}} + \frac{k_{10i}(X_{(i+1)}+Y_{(i+1)} - X_i - Y_i)\Omega}{\alpha_{(i+1)} - \alpha_i}\right] - \text{Ar}\cos(\alpha_i+\tau) + \xi[X_i - A\sin(\alpha_i + \tau)]\right\}\right] + C_{12i}\{X_i - A\sin(\alpha_i+\tau)\}$$
$$+ A\Omega\cos(\alpha_{(i+1)} + \tau)\ ,\ i = 1, 2---N \qquad \text{(A2.10)}$$

by substituting the a_i and b_i directly from equation (3.18) and (3.5), respectively, and by using $\dot{X}_{(i+1)b}$ from equation (3.16) with subscript (i+1) replacing i. The newly introduced coefficients k_{7i} through k_{10i} are given in terms of μ and R_i by

$$k_{7i} = \frac{R_i - \mu}{1 + R_i} , \qquad k_{8i} = \frac{1 + \mu}{1 + R_i} \tag{A2.11a}$$

and

$$k_{9i} = \frac{R_i (1+\mu)}{1 + R_i} , \qquad k_{10i} = \frac{1 - \mu R_i}{1 + R_i} \tag{A2.11b}$$

with i = 1, 2----N invariably.

Slight difficulties arising when i equals one in terms like $(\alpha_i - \alpha_{(i-1)})$ of equation (A2.9) and (A2.10) are avoided by the substitution $[\alpha_{(i+N)} - \alpha_{(i+N-1)}]$ obtained from the periodicity equation (2.13). Then equation (A2.9) and (A2.10) can be rewritten as

$$\begin{aligned} X_{i+1} = \quad & C_{9i}\left[\frac{G_{1i}}{\eta\omega} \{X_i + Y_i - X_{(i-1)} - Y_{(i-1)}\} \right. \\ & + \frac{G_{2i}}{\eta\omega} \{X_{(i+1)} + Y_{(i+1)} - X_i - Y_i\} - \frac{Ar}{\eta}\cos(\alpha_i + \tau) \\ & \left. + \frac{\xi}{\eta} \{X_i - A\sin(\alpha_i + \tau)\} \right] + C_{10i} [X_i - A\sin(\alpha_i + \tau)] \\ & + A\sin(\alpha_{(i+1)} + \tau) , \quad i = 1, 2----N \end{aligned} \tag{A2.12}$$

and

$$G_{3i}\,[X_{(i+1)} + Y_{(i+1)} - X_i - Y_i] + G_{4i}\,[X_{(i+2)}+Y_{(i+2)}-X_{(i+1)}-Y_{(i+1)}]$$

$$= C_{11i}\left[\frac{G_{1i}}{\eta\omega}\,\{X_i+Y_i - X_{(i-1)}-Y_{(i-1)}\} + \frac{G_{2i}}{\eta\omega}\,\{X_{(i+1)}\right.$$

$$\left. + Y_{(i+1)} - X_i - Y_i\} - \frac{Ar}{\eta}\cos(\alpha_i+\tau) + \frac{\xi}{\eta}\,\{X_i - A\sin(\alpha_i+\tau)\}\right]$$

$$+ C_{12i}\,[X_i - A\sin(\alpha_i+\tau)] + A\Omega\cos(\alpha_{i+1}+\tau)\ ,\quad i = 1, 2\text{----}N \qquad \text{(A2.13)}$$

by also employing variables

$$\left.\begin{aligned} G_{1i} &= \frac{\Omega k_{9i}}{\alpha_{(i+N)} - \alpha_{(i+N-1)}}\ ,\ G_{2i} = \frac{\Omega k_{10i}}{\alpha_{(i+1)} - \alpha_i} \\ \text{and} \\ G_{3i} &= \frac{\Omega k_{7(i+1)}}{\alpha_{(i+1)} - \alpha_i}\ ,\ G_{4i} = \frac{\Omega k_{8(i+1)}}{\alpha_{(i+2)}-\alpha_{(i+1)}} \\ & \qquad i = 1, 2\text{----}N \end{aligned}\right\} \qquad \text{(A2.14)}$$

introduced for convenience. If the trigonemetric terms like $\cos(\alpha_i+\tau)$ are expanded and coefficients of the X_i, $A\sin\tau$ and $A\cos\tau$ are collected, equation (A2.12) and (A2.13) can be demonstrated to become

$$X_{(i+1)}\left[1-\frac{C_{9i}\cdot G_{2i}}{\eta\omega}\right]+X_i\left[(+G_{2i}-G_{1i}-\xi\omega)\frac{C_{9i}}{\eta\omega}-C_{10i}\right]$$

$$+X_{(i-1)}\cdot\frac{G_{1i}\cdot C_{9i}}{\eta\omega}+A\cos\tau\left[C_{9i}\left\{\frac{r}{\eta}\cos\alpha_i+\frac{\xi}{\eta}\sin\alpha_i\right\}\right.$$

$$\left.+C_{10i}\sin\alpha_i-\sin\alpha_{(i+1)}\right]+A\sin\tau\left[C_{9i}\left(-\frac{r}{\eta}\cdot\sin\alpha_i\right.\right.$$

$$\left.\left.+\frac{\xi}{\eta}\cos\alpha_i\right)+C_{10i}\cos\alpha_i-\cos\alpha_{(i+1)}\right]$$

$$=\frac{C_{9i}}{\eta\omega}\left[G_{1i}\{Y_i-Y_{(i-1)}\}+G_{2i}\{Y_{(i+1)}-Y_i\}\right],\ i=1,2\text{---}N \qquad (A2.15)$$

and

$$X_{(i+1)}\left[G_{3i}-G_{4i}-\frac{C_{11i}G_{2i}}{\eta\omega}\right]+X_i\left[-G_{3i}-C_{12i}\right.$$

$$\left.-\frac{C_{11i}}{\eta\omega}\{+G_{1i}-G_{2i}+\xi\omega\}\right]+X_{(i+2)}\cdot G_{4i}$$

$$+X_{(i-1)}\left[+\frac{C_{11i}}{\eta\omega}\cdot G_{1i}\right]+A\cos\tau\left[C_{11i}\left\{\frac{r}{\eta}\cdot\cos\alpha_i\right.\right.$$

$$\left.\left.+\frac{\xi}{\eta}\cdot\sin\alpha_i\right\}+C_{12i}\cdot\sin\alpha_i-\Omega\cos\alpha_{(i+1)}\right]$$

$$+A\sin\tau\left[C_{11i}\left(-\frac{r}{\eta}\sin\alpha_i+\frac{\xi}{\eta}\cos\alpha_i\right)+C_{12i}\cos\alpha_i+\Omega\sin\alpha_{(i+1)}\right]$$

$$=-G_{3i}\left(Y_{(i+1)}-Y_i\right)-G_{4i}\left(Y_{(i+2)}-Y_{(i+1)}\right)$$

$$+\frac{C_{11i}}{\eta\omega}\left[G_{1i}\{Y_i-Y_{(i-1)}\}+G_{2i}\{Y_{(i+1)}-Y_i\}\right],$$

$$i=1,\ 2\text{----}N\ . \qquad (A2.16)$$

The periodicity equation (2.13) relating to terms like $X_{(i+N-1)}$ is applied next so that the last two sets of equation can be shown to take the forms

$$\left.\begin{aligned} & W2_i X_i + (1-W1_i)X_{(i+1)} + W3_i X_{(i+N-1)} \\ & \\ & + W4_i \cdot A\cos\tau + W5_i\, A\sin\tau \end{aligned}\right\} = W6_i,\ i = 1, 2\text{---}N \qquad \text{(A2.17)}$$

and

$$\left.\begin{aligned} & V1_i X_i + V2_i X_{(i+1)} + V3_i X_{(i+2)} \\ & \\ & + V4_i X_{(i+N-1)} + V5_i\, A\cos\tau \\ & + V6_i\, A\sin\tau \end{aligned}\right\} = V7_i,\ i = 1, 2\text{---}N\ . \qquad \text{(A2.18)}$$

The above equations have been simplified by the introduction of the coefficients defined by

$$\left.\begin{aligned} W1_i &= \frac{C_{9i}\cdot G_{2i}}{\eta\omega} \\ W2_i &= \frac{C_{9i}}{\eta\omega}(G_{2i} - G_{1i} - \xi\omega) - C_{10i} \\ W3_i &= \frac{G_{1i}\cdot C_{9i}}{\eta\omega} \\ W4_i &= C_{9i}\left\{\frac{r}{\eta}\cos\alpha_i + \frac{\xi}{\eta}\sin\alpha_i\right\} + C_{10i}\sin\alpha_i \\ &\quad - \sin\alpha_{(i+1)} \\ W5_i &= C_{9i}\left(-\frac{r}{\eta}\sin\alpha_i + \frac{\xi}{\eta}\cos\alpha_i\right) + C_{10i}\cos\alpha_i \\ &\quad - \cos\alpha_{(i+1)} \\ W6_i &= \frac{C9_i}{\eta\omega}\left[G_{1i}\{Y_{(i+N)} - Y_{(i+N-1)}\} + G_{2i}\{Y_{(i+1)} - Y_i\}\right] \end{aligned}\right\} \qquad \text{(A2.19)}$$

and

$$
\left.
\begin{aligned}
V1_i &= -G_{3i} - C_{12i} - \frac{C_{11i}}{\eta\omega}\{+G_{1i} - G_{2i} + \xi\omega\} \\
V2_i &= G_{3i} - G_{4i} - \frac{C_{11i}}{\eta\omega} G_{2i} \\
V3_i &= G_{4i} \\
V4_i &= \frac{C_{11i}}{\eta\omega} \cdot G_{1i} \\
V5_i &= C_{11i}\left\{\frac{r}{\eta}\cdot\cos\alpha_i + \frac{\xi}{\eta}\sin\alpha_i\right\} + C_{12i}\cdot\sin\alpha_i \\
&\quad - \Omega\cos\alpha_{(i+1)} \\
V6_i &= C_{11i}\left(-\frac{r}{\eta}\sin\alpha_i + \frac{\xi}{\eta}\cos\alpha_i\right) + C_{12i}\cos\alpha_i \\
&\quad + \Omega\sin\alpha_{(i+1)} \\
V7_i &= -G_{3i}\,(Y_{(i+1)} - Y_i) - G_{4i}\,(Y_{(i+2)} - Y_{(i+1)}) \\
&\quad + \frac{C_{11i}}{\eta\omega}\left[G_{1i}\,(Y_{(i+N)} - Y_{(i+N-1)}) + G_{2i}\,(Y_{(i+1)} - Y_i)\right] .
\end{aligned}
\right\} \qquad \text{(A2.20)}
$$

Subscript i invariably takes the integer valves of 1, 2----N in equation (A2.19) and (A2.20). Consequently equation (A2.17) and (A2.18) are identical to the required equation (3.19a) and (3.19b) of Chapter 3.

The explicit expressions for all representative components of $[Pi_+]$ in equation (3.20b) given by Masri [59] were modified to incorporate possible changes in the coefficient of restitution, the modification

involves changes in variables k_{1i} through k_{4i}. All the elements of $[Pi_+]$ are given below

$$[Pi_+] = \begin{bmatrix} S_{1oi}+S_{12i} & S_{11i} & S_{13i} & S_{14i} \\ S_{15i}+S_{17i} & S_{16i} & S_{18i} & S_{19i} \\ S_{20i}+S_{22i} & S_{21i} & S_{23i} & S_{24i} \\ S_{5i}+S_{7i} & S_{6i} & S_{8i} & S_{9i} \end{bmatrix} \qquad \text{(A2.21)}$$

where

$$D_{3i} = (1/\Omega)\, V_{ia} - A\cos\theta_{(i+1)} - S_{31i}$$

$$S_{1i} = (1/\eta)(\xi C_{9i} + \eta C_{10i}) \;,\; S_{2i} = \left(\frac{1}{\omega\eta}\right) C_{9i}$$

$$S_{3i} = -(\omega/\eta)\, C_{9i} \;,\; S_{4i} = (1/\omega\eta)\, C_{11i}$$

$$k_{1i} = [1 - \mu R_{(i+1)}]/(1+\mu) \;,\; k_{2i} = \mu[1 + R_{(i+1)}]/(1+\mu)$$

$$k_{3i} = [1 + R_{(i+1)}]/(1+\mu) \;,\; k_{4i} = [\mu - R_{(i+1)}]/(1+\mu)$$

$$S_{5i} = S_{1i}/D_{3i} \;,\; S_{6i} = S_{2i}/D_{3i}$$

$$S_{7i} = -1/D_{3i} \;,\; S_{8i} = -[(\alpha_{(i+1)} - \alpha_i)]/(\Omega D_{3i})$$

$$S_{9i} = [-S_{31i} - AS_{1i}\cos\theta_i + A\Omega S_{2i}\sin\theta_i + \frac{1}{\Omega} V_{ia}]/D_{3i}$$

$$Q_{1i} = A\cos\theta_{i+1} + S_{31i}$$

$$S_{1oi} = S_{1i} + Q_{1i}\, S_{5i} \;,\; S_{11i} = S_{2i} + Q_{1i}\, S_{6i}$$

$$S_{12i} = Q_{1i}\, S_{7i} \qquad , S_{13i} = Q_{1i}\, S_{8i}$$

$$S_{14i} = -AS_{1i}\cos\theta_i + A\Omega S_{2i}\sin\theta_i - S_{31i} + Q_{1i} S_{9i}$$

$$Q_{2i} = S_{32i} - A\Omega\sin\theta_{i+1}$$

$$S_{15i} = k_{1i}\,[S_{3i} + Q_{2i}\, S_{5i}]$$

$$S_{16i} = k_{1i}\,[S_{4i} + Q_{2i}\, S_{6i}]$$

$$S_{17i} = k_{1i}\, Q_{2i}\, S_{7i}$$

$$S_{18i} = k_{1i} Q_{2i} S_{8i} + k_{2i}$$

$$S_{31i} = (1/\Omega)\,[b_i S_{3i} + (\dot{X}_{ia} - A\Omega\cos\theta_i)\, C_{11i}/(\omega\eta)]$$

$$S_{19i} = k_{1i}\,[-AS_{3i}\cos\theta_i + A\Omega S_{4i}\sin\theta_i - S_{32i} + (S_{32i} - A\Omega\sin\theta_{i+1})\, S_{9i}]$$

$$S_{32i} = [(1/\Omega\eta)][-\omega\dot{C}_{11i} b_i + (\eta C_{12i} - \xi C_{11i})(\dot{X}_{1a} - A\Omega\cos\theta_i)]$$

$$Q_{3i} = S_{32i} - A\Omega\sin\theta_{i+1}$$

$$S_{20i} = k_{3i}\,[S_{31i} + Q_{3i} S_{5i}]$$

$$S_{21i} = k_{3i}\,[S_{4i} + Q_{3i}\, S_{6i}]$$

$$S_{22i} = k_{3i}\, Q_{3i}\, S_{7i}$$

$$S_{23i} = k_{3i}\, Q_{3i}\, S_{8i} + k_{4i}$$

$$S_{24i} = k_{3i}\,[-AS_{3i}\cos\theta_i + A\Omega S_{4i}\sin\theta_i - S_{32i} + Q_{3i}\, S_{9i}]$$

APPENDIX A3

PARTICULAR FORM OF IMPACT DAMPER'S EQUATIONS FOR TWO EQUISPACED IMPACTS/CYCLE

The general equations of motion of an impact damper have been developed in Chapter 3 with some details given in Appendix 2. These equations will be shown here to simplify to the particular forms given in reference 53 and 54 for two equispaced impacts/cycle, i.e.

$$N = 2 \text{ and } k = 1 \quad . \tag{A3.1}$$

Unfortunately the final general equations (3.19a) and (3.19b) cannot be used straightforwardly because the different variables X_1, $\dot{X}_{1b}$, $\dot{X}_{1a}$, a_1, b_1 and A were treated essentially as the unknowns in these two references. A slightly different nomenclature was adopted too. To avoid unnecessary confusion, the notation of Chapter 3 will be retained with explanatory notes added to facilitate direct comparisons for the interested reader. For example, subscript ones were omitted previously from X_1, $\dot{X}_{1b}$, $\dot{X}_{1a}$ whilst a_1 and b_1 were replaced by b_1 and b_2 respectively [53, 54]. Derivations will be based upon the more fundamental equations (3.5a) (3.6a), (3.7), (3.16) and (3.17) of Chapter 3 and (A2.4) and (A2.8) in Appendix 2 rather than their off-shoots, general equations (3.19a) and (3.19b). This change leads to a better accommodation of the X_1, $\dot{X}_{1b}$, $\dot{X}_{1a}$, a_1, b_1, A or, in column vector abbreviation, $\{U\}_{6x1}$.

The procedure will be shown to produce six linear simultaneous equations with the matrix form:

$$[\Delta]_{6x6} \{U\}_{6x1} = \{g\}_{6x1} \qquad \text{(A3.2)}$$

where the six components of vector $\{g\}_{6x1}$ depend only upon the known gap size, d. All elements of the 6x6 square matrix $[\Delta]_{6x6}$ will be found explicitly. Unknowns {U} were obtained in reference 53 and 54 by pre-multiplying equation (A3.2) by the inverse of $[\Delta]_{6x6}$, $[\Delta]^{-1}_{6x6}$, so that

$$\{U\}_{6x1} = [\Delta]^{-1}_{6x6} \{g\}_{6x1} \quad . \qquad \text{(A3.3)}$$

In the process, however, an error appears in the evaluation of the determinant, Δ , of $[\Delta]_{6x6}$. The correct Δ will be given here along with the limits needed in Section 4.2.3.

It is assumed in reference 53 and 54 that the first impact occurs on the right side of M in Figure 3.1. Therefore equation (3.7) in Chapter 3 takes the specific form

$$Y_1 = + d/2 \quad \text{and} \quad Y_2 = - d/2 \qquad \text{(A3.4)}$$

for the first two collisions (i.e., i=1, 2). The primary mass' absolute displacements and velocities just before these two collisions must be equal in magnitude but reversed in direction for two symmetrical (equi-

spaced) periodic impacts/cycle [53, 54]. Hence

$$X_1 = - X_2 \text{ and } \dot{X}_{1b} = -\dot{X}_{2b} \quad . \tag{A3.5}$$

Subscript b has been omitted from X_1 and X_2 because the primary mass' displacement, unlike its velocity, is continuous at a collision. (see equation (3.8)). Times between contacts are related through the symmetry and periodicity requirements. They are expressed conventionally in terms of the α_i of equation (2.3). By using equation (A3.1) in conjunction with (2.16), (3.6b) and, for equispaced impacts, equation (3.20) it can be shown straightforwardly that

$$\alpha_0 = 2\pi \ , \ \alpha_1 = 0 \text{ and } \alpha_2 = \pi \ . \tag{A3.6}$$

Other α_i may be determined from the periodicity condition (2.13) with N equal two from equation (A3.1). For example when i equals one, equation (2.13) gives

$$\alpha_3 = \alpha_1 + \alpha_0$$

or, by using equation (A3.6),

$$\alpha_3 = 2\pi \quad . \tag{A3.7}$$

Basic relations (A3.4) through (A3.7) pertinent to periodic, two equispaced impacts/cycle motion will be used next to obtain the particular

solution in appropriate form.

A relationship between two of the unknowns, X_1 and b_1, may be derived by simply taking i equal one in equation (3.5a) so that

$$b_1 = X_1 - A \sin\theta_1 \quad . \tag{A3.8}$$

The θ_1 may be determined from equation (3.6b) as

$$\theta_1 = \tau + \alpha_1$$

or, by using equation (A3.6),

$$\theta_1 = \tau \ .$$

Employing the last relationship in equation (A3.8) produces

$$X_1 - b_1 - A \sin\tau = 0 \quad . \tag{A3.9}$$

The velocity of the primary mass just after the first impact, $\dot{X}_{1a}$, is merely the time derivative of its displacement, X(t) given by equation (3.6a), evaluated at instant $t = 0_+$. Differentiating equation (3.6a) and substituting $t = 0_+$ leads to

$$\dot{X}(0_+) \equiv \dot{X}_{1a} = \Omega \frac{\eta}{r} a_1 - \Omega \frac{\xi}{r} b_1 + A\Omega\cos\tau$$

or, by employing equation (3.3),

$$\dot{X}_{1a} - \eta\omega a_1 + \xi\omega b_1 - A\Omega\cos\tau = 0 \quad . \tag{A3.10}$$

Equation (A2.4) with i equal one on the other hand gives

$$X_2 = C_{91}\, a_1 + C_{101}\, b_1 + A\sin(\alpha_2 + \tau)$$

which, in conjunction with equation (A3.5) and (A3.6), leads to

$$X_1 + C_{91}\, a_1 + C_{101}\, b_1 - A\sin\tau = 0 \quad . \tag{A3.11}$$

The two coefficients C_{91} and C_{101} may be determined from equation (A2.3) as

$$C_{91} = \exp\left[-\frac{\pi\xi}{r}\right] \sin\left(\frac{\pi\eta}{r}\right) \tag{A3.12a}$$

and

$$C_{101} = \exp\left[-\frac{\pi\xi}{r}\right] \cos\left(\frac{\pi\eta}{r}\right) \quad . \tag{A3.12b}$$

The two alternative symbols h_1 and h_2 were used respectively for C_{91} and C_{101} in reference 53 and 54. Consequently equation (A3.11) was written there in the form

$$X_1 + h_1\, a_1 + h_2\, b_1 - A\sin\tau = 0 \quad . \tag{A3.13}$$

Unknown velocity $\dot{X}_{1b}$ may be obtained by first substituting i equal one in equation (A2.8) so that

$$\dot{X}_{2b} = C_{111}\, a_1 + C_{121}\, b_1 + A\Omega\cos(\alpha_2 + \tau)$$

and then using equation (A3.5) and (A3.6) to give

$$\dot{X}_{1b} + C_{111}\, a_1 + C_{121}\, b_1 - A\Omega\cos\tau = 0 \quad . \tag{A3.14}$$

Coefficients C_{111} and C_{121} may be evaluated by substituting equation (A3.12a) and (A3.12b) into equation (A2.7) with i equal unity. This procedure may be shown straightforwardly to give

$$C_{111} = \omega \exp[-\frac{\pi\xi}{r}] \,(\eta\cos\frac{\pi\eta}{r} - \xi\sin\frac{\pi\eta}{r}) \tag{A3.15a}$$

and

$$C_{121} = -\omega \exp\,[-\frac{\pi\xi}{r}] \,(\eta\sin\frac{\pi\eta}{r} + \xi\cos\frac{\pi\eta}{r}) \tag{A3.15b}$$

which were termed θ_1 and θ_2, respectively, in reference 53 and 54. However dashed superscripts will be used additionally here to avoid confusion with the θ_i of equation (3.6b). Therefore equation (A3.14) can be rewritten as

$$\dot{X}_{1b} + \theta_1'\, a_1 + \theta_2'\, b_1 - A\Omega\cos\tau = 0 \tag{A3.16}$$

where

$$\theta'_1 \equiv C_{111} \quad \text{and} \quad \theta'_2 \equiv C_{121} \quad . \tag{A3.17}$$

The last two equations required are developed in a similar manner from equation (3.16) and (3.17). For example by substituting i equal one in equation (3.16) and employing the periodicity condition (2.13) with requirement (A3.1), the following equation is derived

$$\dot{X}_{1b} = \begin{cases} \dfrac{k_{71}\,[X_1 + Y_1 - X_2 - Y_2]\,\Omega}{\alpha_3 - \alpha_2} \\ \dfrac{+\,k_{81}\,[X_2 + Y_2 - X_1 - Y_1]\,\Omega}{\alpha_2 - \alpha_1} \end{cases} \quad . \tag{A3.18}$$

Substituting equation (A3.4), (A3.6) and (A3.7) into the last equation and rearranging terms gives

$$\dot{X}_{1b} = (k_{71} - k_{81})\,(2X_1 + d)\,\frac{\Omega}{\pi} \quad . \tag{A3.19}$$

Similarly,

$$\dot{X}_{1a} = (k_{91} - k_{101})\,(2X_1 + d)\,\frac{\Omega}{\pi} \tag{A3.20}$$

starting from equation (3.17). Now the coefficients of restitution R_1, R_2 .... must be equal (to R) for two equispaced impacts/cycle, periodic motion. Consequently differences in the coefficients on the right-

hand of the last two equations can be shown to be

$$k_{71} - k_{81} = \frac{R-2\mu-1}{1+R} \quad \text{and} \quad k_{91} - k_{101} = \frac{R+2\mu R-1}{1+R} \tag{A3.21}$$

from equation (A2.11a) and (A2.11b) of Appendix 2. Substituting these coefficient expressions into equation (A3.19) and (A3.20) produces the last needed equations

$$X_1 + \frac{\pi}{2\Omega}\left(\frac{1+R}{1+2\mu-R}\right) \dot{X}_{1b} = -\, d/2 \tag{A3.22}$$

and

$$X_1 + \frac{\pi}{2\Omega}\left(\frac{1+R}{1-2\mu R-R}\right) \dot{X}_{1a} = -\, d/2 \tag{A2.23}$$

after minor rearrangement. These equations were written in reference 53 and 54 as

$$X_1 + \sigma_1 \dot{X}_{1b} = -\, d/2 \tag{A3.24}$$

and

$$X_1 + \sigma_2 \dot{X}_{1a} = -\, d/2 \tag{A3.25}$$

respectively, where

$$\sigma_1 = \frac{\pi}{2\Omega}\left(\frac{1+R}{1+2\mu-R}\right) \quad \text{and} \quad \sigma_2 = \frac{\pi}{2\Omega}\left(\frac{1+R}{1-2\mu R-R}\right) \quad . \tag{A3.26}$$

Equations (A3.9), (A3.10), (A3.13), (A3.16), (A3.24) and (A3.25) were derived specifically in reference 53 and 54 but in the matrix form

comparable to

$$\begin{vmatrix} 1 & 0 & 0 & 0 & -1 & -\sin\tau \\ 0 & 0 & 1 & -\eta\omega & \xi\omega & -\Omega\cos\tau \\ 1 & 0 & 0 & h_1 & h_2 & -\sin\tau \\ 0 & 1 & 0 & \theta_1' & \theta_2' & -\Omega\cos\tau \\ 1 & \sigma_1 & 0 & 0 & 0 & 0 \\ 1 & 0 & \sigma_2 & 0 & 0 & 0 \end{vmatrix} \begin{Bmatrix} X_1 \\ \dot{X}_{1b} \\ \dot{X}_{1a} \\ a_1 \\ b_1 \\ A \end{Bmatrix} = \begin{Bmatrix} 0 \\ 0 \\ 0 \\ 0 \\ -d/2 \\ -d/2 \end{Bmatrix} . \qquad (A3.27)$$

Equation (A3.27) is the completely detailed version of equation (A3.2). The correct determinant, Δ, of the above 6x6 matrix is

$$\Delta = \begin{cases} h_1 \left[C(\sigma_2 - \sigma_1) - (S + C\sigma_2)\, \sigma_1\, \theta_2' + (S + C\sigma_1)\, \xi\omega\sigma_2\right] \\ + (1 + h_2) \left[(S + C\sigma_2)\, \sigma_1\theta_1' + (S + C\sigma_1)\, \eta\omega\sigma_2\right] \end{cases} \qquad (A3.28)$$

where

$$S = \sin\tau \quad \text{and} \quad C = \Omega\cos\tau \quad . \qquad (A3.29)$$

Finally, the limits of σ_1 and σ_2 given by equation (A3.26) and their ratio are needed in Section 4.2.3 as the mass ratio μ tends to infinity. A physically realizable driving frequency Ω must remain finite whilst $0 < R \leq 1$. Consequently it can be proved from equation (A3.26) that

$$\lim_{\mu\to\infty} \sigma_1 = \lim_{\mu\to\infty} \frac{\pi}{2\Omega} \left(\frac{1+R}{1-R+2\mu}\right) \to 0 \qquad \text{(A3.30)}$$

and similarly,

$$\lim_{\mu\to\infty} \sigma_2 = \lim_{\mu\to\infty} \frac{\pi}{2\Omega} \left(\frac{1+R}{1-R-2\mu R}\right) \to 0 \quad . \qquad \text{(A3.31)}$$

By straightforward algebraic manipulation

$$\lim_{\mu\to\infty} \frac{\sigma_1}{\sigma_2} = \lim_{\mu\to\infty} \left(\frac{1-R-2\mu R}{1-R+2\mu}\right) \to \frac{-2\mu R}{2\mu} = -R \quad . \qquad \text{(A3.32)}$$

APPENDIX A4

MEASUREMENT OF THE COEFFICIENT OF RESTITUTION

Several coefficients of restitution were measured in situ by using high speed photography. A camera, Action Master 500 made by Photosonic Ltd., was mounted on a sturdy tripod, levelled and aligned carefully so that cross-wires in its eyepiece coincided with lines etched on the initially stationary secondary mass. The Impact-Pair shown in Figure 2.11 was then set into motion and permitted to reach a stable state before filming at 500 frames/second was started. Various amplitudes and frequencies of the untaped primary mass were employed when using the mature stainless steel secondary mass in order to encompass all contact velocities in the vibroimpact experiments. Restricted funds limited all other measurements to a single frequency of about 35 Hz. Adequate resolution was maintained by ensuring no fewer than ten film shots per cycle of the primary mass' displacement.

Films were developed commercially and analyzed in slow motion with the aid of the Motion Analyzer manufactured by Photographic Analysis Ltd. Appropriate lengths of film were discarded to eliminate the starting acceleration and finishing deceleration phases of the camera and thereby guarantee constant speed photography [92]. Absolute positions of both masses could be determined straightforwardly

by reference to a short rigid pointer fixed to the concrete base of Figure 2.11. A plot of typical displacements is presented in Figure A4.1 where experimental data points have been joined by eye with an appropriate line or sinusoid. Impacts happened between the two masses at points B_1, B_2, B_3.... and, correspondingly, B_1', B_2', B_3'.... in the upper and lower figures respectively. Therefore the slopes just before and after these points give velocities appropriate to the direct application of equation (2.8) and, hence, the coefficient of restitution, R_i. The number of data points used however inadequately described the more rapidly changing slopes near B_1', B_2', B_3'.... compared with B_1, B_2, B_3, etc. Conversely the A, Ω or from equation (2.16) for this illustration of two impacts/cycle, $2\pi/T_o$, and $(\alpha_i + \tau)$ associated with the more particular equation (2.10) for R_i may be measured accurately from Figure A4.1(b). Variables A, T and τ are shown explicitly in this figure. The remaining α_i, or from equation (2.3) Ωt_i, may be calculated after quantifying the last unknowns t_i, the time delays of subsequent impacts after the first one at B_1. The first delay t_1 is specified in Figure A4.1(b). There was little discernible difference in practice between nominally corresponding impacts in different periods. Consequently, parameters were evaluated typically from fifty periods and averaged arithmetically. Finally the V_{ia} and V_{ib} in equation (2.10) were measured similarly from the slopes between

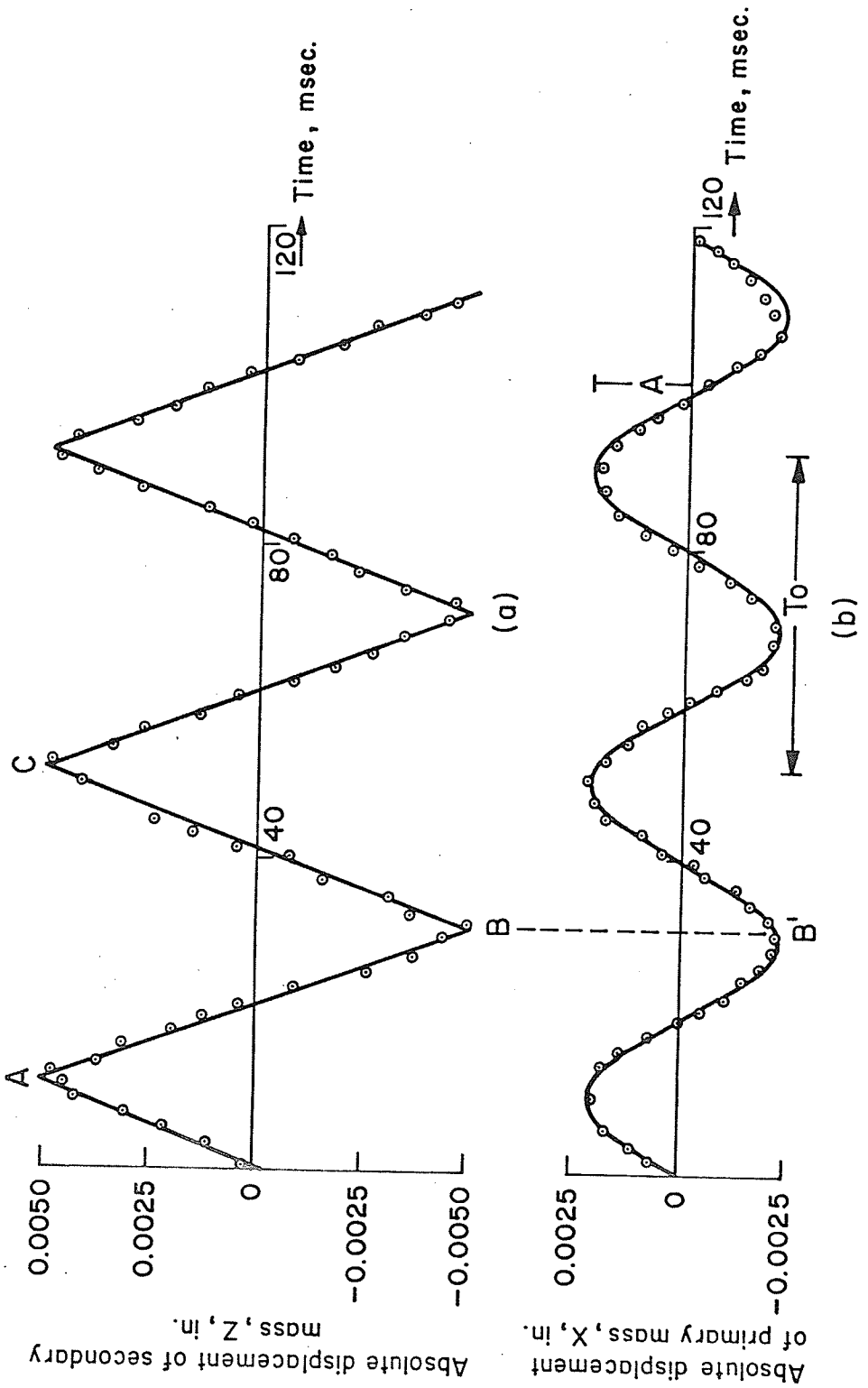

Figure A4.1. Corresponding absolute displacement of (a) secondary mass and (b) primary mass. The full curves - show a line and sinusoid fitted by eye to the experimental data points denoted by ⊙⊙.

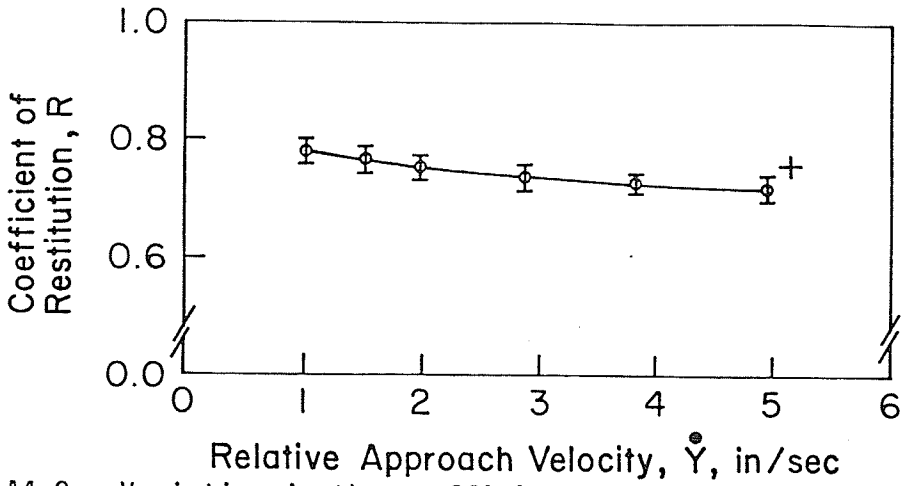

Figure A4.2. Variation in the coefficient of restitution with relative approach velocity for mature stainless steel secondary mass and untaped primary mass.

+The vertical line in the symbol Φ indicates the least and greatest measured values of R at any one Ẏ.

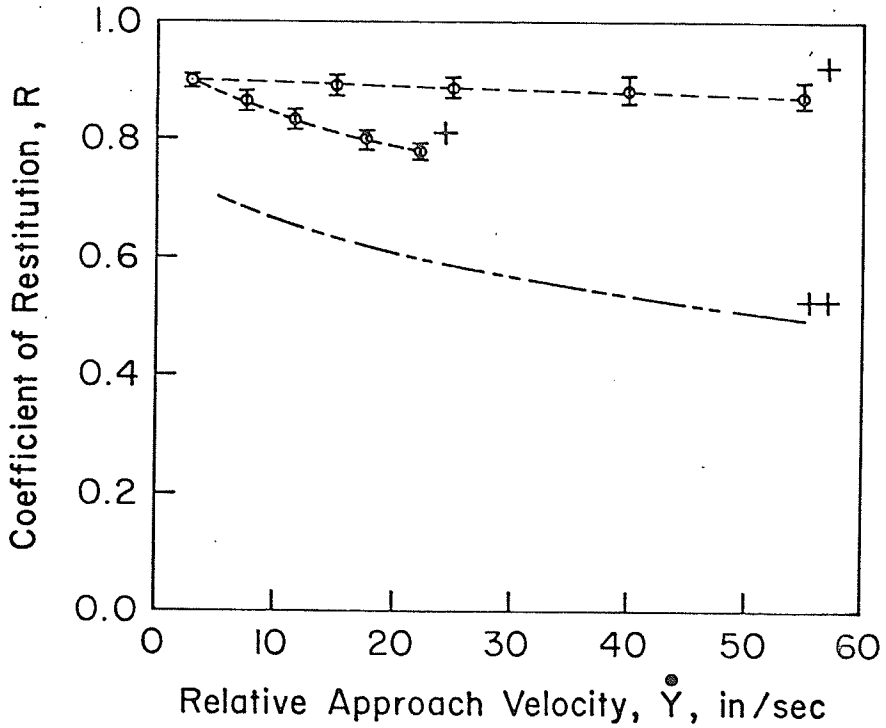

Figure A4.3. Variation in coefficient of restitution with approach velocity. Glass ball hitting a steel plate [36]-----; two impacting steel spheres [35]----; and a steel sphere hitting an aluminium plate [39]-- — -- .

+The vertical line in the symbol Φ indicates the least and greatest measured values of R at any one Ẏ.

++Envelope of the greatest variation which was not given for the lowest curve —— -- —— .

B_1B_2, B_2B_3, etc. Any one of these slopes appeared fairly constant. Therefore, the constant velocity assumption reasonably described the secondary mass' motion between consecutive impacts.

Computations of R_i based upon equation (2.10) at various approach velocities, $\dot{Y}$, are displayed in Figure A4.2 for the untaped primary and mature stainless steel secondary mass. Variations observed in the R_i for consecutive impacts were always within the extreme errors denoted by a symbol's vertical line. Consequently, the assumption that the R_i equal a constant value R in this case is reasonable in the short-term whilst surfaces are hardly affected by contacts. Analogous data obtained previously for comparably hard materials but somewhat different body geometries [35, 36, 39] is presented in Figure A4.3. The coefficients are numerically similar to those in Figure A4.2 and show generally the same tendency to decrease with increasing $\dot{Y}$. Additional effects of repeated collisions do not seem to have been considered in these references.

Coefficients of restitution used theoretically for a given combination of materials and contact surfaces of the primary and secondary masses are noted in Table A4.1. The highest R in this table, 0.75, is the arithmetic average of the greatest and smallest mean values shown in Figure A4.2 over the applicable range of $\dot{Y}$. Remaining information on the other hand corresponds to the average of extreme R

Stainless steel primary mass with contact surfaces:	Material of secondary mass	R
Untaped	stainless steel	0.75
Untaped	brass	0.68
Taped	stainless steel	0.61

Table A4.1 Coefficient of restitution, R, used in theory. Any two, short-term experimental extremes fluctuated about the given R but within $\pm$ 3%.

observed over the short-term again but only at a single $\dot{Y}$. This $\dot{Y}$ was selected to be approximately midway in the range of the $\dot{Y}$ for the true vibroimpact experiments. Then the extreme R were found to be always within its average value $\pm$ 3%.

APPENDIX A5

COMPONENT PROPERTIES OF THE IMPACT DAMPER

The properties of the experimental impact damper shown in Figure 3.6, unlike the theoretical ones in Figure 3.1, are mostly distributed. Procedures used to make the experimental and idealised behaviours largely equivalent will be described here.

The predominant frequency range of interest just encompassed the first natural frequency of the primary when acting independently of the secondary system. All natural frequencies and corresponding viscous damping ratios were measured in standard resonance tests [91]. The fundamental frequency and damping ratio of the primary system alone are given for convenience in Table A5.1. This fundamental was found to be over twenty times smaller than any other, lightly damped natural frequency. Consequently the first mode of the primary system can be reasonably assumed to act alone over the frequencies of interest. Therefore the distributed weight of each cantilevered supporting beam behaved effectively as a weight 33/140 times the beam's total weight concentrated at its free tip [5]. The weight of the beam was measured like that of remaining components on an accurate laboratory weigh scale. Hence the effective weights of both beams were calculated

straightforwardly. These effective weights were added to the measured and essentially tip weights of the accelerometer and aluminium brackets to form the equivalent weight, W_{eq}, of the ideal primary system. The corresponding equivalent stiffness, K_{eq}, was approximated fairly for the very light damping by the square of the experimental fundamental circular frequency times W_{eq} divided by the gravitational constant. Both W_{eq} and K_{eq} of the primary system are presented for convenience in Table A5.1.

The first natural frequency of the secondary mass alone was more than 500 times greater than the frequencies of concern. Therefore it was considered rigid. Its weight was measured as 0.044 ± 0.002 lb.

Property	Methodology	Value
Equivalent weight, W_{eq}	Computation	1.61 lb
Equivalent stiffness, K_{eq}	Computation	65.01 lb/in
Fundamental natural frequency of primary alone	Measurement	19.87 $\pm$ 0.03 Hz
Effective viscous damping ratio	Measurement	0.0114 $\pm$ 0.0005

Table A5.1 Component properties of the impact damper's primary system.